NONLINEAR MATERIAL BEHAVIOR AND FATIGUE-ACCUMULATED DAMAGE OF WOOD PLASTIC COMPOSITES

By

DEREK A. BROSIOUS

A thesis submitted in partial fulfillment of
the requirements for the degree of

MASTER OF SCIENCE IN CIVIL ENGINEERING

WASHINGTON STATE UNIVERSITY
Department of Civil and Environmental Engineering

DECEMBER 2008

To the Faculty of Washington State University:

The members of the Committee appointed to examine the dissertation/thesis of DEREK A. BROSIOUS find it satisfactory and recommend that it be accepted.

_____
Chair

_____
Co-Chair

_____

ACKNOWLEDGMENTS

First, I would like to thank the Office of Naval Research (Grant N00014-06-1-0847) for funding this project and providing me with the rare opportunity to explore new territory. I would like to thank my advisor, Dr. Pizhong Qiao, not just for facilitating my project, but for greatly surpassing what some might consider the bare minimum of his role in this process. Professor Qiao has been a true mentor, a colleague, a friend, and the ultimate voice of wisdom for the past two years, whose impact was monumental. I would also like to extend my gratitude to Dr. Michael P. Wolcott for his input and support in this study.

Personally, I would like to thank my family for providing me with the unconditional and everlasting support that has guided me through this experience. The financial contributions, emotional encouragement, and overall positive reinforcement are directly reflected through this work and my collegiate career. Their assistance in laying the foundation for the rest of my life will never be forgotten.

Finally, I would like to offer special thanks to the faculty at the Wood Materials Engineering Laboratory for their assistance in my research, especially Scott Lewis, Bob Duncan, and Brent Olson for providing technical expertise and for being there at times when I was a bit lost. Also, special thanks go to Wei Fan and Steven Greenwood for their technical assistance and advice in computer programming.

NONLINEAR MATERIAL BEHAVIOR AND FATIGUE-ACCUMULATED DAMAGE OF WOOD PLASTIC COMPOSITES

Abstract

by Derek Allen Brosious, M.S.
Washington State University
December 2008

Chair: Pizhong Qiao
Co-Chair: Michael P. Wolcott

Wood-plastic composites (WPC) are quickly growing as useful materials in the development of structural elements by combining some of the advantages of both wood and plastic. However, their structural use has been somewhat limited due to a lack of knowledge concerning the mechanical behavior of WPC, most notably the stress-strain nonlinearity and the lack of design predictability due to damage accumulation. This paper attempts to address and mitigate these two limitations.

The stress-strain behaviors of several formulations of WPC were evaluated in quasi-static tension and flexure under various strain rates, where highly nonlinear performance was observed. A nonlinear hyperbolic tangent constitutive relation was used for stress-strain and force-displacement analysis in an attempt to model the behavior of coupled wood-polypropylene in axial members and in flexural members. It was found that the hyperbolic tangent function is an excellent tool for describing nonlinear stress-strain behavior in tension and flexure, and deflections of structural members in both loading modes can be predicted quite successfully. Through this process, it was also

discovered that the strain rate, or rate of applied load, had a notable effect on material properties. Increases in stiffness and ultimate strength were observed for increased load rates, and the nonlinearity of stress-strain relation reduced as the load rate increased. An analytical model using energy method was proposed to predict the nonlinear load-deformation history of structural components.

A stress-cycle to failure (S-N) curve was developed for a coupled wood-polypropylene by fatiguing flexural samples to failure. The fatigue data indicated that the formulation behaved extremely well at lower stress ratios, although the data was somewhat erratically dispersed. Based on these findings, coupons were conditioned to varying fractions of ultimate failure cycles and then tested in quasi-static flexure to measure reduced stiffness and in dynamic mechanical analysis (DMA) to measure reduced storage modulus. Two cumulative damage models were proposed using random distributions and two-parameter Weibull distributions of the measured fatigue data. Damage parameters were proposed based on cumulative probability density functions, and they were applied in the context of Continuum Damage Mechanics (CDM) to predict reduced stiffness and reduced storage modulus. The Weibull distribution provided good comparisons with test data, but further investigations are recommended. The present study sheds light on nonlinear material behavior of WPCs under quasi-static loading and accumulated damage under fatigue and provides related prediction models for such phenomena.

TABLE OF CONTENTS

Page

LIST OF TABLES

LIST OF FIGURES

DEDICATION

I passionately dedicate this to all those who have dedicated themselves to a passion.

CHAPTER 1 – INTRODUCTION

1.1 Background

The U.S. Office of Naval Research funded this research project with the Department of Civil and Environmental Engineering at Washington State University to investigate the feasibility of using a wood-plastic composite material (WPC) as an alternative source for structural components in marine applications.

Wood-plastic composites, which are described as thermoplastics reinforced with wood fiber, have been produced in the United States for several decades. Although the industrial demand for WPC in structural applications is no match for that of traditional materials like steel, concrete, or timber, the market has steadily grown over recent years with the discovery and understanding of some of the structural advantages associated with WPC. Currently, researchers have been developing formulations that exhibit outstanding structural performance characteristics, and many applications that were once constructed strictly with timber elements are being replaced and retrofitted with WPC.

Many natural fibers, including jute, wheat, hemp, flax straw, sugarcane, etc., can be combined with plastics to improve mechanical performance and dimensional and thermal stability (Bateman, et al., 2008). WPC utilizes the natural fiber of wood flour as an alternative to synthetic filler, which creates a renewable and biodegradable composite with lower density, less abrasiveness, and lower cost (Hamidinia, et al., 2006; Moteei, et al., 2006). Plastic wastes are a major component of global municipal solid waste and provide a new and promising raw material source for the manufacture of WPC. Recyclable plastics that melt and can be processed below the degradation temperature of wood are normally suitable for use in extrusion of WPC. Hamidinia, et al. (2006)

showed that using recycled plastics in WPC rather than virgin plastics resulted in no significant loss in material strength or stiffness, especially for polyethylene, providing conclusive evidence that the expanded use of WPC can be both economically feasible and sustainable.

The combination of wood and thermoplastics is physically advantageous because during mixing and/or extrusion, the plastic compound penetrates into the wood cell lumen, filling the voids in the wood cell structure and imparting better physical and mechanical properties to the composite (Gardner, et al., 2003). Wolcott (2001) found that the addition of about 40-50% wood flour also added a significant amount of thermal stability to the thermoplastic, while the polymer component improved resistance to moisture and corrosion defects. Clemons (2002) showed that WPC absorbs less moisture than wood and at a slower rate when directly exposed, resulting in exceptional performance in waterfront applications due to resistance of fungal damage and increased dimensional stability (i.e., warping). The use of wood flour as the natural fiber filler rather than others like rice hull, newsprint, and kenaf fibers resulted in the lowest amount of water uptake over a 5 week period, proving that there is no efficient natural substitute for wood flour in composites for marine structures (Moteei, et al., 2006). WPC is also appealing because compared to the standard timber products that have been widely used in the past, it is more durable under corrosion from decay, termites, and other marine organisms that have become prevalent in recent years as water pollution levels have declined. Without preservative treatments, there are virtually no major environmental impacts of using WPC, and much of the composite can be manufactured from recycled materials. Due to reduced production costs of WPC, coupled with increased production

costs of next-generation timber preservative treatments, the economic gap between timber and wood-plastics has drastically narrowed, building further incentive for WPC research (Lu, 2002).

WPC have been shown to exhibit increased durability with negligible maintenance requirements when compared to timber products, causing a vast number of consumers to view them favorably (Clemons, 2002; Wolcott and Smith, 2004). Thermoplastics made from recycled materials such as polyethylene (PE), polyvinyl chloride (PVC), and polypropylene (PP) are currently being utilized for a variety of commercial products. Ample research of high-strength engineered plastics has been performed, and Wolcott (2001) concluded that WPC should not be limited to nonstructural applications. Therefore, expansion of the WPC market for structural applications is appropriate, provided that societal incentive exists and feasible applications are developed and accepted by industry.

1.2 Problem Statement and Significance

WPC are currently well-established for use in floor parquets, park benches, picnic tables, and plastic lumber for pedestrian walkways, home décor, fences, and outdoor decking. This clearly indicates that the WPC market is ripe for nonstructural applications, but recently researchers have been working to expand the use of these materials. WPC has been demonstrated to perform adequately when used as a replacement for treated lumber in marine pier components. Additional projects are also investigating the use of WPC in light vehicular and pedestrian bridges as well as building components where moisture performance is vital (Slaughter, 2005).

Along with evident societal demand and economic practicability, WPC design procedures must be well understood enough to ensure that public safety is held paramount in all engineering applications, and the only way to accomplish that is to conduct extensive research. WPC material properties and behavior are still unclear when compared to timber or steel, especially in specialized research areas where the specific traits of composite interaction come into play. One such area is load duration performance, where a member is under various levels of long-term loading or subjected to random and/or cyclic loading, causing damage to accumulate at unknown rates, times, and magnitudes. Little conclusive research has been conducted to classify damage accumulation in WPC. Therefore, its mechanical behavior and the parameters affecting it remain ambiguous. The mechanical and long-term performance of WPC structural members must be established through organized research and statistical modeling in order to develop consistent methods for deriving design methods and addressing serviceability issues. The expansion of the WPC market for structural applications is hence practical and highly necessary for the advancement of structural engineering worldwide, demanding the need for as much research as possible.

1.3 Research Development

During services, engineered structures are subjected to varying or random loadings as well as constant amplitude loadings, represented in empirical study as fatigue analysis. WPC are often designed to be subjected to loads over an extended period of time, so understanding their short-term properties is not sufficient enough to characterize their long-term properties. This concept applies to nearly all structures for the purposes

of this project. The acquisition of data in a member's simulated linear and nonlinear ranges of deformation and its use in analysis, prediction, and extrapolation are important tasks for WPC research.

Many materials display linear viscoelastic behavior over specific ranges of stress, strain, time, and fatigue conditioning, but may be nonlinear over different ranges of these variables. Linear viscoelastic behavior has been well documented and a number of constitutive equations have been presented (Findley, et al., 1976; Findley, 1960; Flugge, 1967; Fung, 1965). A commonality found in many engineering materials, including composites, is a nonlinear stress-strain relationship combined with properties that are dependent on the loading scenario. Nonlinear materials continue to be one of the leading subjects of ongoing research and the basis of a number of articles summarizing attempts to model nonlinear viscoelastic response (Findley, 1960; Lou and Schapery, 1971; Rand, 1995; Schapery, 1969). These nonlinear materials require constitutive relations that are more complex than linear theory and are therefore usually derived empirically. The need for a constitutive relationship to describe nonlinear behavior of WPC over a wide range of applied stress levels is quite obvious and very practical for determining safe design loads in structural components. For modeling purposes, selecting accurate and mathematically tractable constitutive relations is especially important and must be performed with care.

Failure modes of composite materials are quite complicated and much different from failure modes of isotropic materials such as metals and pure homogenous polymers, like the plastic constituents used in this study. Durability and damage assessment of WPC materials under cyclic loading conditions is of utmost concern and requires

investigation into previously uncharted territories. Many authors have developed damage accumulation models in fatigue studies for various materials including fiber-reinforced polymers (FRP) at varying ply angles and short glass fiber reinforced composites (Shirazi, et al., 2007; Dano, et al., 2006; Han, et al., 1986), but little to no research exists for wood-filled polymers. Such damage models have been built upon concepts of fatigue modulus and multi-stress life prediction, stiffness degradation of damaged material, and other parameters. Some models are based purely on geometric shape, temperature, moisture content, cyclic frequency, number of cycles, and stress level (Han, et al., 1986). The time-dependant nature of WPC may also have considerable effect on the stress distribution within a member. It is of equal importance to be able to use viscoelastic analysis methods to predict changes in stress-strain distribution and mechanical properties over time as a function of damage accumulation. Flexural fatigue conditioning can be used to simulate the damage, and coupled with dynamic mechanical analysis (DMA), loss/storage moduli can be used to determine stiffness degradation and characterize material damage. This research strategy can be used to develop a continuum damage mechanics (CDM) model using kinetic theory with probability theory to study damage accumulation and predict changes in mechanical behavior of WPC.

1.4 Objectives

This research project aims to evaluate the nonlinear material behavior of WPCs, investigate their flexural fatigue performance, and assess fatigue-accumulated damage using DMA. WPC are known to display strain rate effects in response to applied stress. A hyperbolic tangent function is considered to fit the testing data of stress vs. strain and

predict the initial modulus of elasticity, ultimate strength, and reduced stiffness at various design strains. A more complete understanding of the stress-strain nonlinearity is needed to fully classify the mechanical behavior of WPC materials. The static tensile and flexural tests are conducted to evaluate the nonlinear stress-strain relation of WPC, and a nonlinear model using energy method is accordingly developed at coupon level, which can be easily scaled up, thus enabling the prediction of nonlinearity in structural components.

Cyclic loading (fatigue) imparts accumulated damage to materials. In this study, DMA is used to measure the loss and storage modulus and mechanical loss factor as a function of fatigue damage accumulation to assess and predict changes in mechanical properties of one coupled wood-polypropylene composite. A one-dimensional CDM model is proposed, and it utilizes the DMA results and a proposed kinetic theory in order to better understand the effect of damage accumulation in WPC. The specific objectives of this research are as follows:

1) Establish the quasi-static tensile and flexural behavior of a known wood-polyethylene and two wood-polypropylene (uncoupled & coupled) formulations and assess their initial mechanical properties.
2) Examine the effects of quasi-static load rates on flexural material properties.
3) Use the hyperbolic tangent function to characterize the stress-strain nonlinearity from all quasi-static testing data.
4) Develop a nonlinear model based on energy method to predict the axial and flexural response of structural components, based on the measured nonlinear stress-strain constitutive law at coupon level.

5) Evaluate flexural fatigue behavior and establish S-N curves for the proposed WPC materials.
6) Condition the WPC samples under flexural fatigue and characterize cumulative damage using dynamic mechanical analysis (DMA).
7) Develop a one-dimensional (1-D) model using Continuum Damage Mechanics (CDM) to describe and assess fatigue-accumulated damage.

1.5 References

American Association of State Highway and Transportation Officials (AASHTO). "Standard Specifications for Highway Bridges." 17th Edition, 2002.

ASTM D3878-07. "Standard Terminology for Composite Materials." American Society for Testing and Materials.

Bateman, S., Gotama, J., Wu, D., and Yuan, Q., "Wood Fiber Reinforced Polyethylene and Polypropylene Composites with High Modulus and Impact Strength," Journal of Thermoplastic Composite Materials, Vol. 21 pp. 195-208, 2008.

Clemons, C. "Wood-Plastic Composites in the United States, The Interfacing of Two Industries." Forest Product Journal, June 2002, Vol. 52, No. 6., pp. 10-18.

Dano, M., Bissonnette, B., Gendron, G., and Maillette, F., "Experimental Characterization of Damage in Random Short Glass Fiber Reinforced Composites," Journal of Thermoplastic Composite Materials, Vol. 19, pp. 79-96, 2006.

Findley, W.N., "Mechanisms and Mechanics of Creep of Plastics." SPEJ, Vol. 16, pp. 57-65, January 1960.

Findley, W.N., Lai, J.S., and Onaran, K., "Creep and Relaxation of Nonlinear Viscoelastic Materials." North-Holland Publishing Company, New York, NY, 1976.

Flugge, W., "Viscoelasticity." Blaisdell, Waltham, MA, 1967.

Fung, Y.C., "Foundations of Solid Mechanics." Prentice Hall, Englewood Cliffs, NJ, 1965.

Gardner, D.J., and Stokke, D.D., "Fundamental Aspects of Wood as a Component of Thermoplastic Composites," Journal of Vinyl & Additive Technology, Vol. 9, pp. 96-104, 2003.

Han, K.S., and Hwang, W., "Cumulative Damage Models and Multi-Stress Fatigue Life Prediction," Journal of Composite Materials, Vol. 20, pp. 125-153, 1986.

Han, K.S. and Hwang, W., "Fatigue of Composites – Fatigue Modulus Concept and Life Prediction," Journal of Composite Materials, Vol. 20, pp. 154-165, 1986.

Lou, Y.C. and Schapery, R.A., "Viscoelastic Characterization of a Nonlinear Fiber-Reinforced Plastic," Journal of Composite Materials, Vol. 5, pp. 208-234, 1971.

Lu, G., "HDPE Wood-Plastic Composite Material Model Subjected to Damage." Master Thesis, Washington State University, May 2002.

Moteei, N., Najafi, S.K., and Tajvidi, M., "Long-Term Water Uptake Behavior of Natural Fiber/Polypropylene Composites," Journal of Applied Polymer Science, Vol. 99, pp. 2199-2203, 2006.

Hamidinia, E., Najafi, S.K., and Tajvidi, M., "Mechanical Properties of Composites from Sawdust and Recycled Plastics," Journal of Applied Polymer science, Vol. 100, pp. 3641-3645, 2006.

Rand, J.L., "A Nonlinear Viscoelastic Creep Model." Tappi Journal. Pp. 178-182, July 1995.

Schapery, R.A., "On the Characterization of Nonlinear Viscoelastic Materials." Polymer Engineering and Science, Vol. 9, No. 4, pp. 295-310, 1969.

Slaughter, A. E., "Design and Fatigue of a Structural Wood-Plastic Composite." Master Thesis, Washington State University, August 2004.

Shirazi, A., Varvani-Farahani, A., "A Fatigue Damage Model for (0/90) FRP Composites Based on Stiffness degradation of 0 and 90 Composite Plies," Journal of Reinforced Plastics and Composites, Vol. 26, pp. 1319-1336, 2007.

Wolcott, M.P. "Wood-Plastic Composites." Encyclopedia of Materials: Science and Technology, 2001.

Wolcott, M.P. and Smith, P.M., "Opportunities and Challenges for Wood-Plastic Composites in Structural Applications." Proceedings of Progress in Woodfibre-Plastic Composites-2004 Toronto, ON, 2004.

CHAPTER 2 – QUASI-STATIC BEHAVIOR OF WPC

2.1 Introduction

The demand for the use of wood-plastic composites (WPC) in structural applications has increased rapidly in recent years. However, there exist limitations in the prediction of WPC behavior, and therefore, in the design of structural members. While these materials have been progressively developed into more commonly used structural components, there is still a significant need to further verify the relevant mechanical properties and in what ways they can be affected by factors such as load rate and mode, composition, and long-term damage accumulation. Fully understanding those mechanical properties under changing variables can lead to efficient and consistent methods for deriving design values for WPC and addressing serviceability needs of this new and unique material. To be able to characterize and accurately predict this strain and deflections under specific loads as the field of engineering so demands, the intrinsic nonlinearity must be expressed in a practical and applicable form. Constitutive relationships for linear viscoelastic behavior have been presented and well documented over the last several decades (Flugge, 1967; Findley, et al., 1976). However, less research has been accomplished in the development of methods for quantifying and calculating this behavior.

This research attempts to provide and illustrate methods for predicting the load vs. deformation response of wood-plastic composites. This chapter explores a constitutive relationship using the hyperbolic tangent function to describe the nonlinear stress-strain and force-displacement behavior as well as stiffness reduction under tension and flexure, all with reliable accuracy. Curve-fitting and evaluation of the function's reliability

incorporated three different WPC compositions: polypropylene (PP), coupled polypropylene (PPC), and high density polyethylene (HDPE), under the anticipation that the function in question could be used to successfully predict the constitutive behavior. Further and more intense analytical investigation was then conducted on the main composition for this research, i.e., the coupled polypropylene. Force-displacement relationships were derived using the constitutive hyperbolic law coupled with principles of elastic beam theory. Those results were compared to actual deflection curves to evaluate the accuracy of the proposed method.

The effect of the rate of applied stress, or load rate, on mechanical properties was also evaluated at six different rates using the HDPE samples. The data for these loading rates were then curve-fit using the hyperbolic tangent function to assess its prognostic ability in predicting mechanical properties at various load rates.

2.2 Materials and Manufacturing

Three compositions of wood-plastic composite were used in this study. One composition was high-density polyethylene (HDPE), composed of 35% recycled high-density polyethylene powder, 58% 60 mesh pine flour, 6% talc, and 1% lubricant. The other two were of polypropylene, one with a coupling agent and the other without. The coupled polypropylene (PPC) contained 33.9% recycled polypropylene powder, 58.8% 60 mesh pine flour, 4% talc, 1% lubricant, and 2.3% maleated coupling agent. The uncoupled polypropylene (PP) contained 34.7% recycled polypropylene powder, 60.2% 60 mesh pine flour, 4.1% talc, 1.1% lubricant, and no coupling agent. The optimum formulae for these composites maximize mechanical properties and are still easily and

cleanly extruded. Specific manufacturer and product details for HDPE and PP(C) can be found in Tables 2.1 and 2.2, respectively, and extruder temperature info is available in Table 2.3.

The formulation components were first dried and blended using a 4-ft. rotating drum and mixed in two individual batches per formulation for 5 minutes each. The dry batches were then manually fed into the 86-mm conical counter-rotating twin-screw extruder (by Cincinnati-Milacron TC86) and cut with a scroll saw into 5-6 ft. increments as the composites left the extruder. The extrusion process produced about 240 ft. of HDPE and about 380 ft. of PP(C) at about 0.4" thickness and 1.5" width. Nearly all of the HDPE and about one-third of the PP(C) samples were then planed down to 0.25" thick using a Delta planer and narrowed down to 1" wide using a 12" band saw. The planing and narrowing of the samples were conducted in several runs, cutting off equal amounts from all sides so that the original centerlines would remain true in both dimensions. The materials were then cut into individual 5" long samples so that they would fit the Instron and MTS 3-point bending fixture with a clear span of 4" (see Figure 2.1). The rest of the HDPE and an additional one-third of the PP(C) samples were cut into Type III dog-bone samples for tensile tests (see Figure 2.2). They were also planed down to ¼" thick using the Delta planer but then sent to a separate lab to be thinned to 1/8" by a milling machine so that they would later fit the dynamic mechanical analysis (DMA) 3-point bending fixture.

The HDPE and PP(C) specimens, with dimensions of 5"x1"x1/4", were used in all quasi-static flexural studies for this research following the requirements provided in ASTM D790 (2007), where $L/h \geq 16$ and $L/b \geq 4$ (In this study, $L/h = 16$ and $L/b = 4$ are

considered). Only HDPE was used to study the effects of loading rate on mechanical properties since that portion of the research occurred much earlier than the extrusion of the polypropylene. The PP(C) and HDPE specimens of Type III dog-bone shape and at 1/8" thickness were used in quasi-static tensile experiments. Only PP(C) specimens, with dimensions of 5" x 1" x ¼", were used in flexural fatigue conditioning and DMA. See Chapters 3 and 4 for manufacturing and preparation methods concerning the samples for fatigue and DMA tests. All specimens were conditioned for a minimum of 40 hours at 23±2°C and 50±5% relative humidity (RH) per ASTM D 618 (2005) before the tests were conducted. The environmental conditions at the time of testing consisted of a temperature of 22.8°C and RH of 44.6%.

2.3 Material Properties

2.3.1 Mechanical Testing Methods

Five samples of HDPE were tested quasi-statically under 3-point bending configuration in accordance with ASTM D790 (2007) using a displacement control mode at a load rate of 2.7 mm/min to obtain material properties. Additionally, five samples at rates of 5, 10, 20, 30, and 40 mm/min were tested to study the load rate effect. The tests conducted at 2.7 mm/min for static properties were performed on two separate loading frames that would both be used for later tests within the study in order to verify their comparative accuracy. A 3-point bending apparatus was fixed on both a 22-kip MTS 810 testing frame and a 2-kip Instron 4466 testing frame with a loading nose radius of 1" so as to maximize the stress concentration during the test. Figure 2.3 shows a picture of the setup used repeatedly throughout this study, the 22-kip MTS 810. The results of the

quasi-static flexural tests are provided in Tables 2.4 and 2.5 for the 2-kip Instron and 22-kip MTS, respectively, and the stress-strain diagram from the 22-kip test is shown in Figure 2.4.

Six samples of PP(C) were tested on the 2-kip Instron testing machine under 3-point bending configuration in compliance with ASTM D6109 (2005) and ASTM D790 (2007), using displacement control at the same standard load rate of 2.7 mm/min. The results of the quasi-static flexural test for both coupled and uncoupled polypropylene samples are shown in Tables 2.6 and 2.7, and the stress-strain relationships are plotted in Figures 2.7 and 2.8, respectively.

Five samples of PP(C) and six samples HDPE were tested on the 2-kip Instron testing machine under tension-tension configuration, following ASTM D638 (2008), using the displacement control mode at the same load rate of 2.7 mm/min. The tension clamps were pinned to the load cell and base and fastened using a similar 2-nut system so that the specimens were securely clamped in to avoid any slippage. The tension setup on the Instron is displayed in Figure 2.6. The results of the quasi-static tension tests for both coupled and uncoupled polypropylene samples are provided in Tables 2.8 and 2.9, and the stress-strain relationships are plotted in Figures 2.9 and 2.10, respectively. The results of the quasi-static tension tests for HDPE samples are provided in Table 2.10, and the stress-strain curve is displayed in Figure 2.5.

2.3.2 Mechanical Properties – Results and Discussion

In general, the modulus of elasticity (MOE) and modulus of rupture (MOR) obtained from samples in both quasi-static flexure and tension tests for all formulae were

agreeable with each other and with other research results. Stress-strain relationships in all loading modes and for all compositions were observed to be rather nonlinear with the linear region of deformation accounting for less than about 25% of the total deformation recorded before rupture. Obvious evidence of nonlinearity occurred in all stress-strain relationships except for PPC in both loading modes (i.e., tension and flexure), but namely in flexure, which appears more gradual and more linear until sudden brittle failure at about $\varepsilon = 0.015\%$. Both PP and HDPE (without coupling agents) shared the tensile stress-strain plots that appeared nearly identical by inspection to the generic hyperbolic tangent curve with more of a distinct separation between elastic and plastic deformation. The same two compositions looked similar to one another in flexure as well but did not resemble the hyperbolic tangent curve as closely with no real distinguished boundary between elastic and plastic deformation. Coupled PP exhibited more linearity than HDPE or its uncoupled PP counterpart, in agreement with prior findings. As suggested by numerous other papers, the addition of a coupling agent enhances the tensile or flexural modulus as well as the ultimate stress due to the improved adhesion at the wood-polymer interface, which completely changes the deformation mechanism and hence the material behavior (Correa, et al., 2007; Danyadi, et al., 2007).

2.3.2a Flexure

Flexural properties for PP(C) were obtained for the purpose of establishing a benchmark for stress ratios to be used later in fatigue analysis and to study the accuracy of the hyperbolic tangent function in characterizing the nonlinear stress-strain behavior of WPC. The composition containing the coupling agent, referred to as PPC, was stiffer and

stronger as expected and maintained consistency with other authors' findings (Yang, et al., 2008; Slaughter, 2004). Failure was more sudden and brittle compared to both HDPE and uncoupled PP, verifying that a lower level of material compliance be associated with the addition of the coupling agent. MOR was calculated using the ultimate load at failure, the sample dimensions, and by employing the equations of Appendix A.2. Due to the apparent nonlinearity of the stress-strain relationship, the bending MOE was calculated by taking the slope of the stress-strain curve between values of 10% and 20% of MOR in an attempt to capture the largest section of linear data available. This region of the curve gave the best representation of MOE as it didn't include initial settling effects from the test apparatus and it appeared to incorporate only linear data. An example of a spreadsheet used to reduce raw flexural data is located in Section A.3 of the Appendix, which represents the method used for all data reduction. The flexural properties of either mixture can be found in Tables 2.5 – 2.7. All COV values were under 10%, and MOE appeared to be especially reliable, although a bit higher than some other results (Yang, et al., 2008).

The flexural properties of HDPE were obtained for the purpose of studying the effect of load rate on mechanical behavior and to observe the reliability of the hyperbolic tangent function in predicting the nonlinear stress-strain relationship. Both the bending MOE and MOR were calculated using the same procedure as the polypropylene wood-plastics outlined in Appendix A. Average MOE and MOR using the 22-kip MTS frame at the standard load rate, from Table 2.4, were 570,940 psi and 3,703 psi with coefficients of variation (COV) of 6.83% and 4.17%, respectively. While on the 2-kip Instron testing frame, MOE and MOR from Table 2.5 were 524,000 psi and 3,767 psi with COV of

6.35% and 5.03%, respectively. One can observe that the difference in the properties obtained from both machines was nearly negligible, especially for MOR, so the data from the 22-kip test frame was selected both by preference and considering that the 22-kip frame would be utilized later in the research for flexural fatigue.

2.3.2b Tension

Tensile properties of PP(C) were obtained to study the fit of the hyperbolic-tangent function in characterizing the tensile stress-strain relationship and to compare its utility with the fitting of flexural data. MOE and MOR were calculated using ultimate load at failure, cross-sectional dimensions, and by employing the equations of Appendix A.2. Refer to Appendix A.4 for an example of the spreadsheet used to reduce raw tensile data. The results for MOE and MOR were agreeable with other studies (Slaughter, 2005; Correa, et al., 2007; Bateman, et al., 2008). The test results of both PP and PPC can be found in Tables 2.8 and 2.9. The variation of properties from sample to sample was slightly higher than it was in flexure for the same mixtures. This increased error was most likely due to the relatively small cross-sectional dimensions of the Type III dog-bone coupons that were used in order to control and isolate stress concentration at the grips, ensuring that rupture would occur very close to the mid-span of the samples.

Tensile properties of HDPE were obtained solely to include in the evaluation of the hyperbolic-tangent function in predicting the tensile stress-strain relationship and to compare results to that of PP(C) in tension. MOE and MOR were both significantly lower for HDPE in tension than they were for the two polypropylene mixtures. The HDPE material compliance and the stress-strain diagram in Figure 2.5 show that it is

slightly more ductile and deformable than PP and much softer and weaker than PPC, which is also consistent with other recent findings (Bateman, et al., 2008). Also, the HDPE tensile strength was the lowest of all three mixtures at almost half the ultimate strength of PPC.

2.3.3 Load rate Effect

As previously mentioned, the need and applications for wood-plastic composites are rapidly increasing as a natural and efficient alternative to wood and metal, especially in waterfront applications. The dependence of mechanical properties on outside variables like temperature and time-dependent scenarios is being heavily researched today (Schildmeyer, 2006). Creep behavior of WPC has been shown to depend on the loading mode and magnitude and can indeed be characterized by various models such as Findley's power law, but almost every model carries the restriction that it cannot describe nonlinear tertiary creep, which is the region just before rupture occurs (Kobbe, 2005). Therefore, in understanding time-dependent behavior of this relatively new material, it is of high interest to study the rate of applied load and its effect on stiffness and compliance, strain at failure and ultimate strength. Knowing how load rate affects material properties can help us as engineers evaluate probable failure mechanisms and decide how to incorporate that information to design and industry.

Table 2.11 shows the values of MOE and MOR and Table 2.12 provides the stress and strain values at failure according to six different load rates: 2.7, 5, 10, 20, 30, and 40 mm/min. The range of load rate is chosen based on the capability of testing machine. The stress-strain curves show slightly decreasing nonlinearity with increased rate but are

all shaped similar to the base curve in Figure 2.4 so it would be unnecessary to display them all here. However, for reference the curves for all load rates are located in Appendix B.2, Figures B.2.1 – B.2.6. For convenience, Figure 2.11 shows a representative average curve chosen at each load rate to make it easier to visualize the contrast in stress-strain behavior.

There appears to be a fairly solid trend in that MOE and MOR both increased as a function of load rate and failure strain decreased. MOR increased by 17.4% between the standard rate of 2.7 mm/min up to 30 mm/min and ultimate strain decreased by precisely the same amount, whereas MOE rose by 13.1%. As expected, the polymer-based WPC are strain-rate dependent, and the higher the strain rate (load rate), the higher MOE and MOR. It is well known that the mechanical properties of polymer composites depend primarily on the interaction between the polymer matrix and reinforcing filler, in this case the wood flour (Bateman, et al., 2008). The deformation mechanisms in most unmodified WPC, that is those without coupling agents, are matrix brittle fracture and fiber debonding followed by fiber pullout at intermediate to higher stresses. Debonding and matrix cavitation on the tensile surface of the flexural member most likely causes observed plasticity (although minimal) in the lower load rate tests (Hristov, et al., 2004). The apparent increase in mechanical properties with less strain deformation at elevated load rates is probably due to the failure mechanism of fiber pullout at advanced stresses caused by the sudden simulated "impact" load. Matrix cavitation would require proper time to occur and would result in larger strains, which holds consistent with this study.

It's also important to note that the COV between the properties of the five samples also increased with load rate. This result follows intuition for two reasons

Firstly, the sample collection rates were kept constant throughout the study so when a specimen took a tenth of the time to fail at a higher load rate, the LabView file naturally recorded a tenth of the data points. Since MOE was always calculated based off of the same stress limits in the stress-strain slope, it became more scattered at extreme load rates as the value was taken from fewer data points. Second, the material was forced to react at a quicker rate as the load was applied faster and faster. When the load rate reaches a certain level, the response of the material should be considered almost purely dynamic rather than quasi-static. Higher load rates, such as 40 mm/min and greater in this study, create impact loads that cause the WPC to behave differently. Thus, MOR seems to be an unreliable parameter at rates higher than around 30 mm/min. Therefore, the 40 mm/min data was omitted from Figures 2.11 – 2.13 and the analysis of the load rate trend, but noting that the data is available in Table 2.11.

Using a linear regression technique, mechanical properties for this blend of WPC may be approximated by the below curve equations. The log-scale curves are shown in Figures 2.12 and 2.13 along with regression equations and coefficients of correlation (COV). For reference, the standard scale curves are presented in Appendix B.4. The bending MOE (E_b) and MOR (σ_{ult}) in relation to the load rate (dD/dt) are given as (be aware that they are only applicable to the tested load rate range, i.e., dD/dt = 2.7 mm/min to 30 mm/min).

$$\log(E_b) = 0.0577\log(dD/dt) + 5.724 \qquad (\text{Coefficient of Correlation } R^2 = 0.879)$$

for Modulus of Elasticity (2.1)

$$\log(\sigma_{ult}) = 0.678\log(dD/dt) + 3.5496 \quad \text{(Coefficient of Correlation } R^2 = 0.861\text{)}$$

for Modulus of Rupture (2.2)

It is evident that the rate of applied load does have a significant effect on the mechanical properties of HDPE in flexure. Results obtained at the standard load rate are more reliable than those at higher load rates as they are derived from a quasi-static load rather than an abruptly applied "dynamic" load and it is certainly best to conservatively regard those results as more accurate and conclusive when determining design values of HDPE. However, note that it does not follow true to conclude that as load rate decreases mechanical properties become more reliable. If a load is applied too slowly to almost any WPC, then flexural creep could become a notable player. Findley's Power Law has been shown to accurately model creep strains at stress ratios lower than 60% of ultimate stress but to then deviate from there, which means that tertiary creep and/or creep rupture could drastically affect when and how a member fails (Kobbe, 2005; Findley, et al., 1976). Mechanical properties, especially MOR, could then be deemed defective due to uncertainty in the actual failure mechanism. It appears by inspection that the smaller load rates exhibit a smaller linear elastic range, suggesting that very small rates (less than 1 mm/min) would likely display even further nonlinearity. An entirely nonlinear stress-strain curve would imply that the material began transitioning into the nonlinear viscoelastic range at a smaller strain due to creep effects, making mechanical properties difficult to evaluate. Such a phenomenon may be directly related to when and how quickly micro-cracks form or to the bond at short-fiber interfaces, suggesting that the degradation in material properties may be quantitatively and physically evaluated using a

one-dimensional continuum damage mechanics (CDM) model as introduced in Chapter 5.

2.4 Hyperbolic Tangent Constitutive Relationship

After observing the nonlinear behavior of WPC under bending and tension, a hyperbolic tangent function was used to empirically fit all the stress-strain data, including the curves obtained at varied load rates. The function has been previously used to fit nonlinear shear stress-strain behavior of polymer matrix composites (PMC) and load-deflection data of WPC with fair success (Lockyear, 1999). Kobbe (2005) utilized the hyperbolic tangent function to predict tensile elongation in a wood-polypropylene composite with an average error of 2% and compressive loads with an average error of 6%.

While the study in this project maintains the same basic principles as previous studies, the specific objectives are as follows:

1) Successfully estimate failure strength based on initial modulus and evaluate reduced stiffness at various design strains.
2) Derive constitutive P-Δ relationships using principles of work and energy for axial and pure bending cases. These curves are intended to illustrate useful and applicable methods of predicting service deflections and/or beam curvatures under loading, based on the hyperbolic tangent function of stress-strain fitted with the experimental data.

2.4.1 Stress-Strain Constitutive Law

The flexural stress is represented as a hyperbolic tangent function of the strain as depicted in Figure 2.14. It is described using the following equation

$$\sigma(\varepsilon) = C_2 \tanh\left(\frac{C_1}{C_2}\varepsilon\right) \tag{2.3}$$

The derivative, or slope, of that curve is given as

$$\frac{d\sigma}{d\varepsilon} = (C_1)\sec h^2\left(\frac{C_1\varepsilon}{C_2}\right) \tag{2.4}$$

For the intended interest, C_1 represents the initial flexural modulus E_b, obtained experimentally, and C_2 is the predicted flexural strength based on this procedure. The objective is to employ the Chi-Squared Goodness-of-Fit function, shown below in equation (2.5), to numerically calculate C_2 for each sample in each formulation and loading mode.

$$X^2 = \sum_{i=1}^{k} \frac{(\text{observed} - \text{expected})^2}{\text{expected}} \tag{2.5}$$

The "observed" represents the stresses obtained from the actual quasi-static flexural tests. The "expected" are the theoretical stresses that lay on the generic hyperbolic tangent curve. The principle behind the Chi-Squared function is that the "goodness-of-fit" of the observed data to the expected data increases with a decreasing value of X^2, which is obvious since X^2 is directly proportional to the square of the difference between observed and expected stresses. Therefore, by substituting equation (2.3) into (2.5) for the expected stress, X^2 becomes a function of the only unknown, C_2. This is shown below in equation (2.6).

$$X^2 = \sum_{i=1}^{k} \frac{\left(\sigma(\varepsilon) - C_2 \tanh\left(\frac{C_1}{C_2}\varepsilon\right)\right)^2}{C_2 \tanh\left(\frac{C_1}{C_2}\varepsilon\right)} \tag{2.6}$$

C_2 was calculated numerically using a short program written in Visual Basic by Microsoft. The numerical method works as follows: The summation in the Chi-Squared function is taken from i = 1 to i = n for every corresponding pair of stresses and strains. A logical range of possible values for C_2, say 1,000 to 20,000, was chosen for a loop along with an appropriate increment "i" to use as a step. For a given step, a possible C_2 yielded a Chi-Squared sum and was compared to the sum that resulted from the previous step. If the new sum was smaller than the old sum, then the value was stored as a local minimum. Every step past i = 1 compares the Chi-Squared sums at i and i – 1, along with the value currently in storage and then replaces accordingly. Once the loop is finished running, the absolute minimum sits in the storage cell and is designated as C_2. Refer to Appendix C for raw data and an example of the Visual Basic code used for this procedure.

Once C2 and C1 were established, hyperbolic stress was calculated for a vector of design strains and compared and plotted against the measured stresses at those design strains. Tables 2.19 – 2.21 shows this data and Figures 2.15 – 2.20 show the curves. Measured stress is displayed in blue and predicted stress in red.

2.4.2 P-Δ: Axial Case

To develop the axial load vs. elongation (P-Δ) relationship of a WPC structural member under an axial tensile load based on a constitutive function such as the

hyperbolic tangent function of the stress-strain relation, the principles of work and energy are considered to account for behavioral change along the volume of the samples. Force and displacement can be related to stress and strain by way of simple mathematics, but only under specific and often assumed conditions. For the axial case, the following mathematical procedure was used to develop P-Δ. The strain energy through the length of the member under stress is the same as the work accomplished by the axial force. The work (W) and strain energy (U) in an axial member can be expressed as

$$U = \int \left(\int_0^{\varepsilon} \sigma(\varepsilon) d\varepsilon \right) dV = \int_0^{L} \left(\int_0^{\varepsilon} \sigma(\varepsilon) d\varepsilon \right) A dx \tag{2.7}$$

$$W = \int_0^{\Delta} P(\Delta) d\Delta = \int_0^{L} P(\Delta) \varepsilon dx \tag{2.8}$$

Equating work and strain energy in terms of unit strain, integrating the like parameter x on both sides and then inserting the hyperbolic stress-strain relation, produces the following:

$$F(\varepsilon) = A \int_0^{\varepsilon} \frac{C_2}{\varepsilon} \tanh\left(\frac{C_1 \varepsilon}{C_2} \right) d\varepsilon \tag{2.9}$$

The hyperbolic tangent function can be approximated as a series expansion containing polynomials that show the natural decay of the hyperbolic function. For the purposes of this study, the first 2 terms of the following expression will be used for substitution:

$$\tanh(z) = z - \frac{1}{3} z^3 + \frac{2}{15} z^5 - \frac{17}{315} z^7 + \cdots \tag{2.10}$$

Substituting the series expansion and integrating with respect to strain yields:

$$F(\varepsilon) = C_1 A \varepsilon \left[1 - \frac{C_1{}^2 \varepsilon^2}{9 C_2{}^2} \right] + C \tag{2.11}$$

Unit strain is equivalent to extension over the extensometer length, or:

$$\varepsilon = \frac{\Delta}{L} \tag{2.12}$$

Substituting this for strain and b (width) x d (thickness) for A (the cross-section area) produces the final force-displacement law where L is the extensometer length, b is the sample width, and d is the sample depth as:

$$F(\Delta) = \frac{C_1 bd\Delta}{L}\left(1 - \frac{C_1{}^2\Delta^2}{9C_2{}^2L^2}\right) \tag{2.13}$$

Figure 2.21 displays P-Δ as it was measured experimentally and as it was predicted using the constitutive equation (2.13) based on the hyperbolic tangent stress-strain function given in equation (2.3). Table 2.22 compares the average actual and model-predicted extensions at failure.

2.4.3 P-Δ: Pure Bending Case

The pure bending case is more complex to derive because the stress and strain are dependent on moment, which changes along the length of the sample. However, the bending moment M(x) is known, and the stress-strain relationship is assumed as the hyperbolic tangent constitutive relationship. Therefore, the following mathematical and numerical procedure was used to characterize the transverse load vs. displacement relation (P-Δ) for a given cross-section at any point along the beam. P-Δ at mid-span was then numerically calculated for a vector of forces and compared to actual measured deflections, similar to the axial case. Strain energy through the length of the member under stress is the same as the work accomplished by axial force, meaning virtual work is

conserved and the total rate at which it is expended is always zero. We can express total virtual work as follows:

$$\delta\Pi = \int_V \int \sigma_{xx}\delta\varepsilon_{xx}dV - \int F\langle x - L/2\rangle^{-1}\delta\Delta dx = 0 \tag{2.14}$$

And strain can be related to deflection along x using curvature as follows:

$$\varepsilon_{xx} = y\kappa = y\left(\frac{\partial^2\Delta}{\partial x^2}\right) \tag{2.15}$$

where y is the beam depth and κ is beam curvature. Substituting equations 2.3, 2.10, and 2.15 into equation 2.15 and then rearranging and integrating yields the governing expression observed below:

$$C_1\left(\frac{\partial^2\Delta}{\partial x^2}\right)\frac{h^3}{12} - \frac{{C_1}^3 h^5}{240{C_2}^2}\left(\frac{\partial^2\Delta}{\partial x^2}\right)^3 - F\langle x - L/2\rangle^{-1} + \frac{Fx}{2} = 0 \tag{2.16}$$

This expression is especially interesting as it seems to be comprised of distinct regions of linear elasticity and nonlinear decay in curvature and hence deflection. It can be reduced and represented as a depressed cubic for curvature in the following form:

$$-A\kappa^3 + B\kappa + CFx = 0 \tag{2.18}$$

where A, B, and C are scalar constants that depend on sample dimensions and the hyperbolic constants obtained in Section 2.4.1. The deflection can be found by solving the cubic in equation (2.18) for curvature and then double integrating to obtain deflection. However, deflection cannot be represented in terms of x symbolically because the curvature function is too difficult to integrate, so Matlab was used to numerically calculate deflections for a given force and location. The code, found and commented in Appendix C, is comprised of a series of functions written inside a short loop that pre-selects x as L/2 (e.g., a beam under a mid-span load) and incrementally inputs forces,

thereafter generating a vector for Δ and plotting it against those corresponding forces. See Appendix C for further detail. Figure 2.22 displays P-Δ at beam mid span as it was measured experimentally and as it was predicted using the constitutive equation (2.16) and numerical analysis. Table 2.22 compares the average actual and model-predicted deflections at failure.

2.4.4 Results and Discussion

Comparison of average values of C_2 to average test values of MOR can enable assessment of the validity of the hyperbolic tangent function as a means of predicting the material performance. By developing an accurate method to measure reduced stiffness, researchers and designers may be able to better understand WPC nonlinearityity and use that information to predict loss of stiffness. For illustrative purposes, Figure 2.23 shows the hyperbolic secant function of equation 2.4 applied to strains from 0 to a representative ultimate, about 0.017.

The numerical results and comparison between MOR and C_2 for the standard load rate of 2.7 mm/min for all six test scenarios can be found in Tables 2.13 – 2.16. At the standard load rate, the hyperbolic tangent function appears to accurately describe stress-strain nonlinearity, overall. The data in Tables 2.19 – 2.21 suggests that if material properties are known or can be estimated, nonlinear behavior can be predicted with tolerances ranging from 2 – 6%. This notion, along with the low variances between MOR and C2 provide quite convincing evidence that the function can be used to successfully predict the behavior in all six test scenarios, although it does tend to over predict the ultimate strength in most cases. On average, MOR was overshot by only

5.11% for HDPE in flexure and by just 0.14% for PP in flexure, as seen in Tables 2.13 and 2.14. Tables 2.15 and 2.16 show that all compositions yielded good results in tension. The function over calculated MOR by 2.40% for PPC and under calculated MOR by 4.30% for PP, both within 5% error. All COV in each test scenario for C_2 and MOR were practical and comparable to each other, with the highest variation appearing in PP tensile data at 14.29% for C_2 and 12.34% for MOR. The rest of the observed variations among C_2 and MOR at the standard loading were under 10%, suggesting strong dependability of the produced averages and hence a dependable correlation between experimental and predicted material properties.

It is reasonable to presume from this data that the hyperbolic tangent function is a reliable predictor of stress-strain behavior in wood-plastic composites. This conclusion was based mainly around two reasons. First, assuming that an acceptable error between C_2 and actual MOR of 10% was considered, five of the six test scenarios yielded accurate results and errors under 6%. Second, PPC under flexure was the only test scenario that challenged the consistency of the hyperbolic tangent function in terms of variance. In comparison to the other test scenarios, C_2 seemed to exceed actual MOR by leaps and bounds but even 21% is not that dramatic of an error for a non-homogeneous material. This disparity also follows logic as the coupling agent used in this wood-polypropylene blend caused an evident improvement in stress-strain linearity, especially under flexure as seen in Figure 2.7. With a longer and steeper linear portion of the total curve and a larger measured MOE, the PPC data fitted by the hyperbolic tangent function will always predict a higher ultimate strength than the material may actually provide. Further

investigation involving more samples and a large variety of compositions is suggested to assess the function's validity, but the results of this study are certainly supportive.

The hyperbolic tangent's validity was also tested under the load rates described in Section 2.3.3 for only the HDPE specimens. Table 2.17 shows C_2 for every sample at each load rate, along with the average and COV. More significantly, average C_2 and average experimental MOR for each load rate are compared in Table 2.18. The function proved less reliable in characterizing stress-strain behavior at higher load rates, as expected and explained in the previous section. While the standard load rate of 2.7 mm/min yielded good results as aforementioned, the error is more significant at higher load rates with almost 20% at just 10 mm/min and over 10% at greater rates. The relationship between C_2 and actual MOR is not proportional or linear by any means, but the data suggests the only statistic that is important. That is the hyperbolic tangent function should not be used to fit flexural data obtained at load rates higher than around 5 mm/min, or 0.1969 in/min. The most obvious explanation for the inaccuracy of the function at excessive load rates is similar to the stiffening and strengthening effect of the coupling agent on data of nonlinearity. The increased load rate has been shown to have a dynamic "hardening" effect on the compliance of the material and induced less nonlinearity in the material. An increased MOE, a.k.a., the C_1 coefficient in the function, raises X^2 at every point on the stress-strain curve. In order to minimize the sum of those values, the Visual Basic program produces a higher C_2 than is really indicative of the material's ultimate strength.

The force-displacement relationships in equations (2.14) and (2.17), which were derived in sections 2.4.2 and 2.4.3, appeared to be quite successful in modeling the

experimental relationships, specifically the numerical method for the bending case. The derived relationships seem to mimic the test samples closely. Figures 2.21 and 2.22 show the model curves in black with the curve fitted cubic equation displayed and Table 2.22 shows the measured and predicted failure deflections for both cases. The tension model underestimates by 21%, but the numerical program for bending does so by just over 7%, a logical finding considering the bending procedure uses a more exact solution. The upscale of the coupon test data of hyperbolic tangent function of stress vs. strain relation to the behavior of a structural component is thus demonstrated in this study. More test data should be considered in the future study, and the experimental measured behavior of the structural components should be used to correlate the prediction model based on the coupon test data.

The concepts that this chapter has explored and established could prove very useful in design with some further investigation and fine-tuning. If material properties and geometry for a composite structural member such as a WPC stringer are known or can be measured, then strain and deflections can be predicted under given loads. In theory, if a beam has a certain deflection criterion, say L/180 or L/360, then accurately predicting the structural member deflection using coupon measured data can actively aid design. Since WPC display high nonlinear stress-strain behavior at the coupon level as shown in this study, the WPC structural components (e.g., larger members or thin-walled composite sections) are expected to exhibit nonlinear P-Δ behavior as well. The preliminary results shown in this section indicate that the stress-strain curve represented by the hyperbolic tangent function and fitted from the coupon measurement can be used

in equations (2.13) and (2.16) to predict the nonlinear structural component behavior and can thus be implemented in design practice.

2.5 Concluding Remarks

In this chapter, quasi-static mechanical properties of coupled and uncoupled polypropylene (PP and PPC) and high density polyethylene (HDPE) were evaluated in tension and flexure. PP and HDPE in flexure were very comparable in all aspects, including physical characteristics such as color, texture, and the ductile splitting that occurred at failure. PPC exhibited better material properties than PP and a more brittle snapping at rupture due to the improved interface adhesion by the coupling agent. It had a 20% higher bending modulus and 52% greater ultimate strength than its uncoupled counterpart, making it the optimum formulation for structural performance. Consistent results were achieved for all mixtures loaded in tension. Again, PPC performed the best with nearly double the yield strength as HDPE.

It was evident in this study that an increased rate of applied stress improved mechanical properties, but only at the expense of reliability and ambiguity in the true failure mechanism. Properties were affected by uncontrollable variables in the study, such as sample collection rate and the effect of simulated dynamic loads at higher rates. For testing purposes, the load rates between 1 and 5 mm/min would likely achieve the most reliable results for field application.

The work in this chapter verified that the hyperbolic tangent function can be used to fit tensile and flexural stress-strain data and demonstrated great potential for load-deflection analysis of structural members under axial or bending loading. The function

can fairly predict modulus of rupture for all test scenarios under a given data set. The relationship can be used to predict strains as a function of stress at a wide range of points on the modeled curves with excellent precision, but tends to slightly underestimate initial stiffness in tension and flexure. The P-Δ laws for tension and bending can numerically calculate member elongation and transverse displacements at any point along a beam under an applied loading. The only prominent limitation of the function proved to be in fitting data at high load rates. Structural members to be used in the field that may be susceptible to controlling or critical impact loads should not be designed to resist those loads using these methods.

The usefulness of hyperbolic tangent fitting of nonlinear stress-strain constitutive relation and the upscale of the coupon test data to predict the nonlinear behavior of structural components are illustrated in this study. It is useful in design that the nonlinear P-Δ behavior of the structural members can be predicted using the nonlinear tangent function of stress-strain obtained at coupon level, thus eliminating the necessity of the full-scale structural tests and aiding engineering design of WPC members.

2.6 References

ASTM D3878-07. "Standard Terminology for Composite Materials." American Society for Testing and Materials.

ASTM D618-05. "Standard Practice for Conditioning Plastics for Testing." American Society for Testing and Materials.

ASTM D638-08. "Standard Test Methods for Tensile Properties of Plastics." American Society for Testing and Materials.

ASTM D6109-05. "Standard Test Methods for Flexural Properties of Unreinforced and Reinforced Plastic Lumber." American Society for Testing and Materials.

ASTM D790-07. "Standard Test Methods for Flexural Properties of Unreinforced and Reinforced and Electric Insulating Materials." American Society for Testing and Materials.

Bateman, S., Gotama, J., Wu, D., and Yuan, Q., "Wood Fiber Reinforced Polyethylene and Polypropylene Composites with High Modulus and Impact Strength." Journal of Thermoplastic Composite Materials, Vol. 21 pp. 195-208, 2008.

Correa, C.A., Hage Jr, E., "Role of Maleated Coupling Agents on the Interface Adhesion of Polypropylene – Wood Composites." Journal of Thermoplastic Composites, Vol. 20, pp. 323-339, 2007.

Danyadi, L., Moczo, J., Pukanszky, B., Renner, K., "Wood Flour Filled Polypropylene Composites: Interfacial Adhesion and Micromechanical Deformations." Journal of Polymer Engineering and Science, Vol. XX, pp. 1246-1255.

Findley, W.N., Lai, J.S., and Onaran, K., "Creep and Relaxation of Nonlinear Viscoelastic Materials." North-Holland Publishing Company, New York, NY, 1976.

Flugge, W., "Viscoelasticity." Blaisdell, Waltham, MA, 1967.

Hristov, V.N., Lach, R., Michler, G.H., Vasileva, S.T., "Deformation Mechanisms and Mechanical Properties of Modified Polypropylene/Wood Fiber Composites." Polymer Composites, Vol. 25, pp. 521-526, 2004.

Kobbe, R.G., "Creep Behavior of Wood-Polypropylene Composites." Master Thesis, Washington State University, June 2005.

Lockyear, S.A., "Mechanical Analysis of Transversely Loaded Wood/Plastic Sections." Master Thesis, Washington State University, December 1999.

Murphy, J.F., “Characterization of Nonlinear Materials.” Unpublished Paper. USDA Forest Products Laboratory Technical Note, Madison, WI.

Schildmeyer, A.J., “Temperature and Time-Dependent Behaviors of a Wood-Polypropylene Composite.” Master Thesis, Washington State University, August 2005.

Slaughter, A.E., "Design and Fatigue of a Structural Wood-Plastic Composite." Master Thesis, Washington State University, August 2004.

Yang, H-S, Qiao, P., and Wolcott, M.P., “Flexural Fatigue and Reliability Analysis of Wood Flour/High Density Polyethylene Composites,” Journal of Reinforced Plastics and Composites, in press, 2008.

2.7 Tables

Table 2.1. Product details and quantities for extruded HDPE.

Material	Quantities	Manufacturer	Product
	Uncoupled		
HDPE	35%	Equistar Petrothene	LB 0100-00
60 Mesh Pine Flour	58%	American Wood Fibers	#6020
Talc	6%	Luzenac	Nicron 403
Lubricant	1%	Honeywell	OP100

Table 2.2. Product details and quantities for extruded PP(C).

Material	Quantities	Manufacturer	Product
	Uncoupled (Coupled)		
Polypropylene	34.7% (33.9%)	Equistar Petrothene	LB 0100-00
60 Mesh Pine Flour	60.2% (58.8%)	American Wood Fibers	#6020
Talc	4.1% (4%)	Luzenac	Nicron 403
Lubricant	1% (1%)	Honeywell	OP100
Coupling Agent	0% (2.3%)	Honeywell	950P

Table 2.3. Extruder temperature profile for all materials produced.

		Temperature (°F)
Barrel Zone	1	325
	2	325
	3	325
	4	325
Screw		325
Die Zone	1	340
	2	340
	3	340

Table 2.4. HDPE quasi-static flexural properties (MTS 22-kip frame).

Sample	MOE (psi)	MOE (GPa)	MOR (psi)	MOR (GPa)
1	610,860	4.21	3,822	0.0264
2	595,228	4.10	3,694	0.0255
3	522,724	3.60	3,660	0.0252
4	589,770	4.07	3,867	0.0267
5	536,118	3.70	3,474	0.0240
Average	**570,940**	**3.94**	**3,703**	**0.0255**
COV (%)	6.83	6.83	4.17	4.17

Table 2.5. HDPE quasi-static flexural properties (Instron 2-kip frame).

Sample	MOE (psi)	MOE (GPa)	MOR (psi)	MOR (GPa)
1	549,310	3.79	4,077	0.0281
2	533,900	3.68	3,557	0.0245
3	475,301	3.28	3,736	0.0258
4	555,600	3.83	3,748	0.0258
5	506,092	3.49	3,719	0.0256
Average	**524,041**	**3.61**	**3,768**	**0.0260**
COV (%)	6.35	6.35	5.03	5.03

Table 2.6. PP quasi-static flexural properties.

Sample	MOE (psi)	MOE (GPa)	MOR (psi)	MOR (GPa)
1	542,926	3.74	4,333	0.0299
2	532,607	3.67	4,935	0.0340
3	524,232	3.61	4,023	0.0277
4	503,628	3.47	3,847	0.0265
5	529,271	3.65	4,696	0.0324
6	557,502	3.84	4,073	0.0281
Average	**531,694**	**3.67**	**4,318**	**0.0298**
COV (%)	3.41	3.41	9.79	9.79

Table 2.7. PPC quasi-static flexural properties.

Sample	MOE (psi)	MOE (GPa)	MOR (psi)	MOR (GPa)
1	649,932	4.48	6,362	0.0439
2	662,411	4.57	7,057	0.0487
3	645,035	4.45	6,778	0.0467
4	610,750	4.21	6,476	0.0447
5	633,783	4.37	6,994	0.0482
6	614,440	4.24	5,744	0.0396
Average	**636,058**	**4.39**	**6,569**	**0.0453**
COV (%)	3.21	3.21	7.44	7.44

Table 2.8. PP quasi-static tensile properties.

Sample	MOE (psi)	MOE (GPa)	MOR (psi)	MOR (GPa)
1	741,239	5.11	1,815	0.0125
2	668,980	4.61	1,747	0.0120
3	722,764	4.98	1,916	0.0132
4	805,233	5.55	2,365	0.0163
5	762,351	5.26	1,937	0.0134
Average	**740,113**	**5.10**	**1,956**	**0.0135**
COV (%)	6.79	6.79	12.34	12.34

Table 2.9. PPC quasi-static tensile properties.

Sample	MOE (psi)	MOE (GPa)	MOR (psi)	MOR (GPa)
1	834,444	5.75	2,810	0.0194
2	777,474	5.36	2,656	0.0183
3	868,937	5.99	3,139	0.0216
4	891,694	6.15	3,204	0.0221
5	882,948	6.09	3,237	0.0223
Average	**851,100**	**5.87**	**3,009**	**0.0207**
COV (%)	5.47	5.47	8.66	8.66

Table 2.10. HDPE quasi-static tensile properties.

Sample	MOE (psi)	MOE (GPa)	MOR (psi)	MOR (GPa)
1	776,030	5.35	1,692	0.0117
2	710,358	4.90	1,594	0.0109
3	729,022	5.03	1,639	0.0113
4	707,275	4.88	1,634	0.0113
5	688,802	4.75	1,668	0.0115
6	729,826	5.03	1,694	0.0117
Average	**723,552**	**4.99**	**1,654**	**0.0114**
COV (%)	4.13	4.13	2.33	2.33

Table 2.11. Average mechanical properties of HDPE in flexure at all load rates.

dD/dt (mm/min)	MOE (psi)	MOE (GPa)	COV (%)	MOR (psi)	MOR (GPa)	COV (%)
2.2	570,940	3.94	6.83	3,703	0.0255	4.17
5	575,478	3.97	2.24	3,980	0.0274	3.46
10	586,815	4.05	5.15	4,310	0.0297	3.01
20	642,814	4.43	4.65	4,361	0.0301	5.78
30	645,712	4.45	10.38	4,347	0.0300	7.96
40	581,471	4.01	25.09	4,140	0.0285	16.41

Table 2.12. Stress and strain at failure of HDPE in flexure at all load rates.

dD/dt (mm/min)	σ_u (psi)	COV (%)	ε_u (in/in)	COV (%)
2.7	3,703	4.17	0.01357	7.78
5	3,980	3.46	0.01281	4.01
10	4,310	3.01	0.01225	7.38
20	4,361	5.78	0.01181	4.78
30	4,347	7.96	0.01122	11.78
40	4,140	16.41	0.01268	12.06

Table 2.13. C_2 and MOR for HDPE in flexure.

Sample #	1	2	3	4	5	**Average**	COV (%)
C_2	3,986	3,880	3,794	4,068	3,734	**3,892**	3.51
MOR (psi)	3,822	3,694	3,660	3,867	3,474	**3,703**	4.17
% Difference	4.30	5.04	3.67	5.20	7.50	**5.11**	--

Table 2.14. C_2 and MOR for PP(C) in flexure.

PP Sample #	1	2	3	4	5	6	**Average**	COV (%)
C_2	4,552	4,821	4,033	3,772	4,691	4,074	**4,324**	9.73
MOR	4,333	4,935	4,023	3,847	4,696	4,073	**4,318**	9.79
% Difference	5.06	2.32	0.25	1.94	0.10	0.03	**0.14**	--
PPC Sample #	1	2	3	4	5	6	**Average**	COV (%)
C_2	7,715	7,761	8,125	8,048	7,741	8,423	**7,969**	3.53
MOR	6,362	7,057	6,778	6,476	6,994	5,744	**6,569**	7.44
% Difference	21.26	9.98	19.87	24.27	10.68	46.65	**21.32**	--

Table 2.15. C_2 and MOR for PP(C) in tension.

PP Sample #	1	2	3	4	5	**Average**	COV (%)
C_2	1,722	1,637	1,867	2,324	1,809	**1,872**	14.29
MOR (psi)	1,815	1,747	1,916	2,365	1,937	**1,956**	12.34
% Difference	5.11	6.29	2.55	1.73	6.60	**4.30**	--
PPC Sample #	1	2	3	4	5	**Average**	COV (%)
C_2	2,827	2,752	3,149	3,238	3,441	**3,081**	9.34
MOR (psi)	2,810	2,656	3,139	3,204	3,237	**3,009**	8.66
% Difference	0.60	3.63	0.30	1.05	6.30	**2.40**	--

Table 2.16. C_2 and MOR for HDPE in tension.

Sample #	1	2	3	4	5	6	**Average**	COV (%)
C_2	1621	1554	1552	1592	1646	1520	**1,593**	2.59
MOR (psi)	1,692	1,594	1,639	1,634	1,668	1,694	**1,645**	2.25
% Error	4.22	2.53	5.28	2.58	1.30	10.26	**3.19**	--

Table 2.17. C_2 values for HDPE in flexure at all load rates.

dD/dt (mm/min)	Sample 1	Sample 2	Sample 3	Sample 4	Sample 5	**Average**	COV (%)
2.2	3,986	3,880	3,794	4,068	3,734	**3,892**	3.51
5	4,865	3,945	4,324	3,996	4,244	**4,275**	8.58
10	5,016	5,062	5,369	5,142	5,206	**5,159**	2.68
20	5,276	5,294	4,753	5,184	4,174	**4,936**	9.71
30	4,411	4,840	5,336	4,827	5,343	**4,951**	7.96
40	3,448	4,761	4,606	4,601	5,640	**4,611**	16.92

Table 2.18. C_2 and MOR comparison for HDPE in flexure at all load rates.

dD/dt (mm/min)	Average C_2	Average σ_{ult}	% difference
2.2	3,892	3,703	5.11
5	4,275	3,980	7.40
10	5,159	4,310	19.71
20	4,936	4,361	13.20
30	4,951	4,347	13.90
40	4,611	4,140	11.37

Table 2.19. Measured stress vs. predicted stress for HDPE in flexure and tension.

Flexure				Tension			
Strain (in/in)	Measured Stress (psi)	Predicted Stress (psi)	% error	Strain (in/in)	Measured Stress (psi)	Predicted Stress (psi)	% error
0.001	422	429	1.54	0.0005	355	338	5.03
0.002	889	902	1.48	0.0010	665	658	1.02
0.003	1,296	1,312	1.26	0.0015	907	924	1.86
0.004	1,679	1,691	0.68	0.0020	1,098	1,135	3.22
0.005	1,991	1,989	0.10	0.0025	1,234	1,283	3.79
0.006	2,244	2,117	5.98	0.0030	1,340	1,386	3.33
0.007	2,340	2,206	6.06	0.0035	1,422	1,459	2.57
0.008	2,408	2,281	5.57	0.0040	1,480	1,504	1.62
0.009	2,461	2,338	5.28	0.0045	1,528	1,537	0.58
0.01	2,504	2,381	5.16	0.0050	1,560	1,556	0.24
Average Error			**3.31**	**Average Error**			**2.33**

Table 2.20. Measured stress vs. predicted stress for PP and PPC in flexure.

Uncoupled PP				Coupled PP			
Strain (in/in)	Measured Stress (psi)	Predicted Stress (psi)	% error	Strain (in/in)	Measured Stress (psi)	Predicted Stress (psi)	% error
0.0014	590	718	17.91	0.002	936	1,164	19.60
0.0024	1,117	1,216	8.16	0.003	1,578	1,788	11.75
0.0034	1,596	1,681	5.09	0.004	2,227	2,399	7.15
0.0044	2,024	2,111	4.12	0.005	2,834	2,967	4.48
0.0054	2,394	2,491	3.87	0.006	3,395	3,494	2.83
0.0064	2,711	2,815	3.71	0.007	3,947	4,015	1.69
0.0074	2,987	3,093	3.44	0.008	4,431	4,477	1.02
0.0084	3,235	3,335	3.02	0.009	4,864	4,889	0.50
0.0094	3,436	3,526	2.57	0.01	5,245	5,253	0.16
0.0104	3,607	3,680	2.00	0.011	5,472	5,476	0.08
Average Error			**5.39**	**Average Error**			**4.93**

Table 2.21. Measured stress vs. predicted stress for PP and PPC in tension.

Uncoupled PP				Coupled PP			
Strain (in/in)	Measured Stress (psi)	Predicted Stress (psi)	% error	Strain (in/in)	Measured Stress (psi)	Predicted Stress (psi)	% error
0.0005	369	336	9.92	0.0005	431	384	12.21
0.0055	710	676	4.89	0.0055	841	799	5.26
0.0105	983	974	0.91	0.0105	1,207	1,175	2.72
0.0155	1,203	1,216	1.12	0.0155	1,545	1,537	0.54
0.0205	1,358	1,400	3.00	0.0205	1,821	1,823	0.08
0.0255	1,482	1,535	3.47	0.0255	2,061	2,076	0.72
0.0305	1,575	1,639	3.93	0.0305	2,262	2,280	0.75
0.0355	1,645	1,709	3.73	0.0355	2,436	2,456	0.81
0.0405	1,703	1,760	3.26	0.0405	2,577	2,594	0.66
0.0455	1,748	1,794	2.57	0.0455	2,692	2,704	0.43
Average Error			**3.68**	**Average Error**			**2.42**

Table 2.22. Failure strains: actual vs. predicted.

Tension		Flexure	
Sample	$\Delta_{ult\text{-}actual}$	Sample	$\Delta_{ult\text{-}actual}$
1	0.00830	1	0.1410
2	0.00772	2	0.1360
3	0.00864	3	0.1290
4	0.00791	4	0.1620
5	0.00729	5	0.1420
		6	0.1230
Average	0.00797	Average	0.1388
$\Delta_{ult\text{-}model}$	0.0063	$\Delta_{ult\text{-}model}$	0.1288
% error	20.97	% error	7.23

2.8 Figures

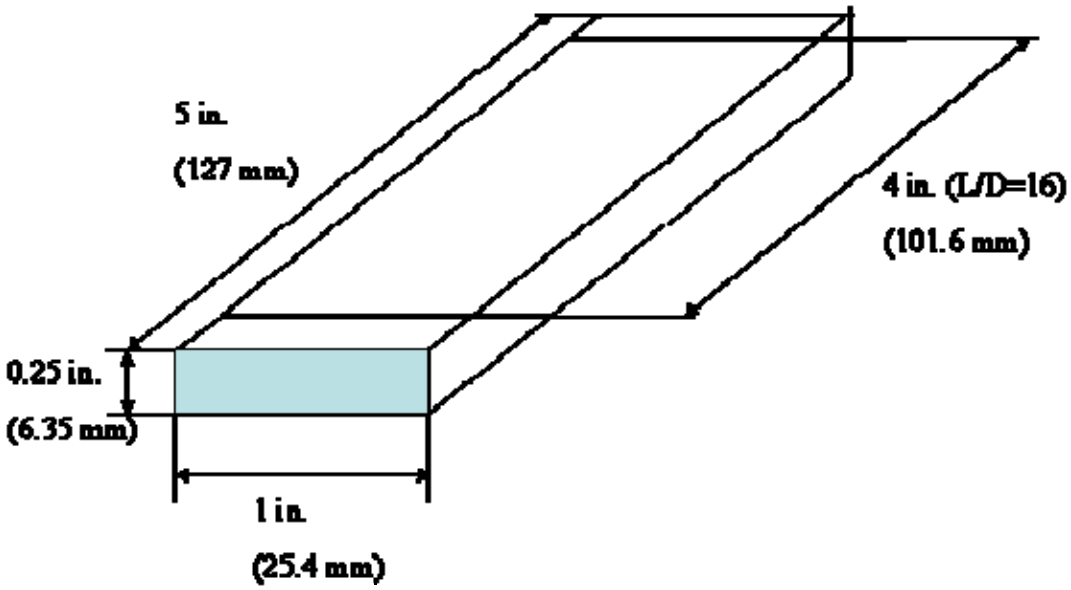

Figure 2.1. Flexural test coupon for all flexural tests.

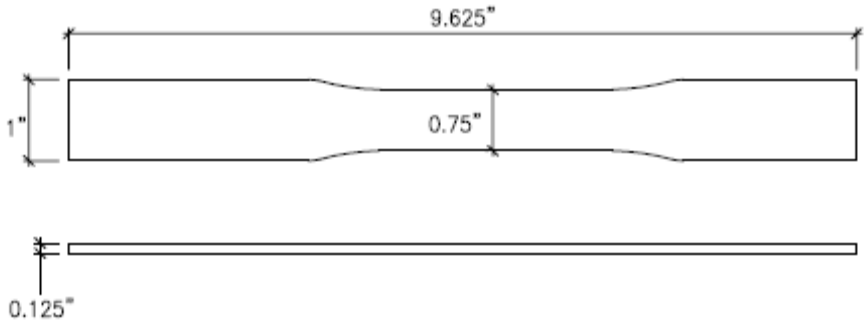

Figure 2.2. Type III dog-bone for tensile testing.

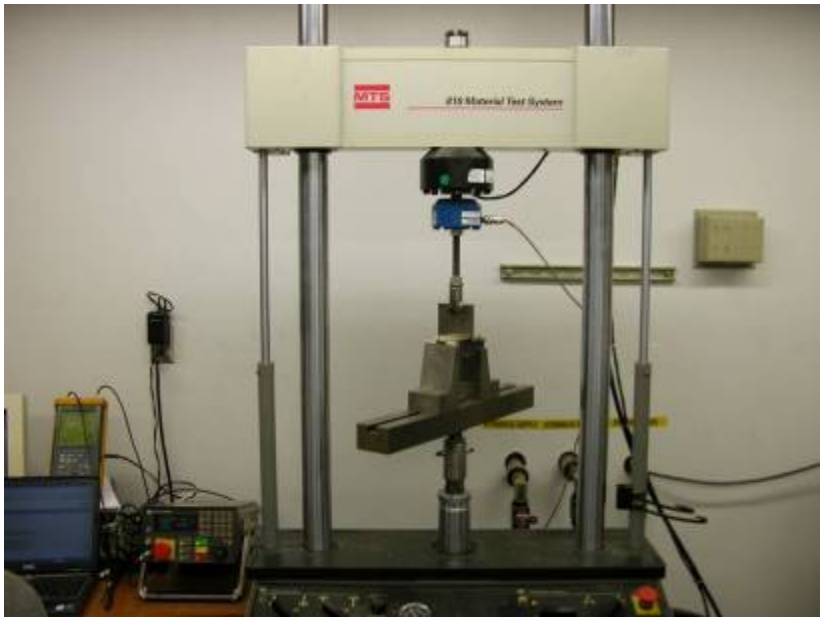

Figure 2.3. 3-point bending test apparatus on 22-kip MTS 810 frame.

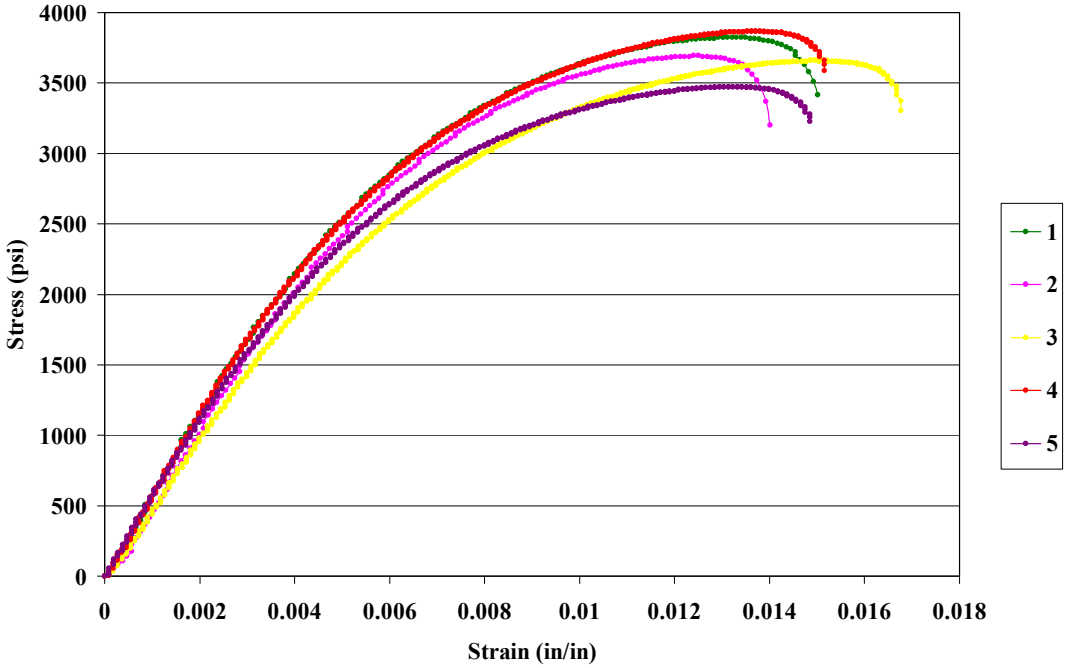

Figure 2.4. HDPE flexural stress vs. strain at 2.7 mm/min.

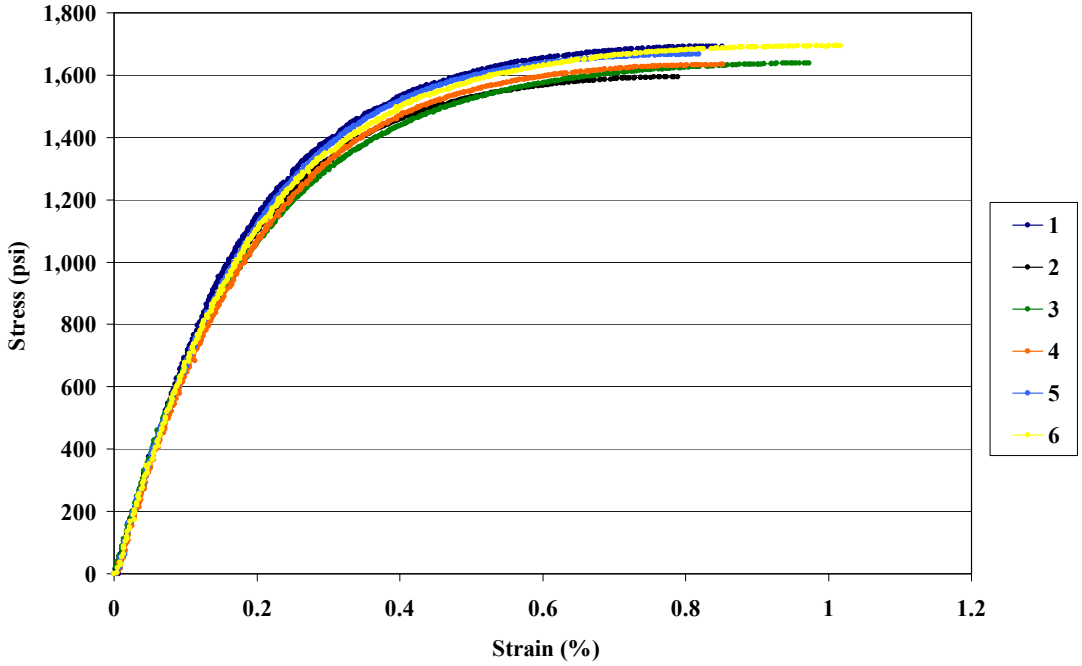

Figure 2.5. HDPE tensile stress vs. strain.

Figure 2.6. Tension-tension test apparatus on 2-kip Instron frame.

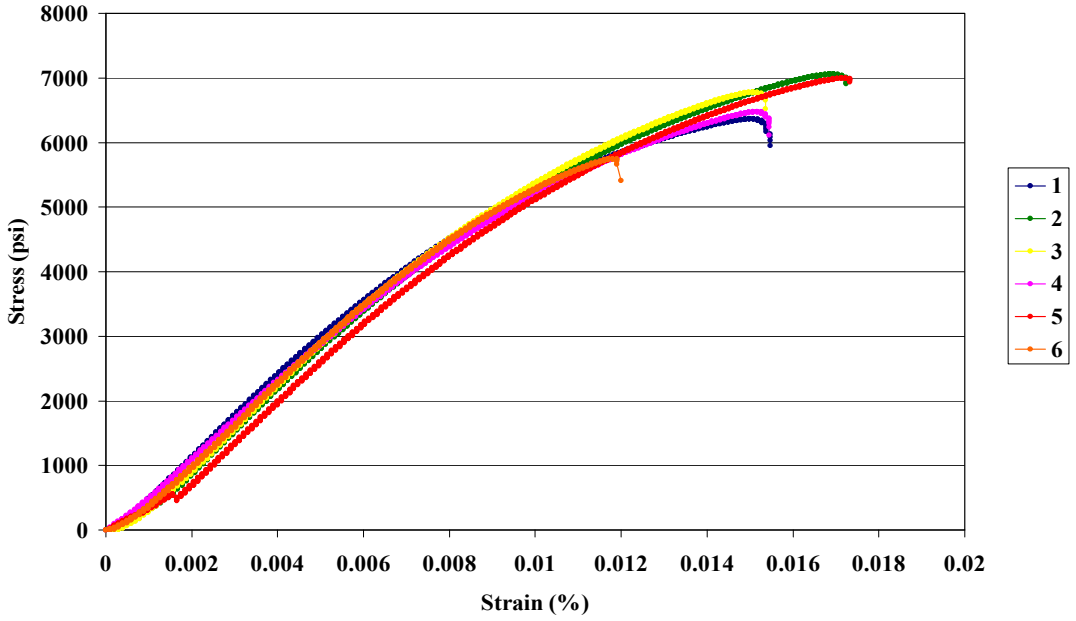

Figure 2.7. PPC flexural stress vs. strain

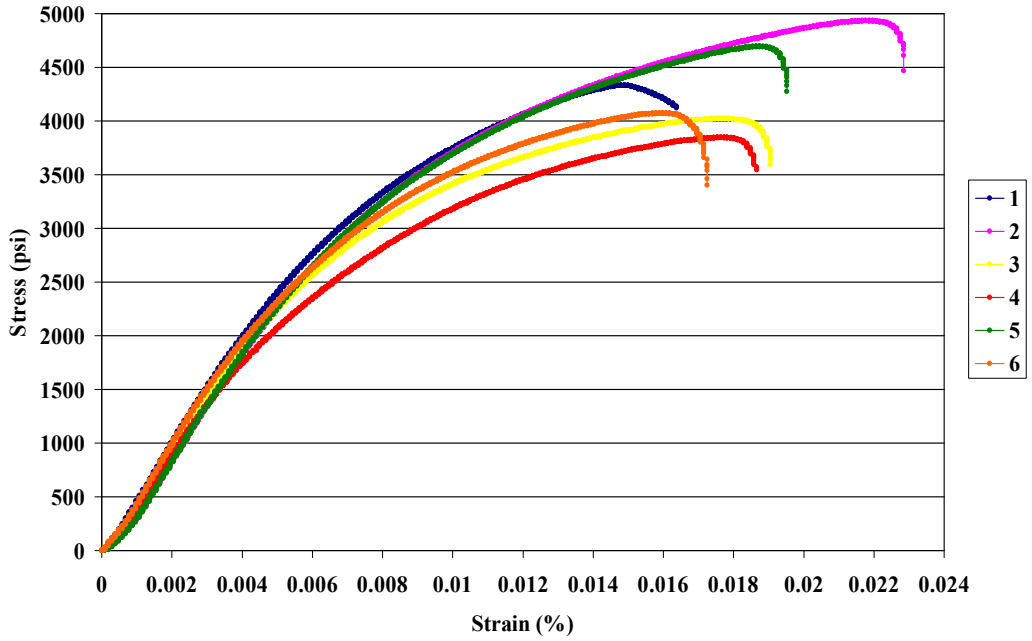

Figure 2.8. PP flexural stress vs. strain.

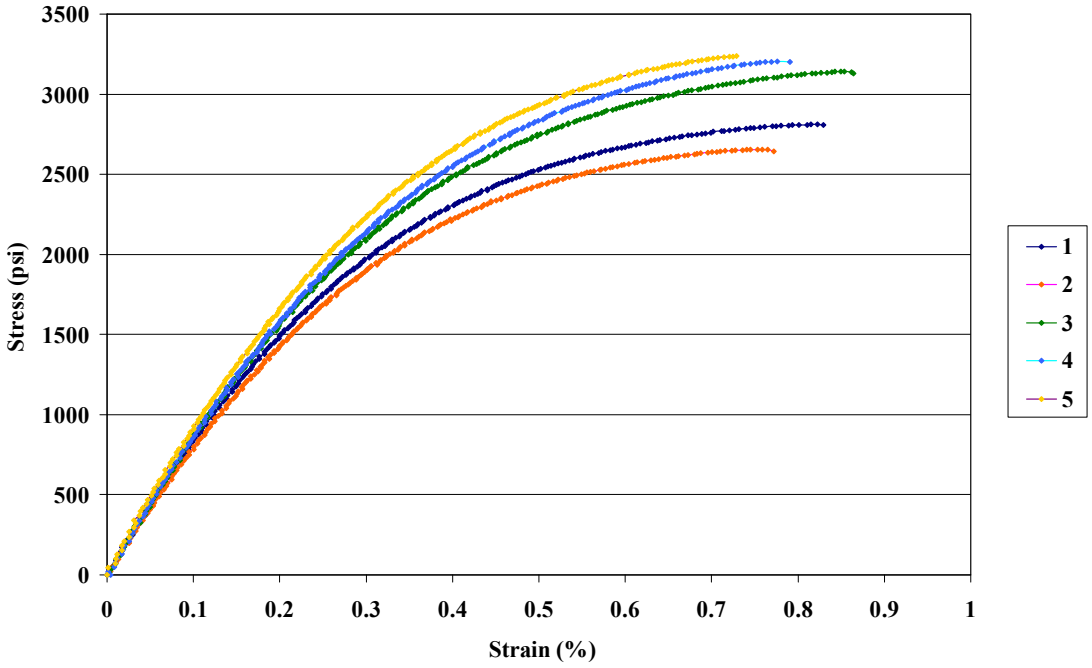

Figure 2.9. PPC tensile stress vs. strain curve.

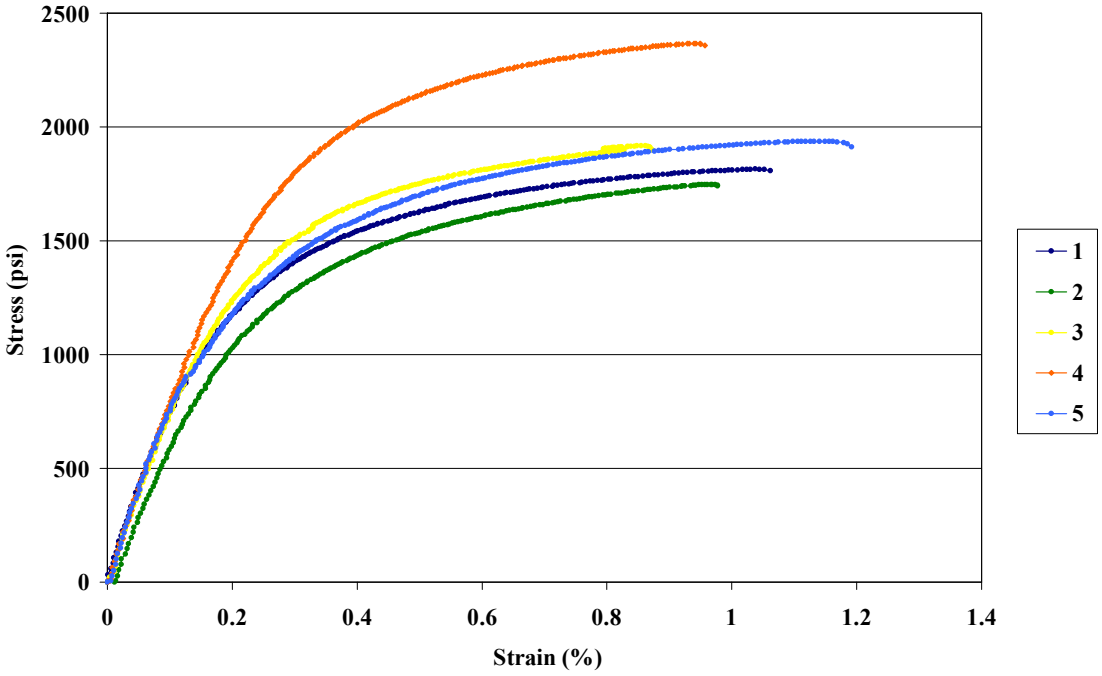

Figure 2.10. PP tensile stress vs. strain curve.

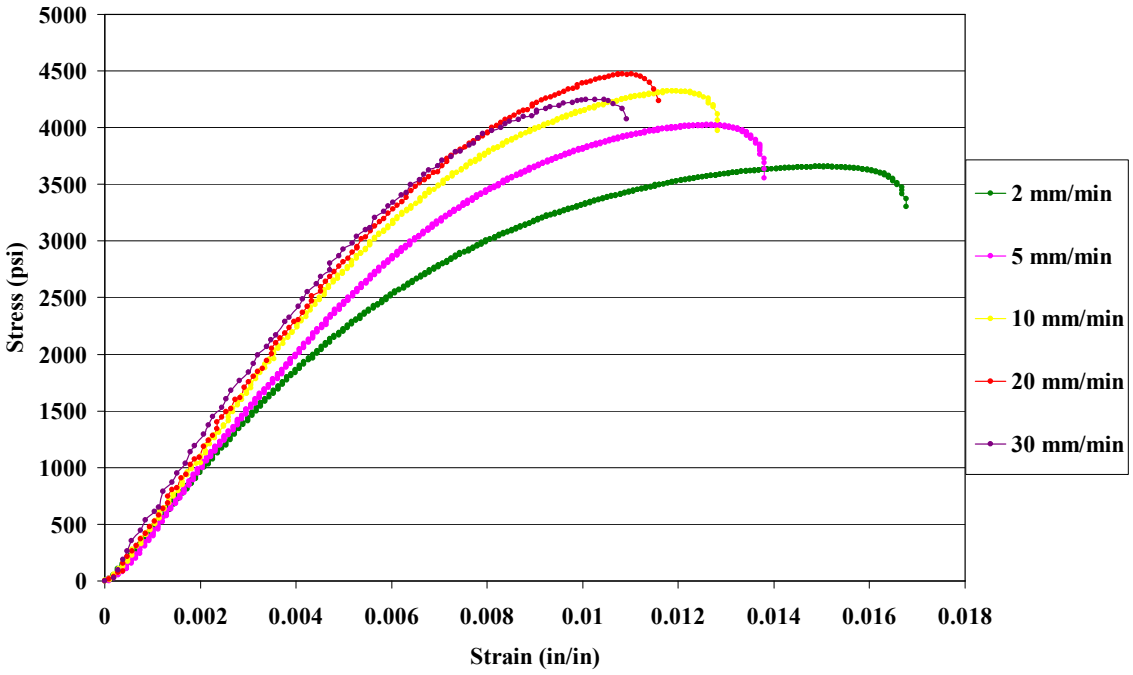

Figure 2.11. Stress vs. strain sampled at varying load rates for HDPE.

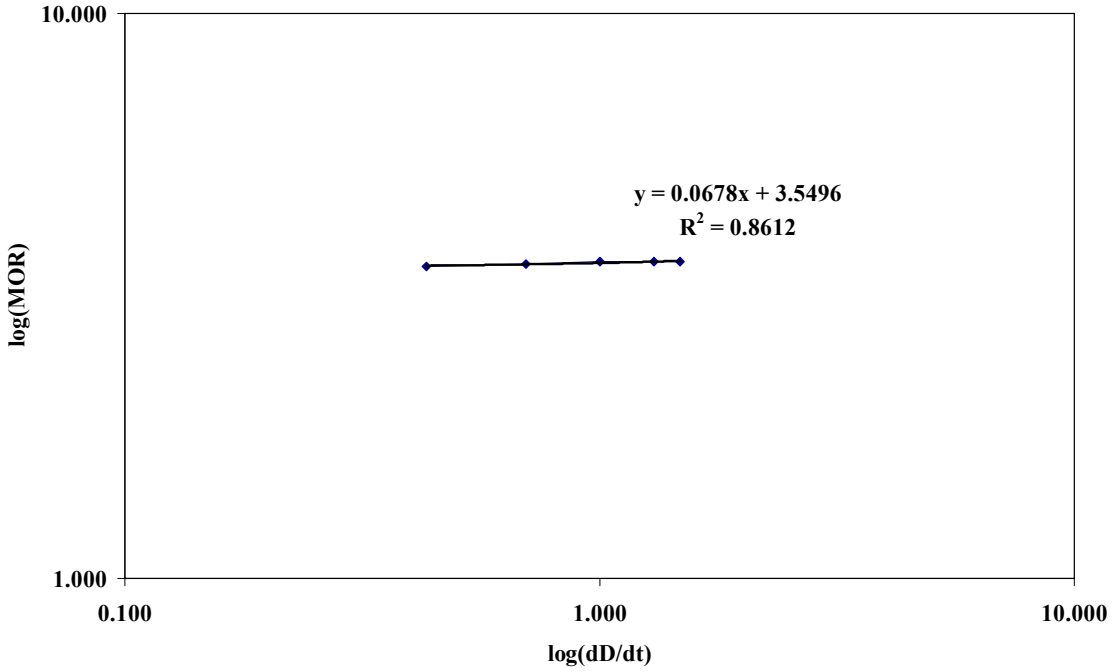

Figure 2.12. Log of MOR vs. load rate for HDPE in flexure ($2.2 \leq dD/dt \leq 30$).

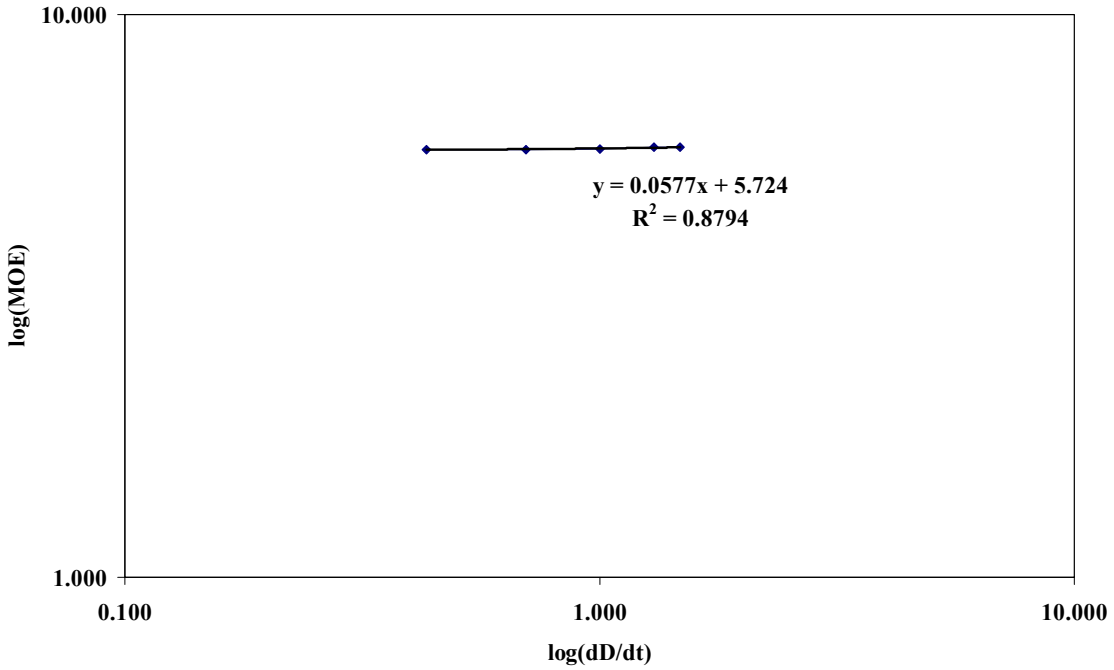

Figure 2.13. Log of MOE vs. load rate for HDPE in flexure ($2.2 \leq dD/dt \leq 30$).

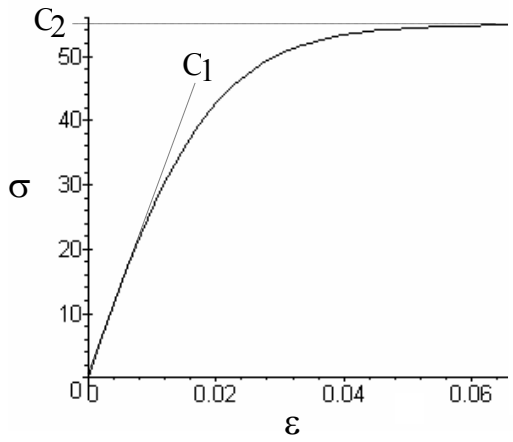

Figure 2.14. Hyperbolic tangent function for nonlinear stress-strain relationship.

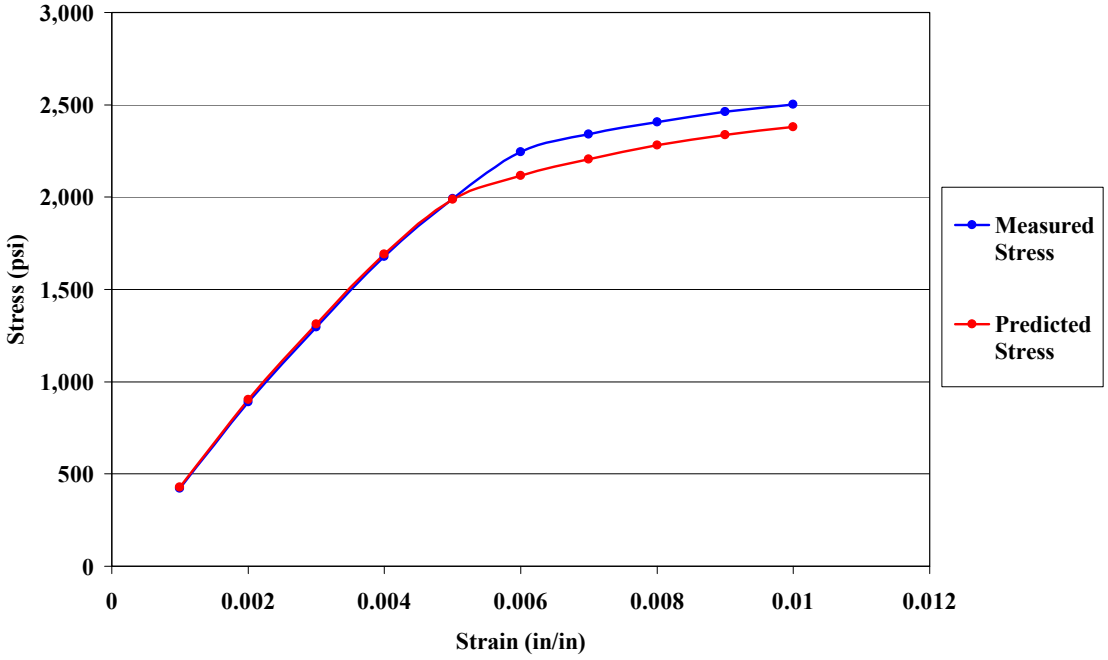

Figure 2.15. Measured stress vs. hyperbolic predicted stress for HDPE in flexure.

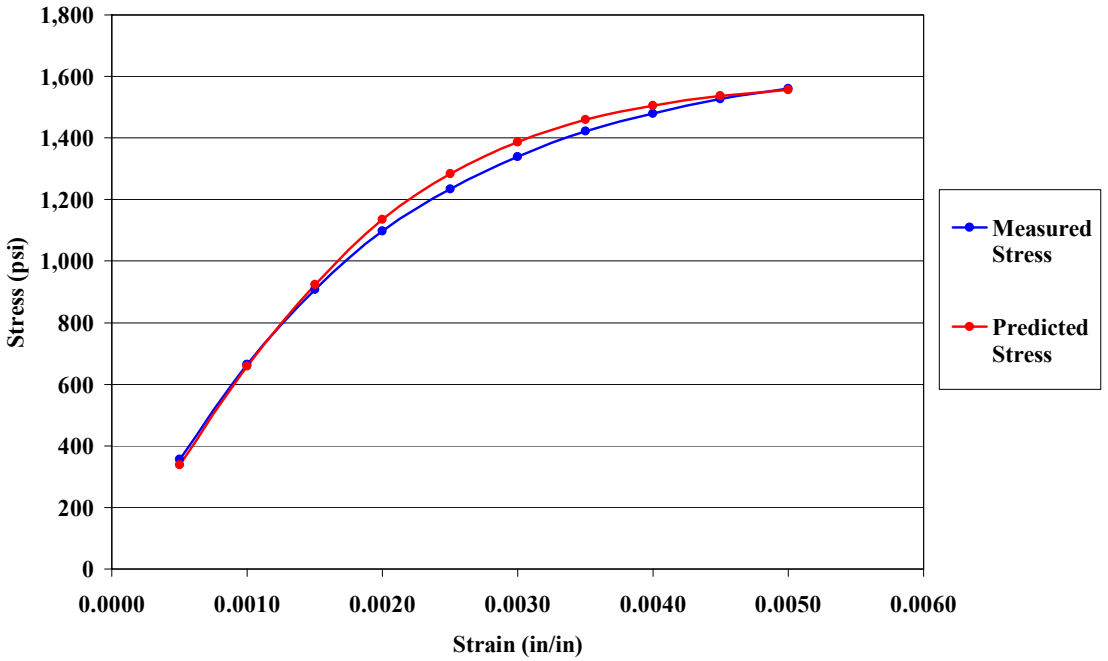

Figure 2.16. Measured stress vs. hyperbolic predicted stress for HDPE in tension.

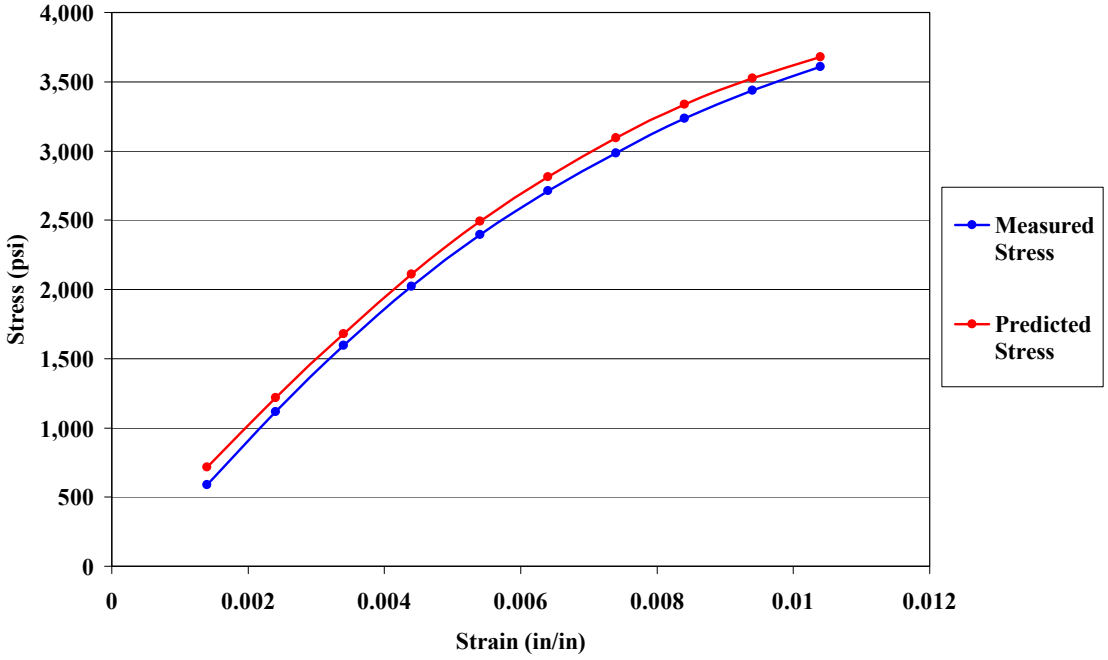

Figure 2.17. Measured stress vs. hyperbolic predicted stress for PP in flexure.

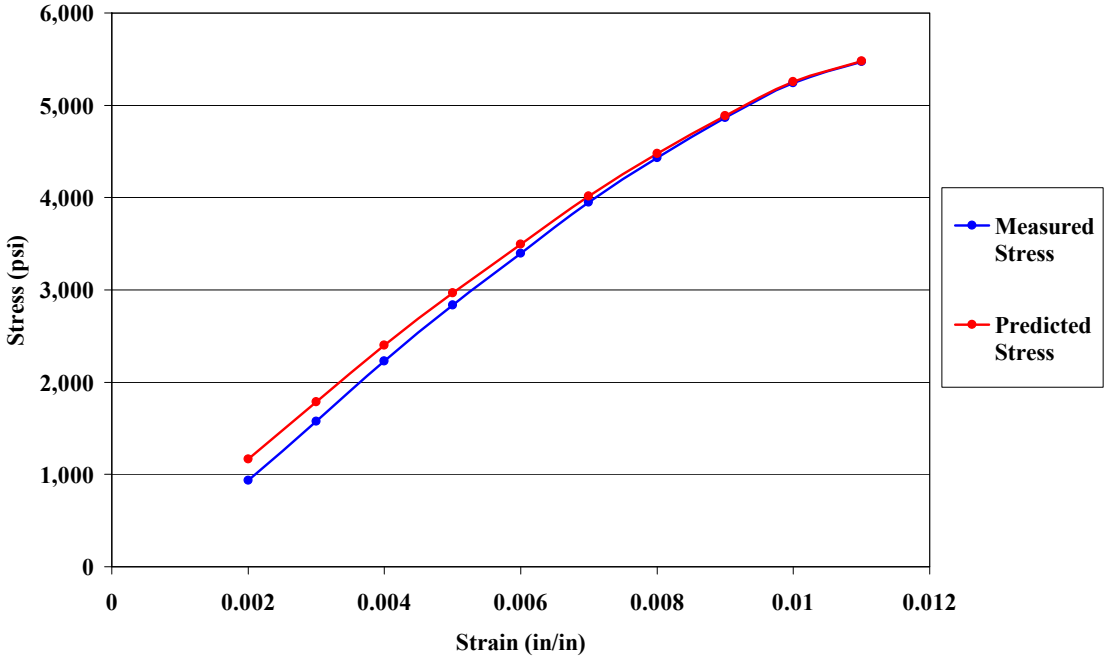

Figure 2.18. Measured stress vs. hyperbolic predicted stress for PPC in flexure.

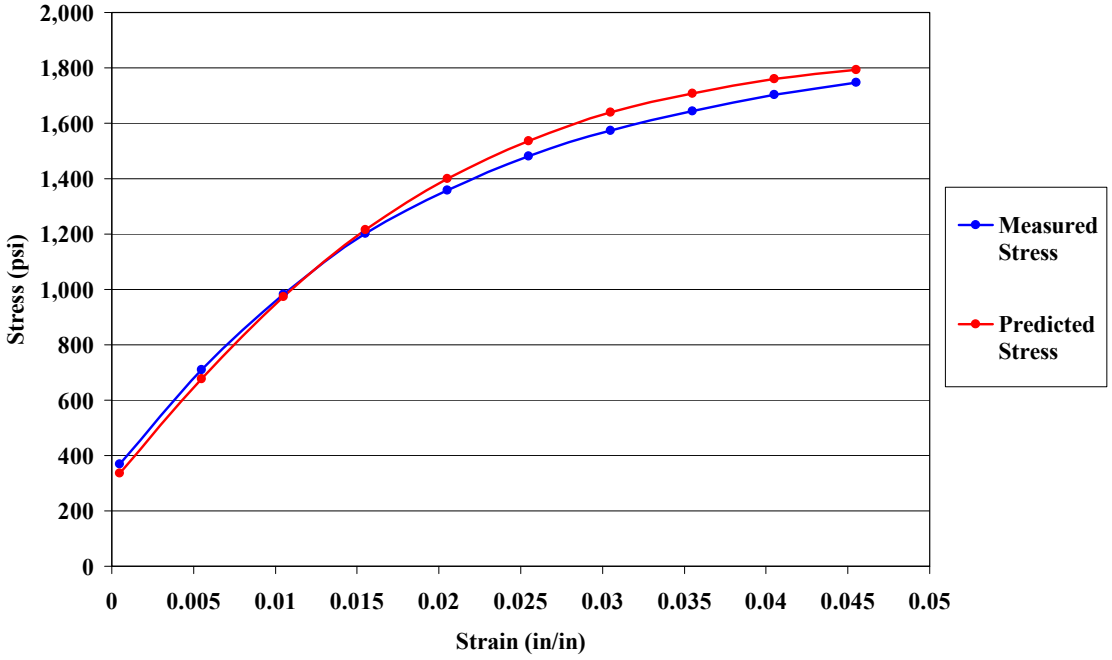

Figure 2.19. Measured stress vs. hyperbolic predicted stress for PP in tension.

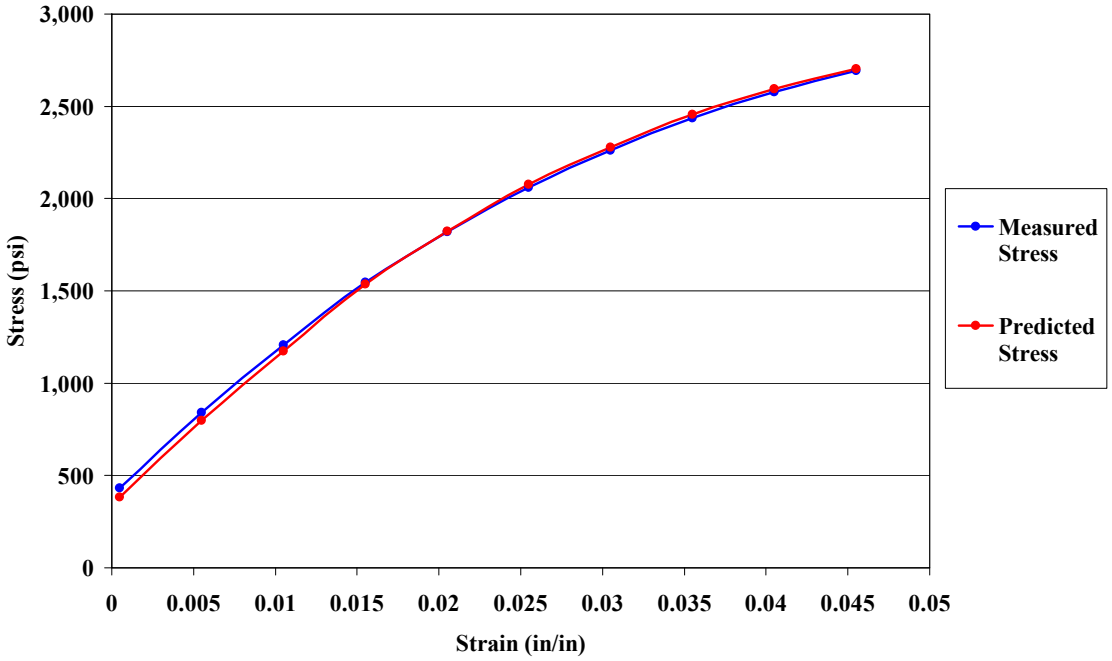

Figure 2.20. Measured stress vs. hyperbolic predicted stress for PPC in tension.

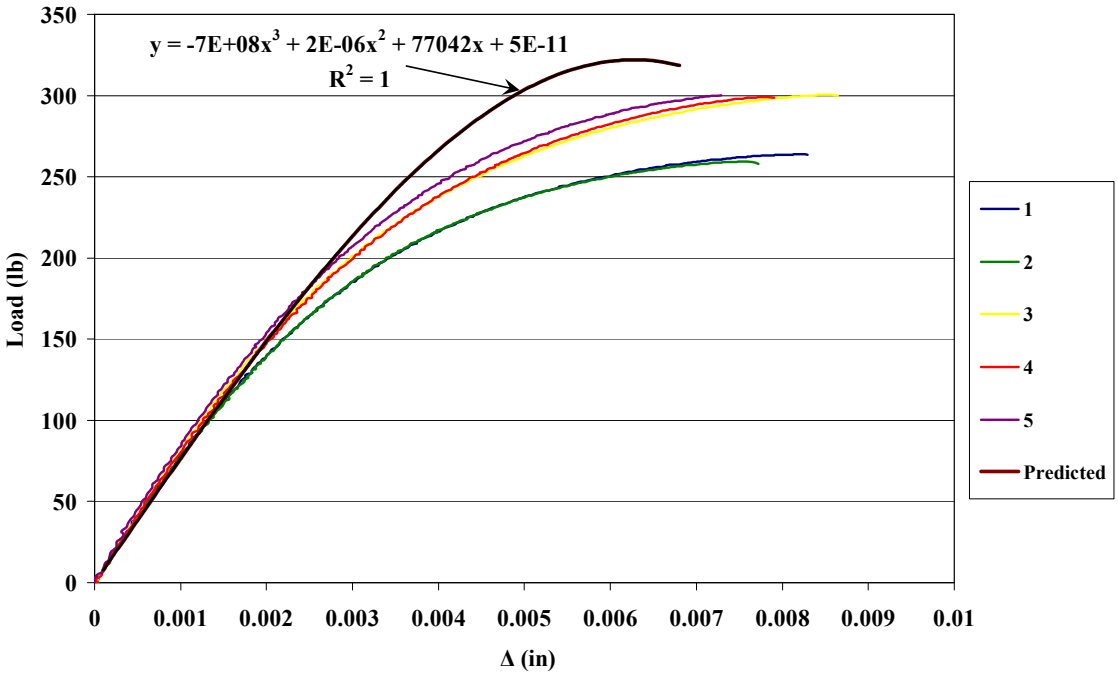

Figure 2.21. Tension force-displacement curves: actual vs. predicted.

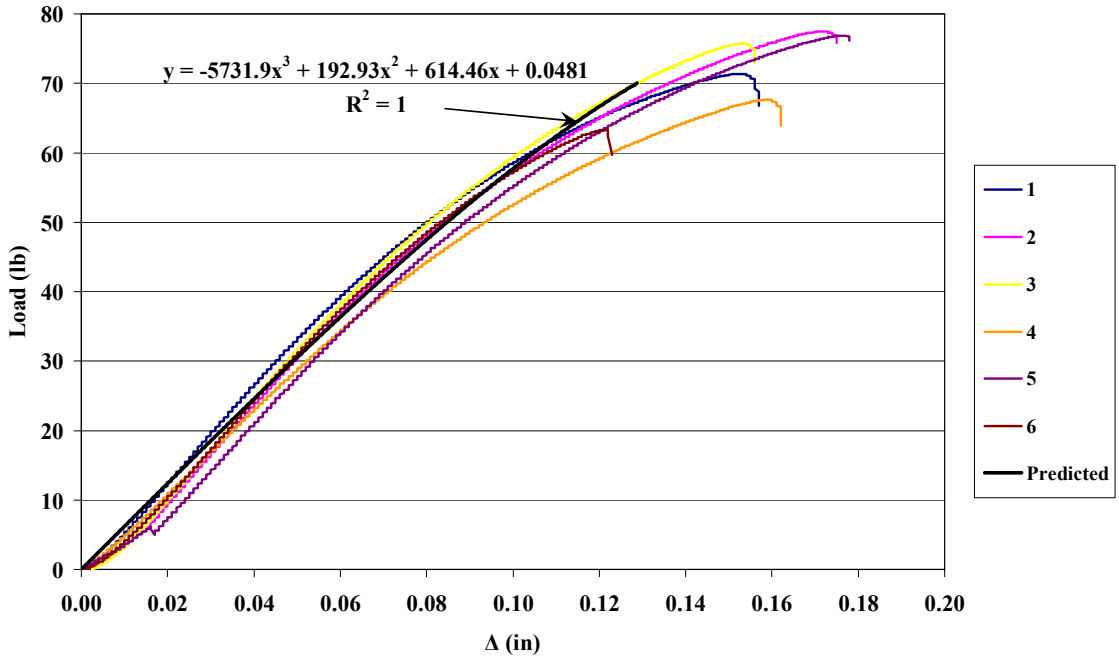

Figure 2.22. Flexural force-displacement curves: actual vs. predicted.

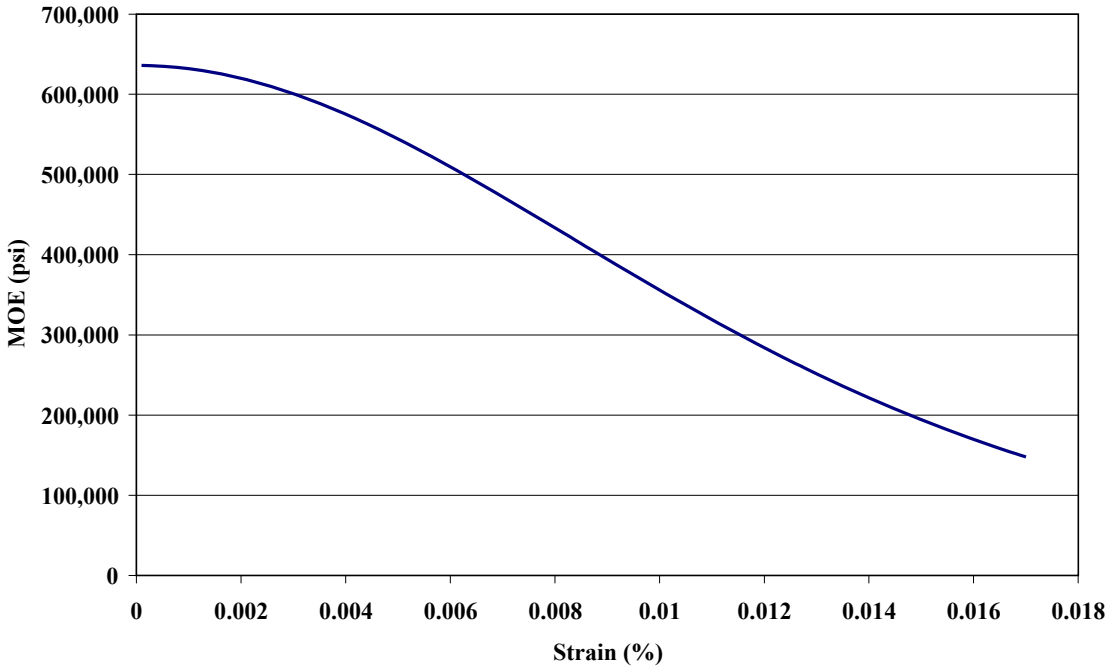

Figure 2.23. Hyperbolic prediction of stiffness degradation vs. strain.

CHAPTER 3 – FATIGUE LIFE AND CONDITIONING

3.1 Introduction

Fatigue is commonly described as the process which causes premature failure or internal physical damage of a material subjected to repetitive or cyclic loading. The process is quite complicated in nature and difficult to accurately describe in homogenous materials, which makes composites especially challenging. According to many available studies, it is suggested that at least half of all mechanical failures are directly related to fatigue loading (Gao, 1994). No exact percentages or even reliable estimates are available for how fatigue contributes to structural failures in general, but the unease in industry is growing and evident in modern research. Recently, concern has spread from fiber-reinforced composites and laminates used in dynamic mechanisms to wood-plastic composites as they become a major player in structurally engineered materials.

Wood-plastic composites are currently being widely used in non-structural applications and in some less demanding load-bearing situations, such as residential decks, rails, and walkways. WPC materials in general have many desirable properties like resistance to corrosion, moisture, and decay and also suitable strength-to-weight ratios. This study utilizes a wood-polypropylene composite with a coupling agent for optimum stiffness and overall performance as suggested in the previous chapter. The same formulation has been shown in recent research as an effective component in some transportation applications such as pedestrian and rural bridge decks. Highway structures produced from other materials have proved less than reliable when fatigue-related loading scenarios come into play (Slaughter, 2004). Fatigue modeling and assessment has quickly become a notable topic of concern in all types of structural composites. As

Clausen and Epaarachchi (2003) observed, glass fiber-reinforced plastics are being integrated into structural situations where fatigue loading is critical. However, while the GFRP is more cost-effective than other fiber-reinforced polymers like graphite and epoxy, it is much more sensitive to fatigue loading and hence requires more accurate modeling before making a real transition into high fatigue load applications. Similarly, WPC elicits the same research incentives as there has been limited research conducted to characterize the fatigue response of WPC. In marine and waterfront applications where WPC may be effectively employed such as heavily trafficked bridge decks, piers, and loading docks, fatigue could also become a significant cause of structural failure. Durability and damage assessment using fatigue conditioning are principal concerns for fully understanding the material behavior and require continued research investigation.

Various authors have derived, studied and supplemented fatigue models for many different composites using the concepts behind logarithmic and power functions, but few focus directly on natural fiber composites like WPC. The models often incorporate various test parameters, including stress ratio, R-value, temperature, test frequency, strain rate, etc. to relate possible field conditions to material fatigue life. Broutman and Sahu, (1972) were among the first to suggest a monotonously decreasing residual strength with cyclic loading, in which the failure was assumed to occur when that strength matched the load amplitude. Hwang and Han (1986) presented a concept called “fatigue modulus”, which is defined as the slope of applied stress and resultant strain at a pre-determined cycle and assumes that the modulus degradation follows a power function of the fatigue cycles “N”. The authors then utilize the physical variables of fatigue modulus and resultant strain to analytically study cumulative damage and propose prediction models

based on S-N relationships. However, this model utilizes one key assumption in that applied stress has a linear relation with resultant strain at any arbitrary loading cycle. Given the conclusive and overwhelming evidence of stress-strain nonlinearity from the last chapter and the results of the present fatigue study, this assumption should be deemed inapplicable for WPC.

Some authors have concentrated their research on stiffness degradation in composite plies. Gao (1994) attempted to relate fatigue failure and fundamental cumulative damage in composite laminates by evaluating internal load redistribution in each lamina from a stiffness reduction model. The author then developed a nonlinear cumulative damage model to predict the critical lamina that controls the fracture of the entire composite. This model utilized a linear function of a crack density parameter to represent damage of the laminate, but no research has shown that crack density can be simply assumed as a parameter for WPC so this model has no application to the material. Shirazi and Varvani-Farahani (2007) proposed a similar damage model based on the actual cracking mechanism and the progression of damage through the varying regions of the laminate (matrix, fiber, and interface). The fatigue damage of the system was found by integrating the effects of cyclic stress magnitude, mean stress, off-axis ply angles, and interfacial bond strength. Again, the concepts of this model relate damage through an evolved micromechanics failure theory where the interaction between fiber and matrix is explicitly analyzed. WPC matrix-fiber interface is physically microscopic and therefore would be more suited for a macroscopic study where it is treated as a homogenously anisotropic continuum. In other words, it more closely relates to many studies conducted on random short glass fiber reinforced composites. Again, plenty of authors have

proposed theories and models for this as well, but they are rarely derived nor implemented for WPC. The immediate objectives of this chapter are two-fold:

1) Evaluate flexural fatigue life of a common wood-polypropylene blend and establish an S-N curve.
2) Apply controlled conditioning at various stress ratios and numbers of cycles in order to study stiffness degradation by DMA and develop a one-dimensional (1-D) continuum damage mechanics (CDM) model. This proposed model will attempt to employ a mechanics of materials approach using kinetic law to evaluate stiffness degradation as a function of fatigue cycles.

3.2 Background

When applying fatigue loading to any specimen, it is ultimately important to pick a consistent set of test parameters, including stress ratio, loading mode, frequency, R-value, and environmental conditions such as temperature and humidity. The loading mode can be 3-point bending, dual cantilever, tension, compression, shear, etc. Flexure in 3-point bending was chosen for this study in order to maintain consistency with DMA analysis and also because tension-tension proved to be a difficult mode to accurately apply stress amplitudes throughout the cycling. Stress ratio is the ratio of maximum applied stress to the ultimate stress, or ($S = \sigma_{max}/\sigma_{ult}$), usually obtained through static tests. The R-value is the ratio of valley to peak stresses within the cyclic loading, or ($S = \sigma_{min}/\sigma_{max}$). For example, if the ultimate bending strength (σ_{ult}) of a coupon was 100 psi and σ_{max} = 70 psi was desired, then the stress ratio is considered 0.7 or 70%. If an R-value of 0.1 is desired, then σ_{min} = 7 psi.

A good deal of conclusive research has been accomplished through fatigue studies that incorporate the variations of such parameters in order to examine their effects on fatigue life and damage accumulation. By considering varying R-values and stress ratios at a constant frequency of 10 Hz on both coupled and uncoupled polypropylene composites, Yang, et al. (2008) showed that fatigue life was inversely related to $\sigma_{max}/\sigma_{ult}$ (S = 0.8 to 0.95) and proportionally related to the R-value (range of 0.09 to 0.19), both of which could be logically hypothesized. Their research also verified that coupled PP behaves better than uncoupled PP due to the improved interfacial bonding between the matrix and wood particles. Additionally, Caprino and D'Amore (1998) performed fatigue tests on glass fiber-reinforced PP composites at constant stress amplitude and frequency and achieved the same results with R-values ranging from 0.1 to 0.5. Frequency is a unique parameter in that it has been shown to exhibit dual effects on the fatigue life of many fiber reinforced polymers, depending on changes in thermal conditions during cyclic loading. A fair amount of literature on this subject indicates that if hysteretic heating is insignificant compared to the material's inherent thermal sensitivity, then fatigue life almost always increases with frequency, but if heating is more relevant than the trend is opposite (Xiao, 1999; Chan & Sun, 1979; O'Brien, et al., 1977). Slaughter (2004) applied this literary interpretation to wood-polypropylene, as he found increasing fatigue life with frequency while observing only small temperature increases (4 to 5 degrees). In Section 3.2.2, the methods used to evaluate fatigue life and condition the specimens along with the selection of all necessary parameters will be fully detailed.

3.2 Materials and Methods

3.2.1 Materials

One particular blend of wood-plastic composite was used for this portion of the study. Wood-polypropylene containing a maleated coupling agent proved to be the strongest and stiffest of the three compositions from Chapter 2 and from previous work (Yang, et al., 2008). The PPC formulation and manufacturing process outlined in Section 2.2 are identical to the process for these specimens, but they were done in separate extrusion batches as there was a need for fresher samples. Refer to Table 2.2 for product details and quantities for the composite and to Table 2.3 for the extrusion temperature profile. Figure 2.7 illustrates the dimensions of the test coupons in both English and metric units.

3.2.2 Fatigue Life and Sample Conditioning

The 22-kip MTS 810 testing frame and 3-point bending fixture were used for all fatiguing in this study just as they were for all quasi-static flexural tests. See Figures 3.1 and 3.2 for images of this test setup. Considering that a standard range of frequencies used in prior research was 1 to 10 Hz, 5 Hz was chosen for this study to reflect a moderate test frequency. Also, the frame could not be tuned as accurately at higher frequencies, and the stress amplitudes probably would have contained too much error to yield reliable results. $R = 0.1$ was selected as it is a common value used in other studies and because higher values often result in significantly high fatigue lives, which would have caused the tests to run too long for the feasibility of this study. Environmental conditions were standard and consistent for all tests as they were conducted in a

conditioning room with T = 70° and RH = 52%. Recall from Chapter 2 that the quasi-static flexural tests were performed on all compositions in this study and ultimate strength for coupled PP are presented in Table 2.7. From those ultimate values, stress ratios of 70%, 80%, and 90% were chosen and four samples in each stress category were tested until rupture. The tests were controlled using an MTS 407 interface that allows the user to monitor the number of cycles, frequency, and other load conditions. The technical details concerning the interface and hydraulic system are outlined in Appendix D along with techniques used to assure quality and accuracy of the stress amplitudes. Table 3.1 shows the intended max and min stress amplitudes and the set points and spans required by the interface. The results for each trial along with their averages and COV are shown in Table 3.2. The S-N curve (stress ratio to number of cycles) is depicted on a logarithmic scale in Figure 3.3.

Once the fatigue lives and S-N curve were established, condition levels were selected based on the number of cycles to failure at each stress ratio. For each category, four samples each were conditioned at N = 50%, 70%, and 90%, a total of 36 samples to be used later in DMA in Chpater 4. Table 3.3 shows the cycles to failure and the corresponding number of required cycles for each condition level.

3.3 Results and Discussion

Referring to Table 3.2, the cycles to failure for stress ratios of 70%, 80%, and 90% were 1,084,928 cycles, 89,715 cycles, and 5,424 cycles, respectively. The dispersion of data can often be most simply and plainly characterized by the coefficient of variation (COV). Average COV for each stress ratio in these samples were 14.89%,

26.88%, and 10.11%, respectively. The scattering of these data is quite reasonable with the exception of S = 80%. A COV of around 20% is generally tolerable when dealing with composites of any type, especially wood-plastics. WPC do not have long fiber reinforcement but only particle fibers so their orientation and microscopic interface with the polymer matrix make their test behavior a bit erratic. The results themselves are particularly intriguing in that at a stress ratio of 70%, it is extremely rare to reach such a high number of cycles in a WPC, regardless of the constituents involved. Slaughter (2004) and Yang, et al. (2008), under similar test parameters, achieved results that are less than an order of magnitude below the million cycles resulting from these tests. However, the consistency in these samples lasting around a million cycles suggests that there may have been some hidden or unknown phenomena acting within the material microstructure that caused them to withstand such duress. For an AS4/PEEK thermoplastic laminate, Xiao (1999) found fatigue cycles upwards of 1,400,000 at stress ratios of 60% that resulted in no failure at all. One possible suggestion for an extremely long life is that there could be a fatigue limit for this particular composition that is sensitive to loading conditions. This particular extrusion batch may have been faulty or on the other hand, the fiber-matrix interface may have been abnormally strong.

3.4 Concluding Remarks

In this chapter, fatigue behavior of wood-polypropylene containing a maleated coupling agent (PPC) was characterized, and the S-N curve for PPC was obtained as (see Figure 3.3)

$$\log\left(\frac{\sigma_{\max}}{\sigma_{ult}}\right) = 0.1318 - 0.0471\log(N)\text{, R = 0.1 and frequency = 5 Hz} \qquad (3.1)$$

The present fatigue study aimed to establish the fatigue life (N) of the wood plastic composites (e.g., PPC in this study) under various stress ratios (S), which can be later used as a guide to condition the samples to certain number of cycles (e.g., a percentage of the fatigue life, %N) and thus accumulate fatigue-induced damage as illustrated in the next chapter.

The fatigue data (e.g., the stress to cycle to failure plots) obtained from the experiment in this chapter can shed light on the nature of failure of WPC under fatigue. More importantly, it can help form an empirical kinetic law for evolving damage in WPC under fatigue and establish a fatigue-accumulated continuum damage mechanics (CDM) model to predict the material degradation due to cyclic loading, as demonstrated in Chapter 5.

3.4 References

Broutman, L.J., Sahu, S. “A New Theory to Predict Cumulative Fatigue Damage in Fiberglass Reinforced Plastics.” Composite Materials Testing and Design (2nd Conference), ASTM STP 497, pp. 170-188, 1972.

Caprino, G. and D’Amore, A. “Flexural Fatigue Behaviour of Random Continuous-Fibre-Reinforced Thermoplastic Composites.” Composite Science and Technology, 1998.

Chan, W.S. and Sun, C.T. “Frequency Effect on the Fatigue Life of a Laminated Composite.” Composite Materials: Testing and Design, ASTM STP 675, Ed. S.W. Tsai, pp. 418-430, 1979.

Clausen, P.D., Epaarachchi, J.A. “An Empirical Model for Fatigue Behavior Prediction of Glass Fibre-reinforced Plastic Composites for Various Stress Ratios and Test Frequencies.” Composites Part A: Applied Science and Manufacturing, Vol. 33, pp. 453-458, 2002.

Gao, Z. “A Cumulative Damage Model for Fatigue Life of Composite Laminates.” Journal of Reinforced Plastics and Composites, Vol. 13, pp. 128-141, 1994.

Han, K.S., and Hwang, W., “Cumulative Damage Models and Multi-Stress Fatigue Life Prediction.” Journal of Composite Materials, Vol. 20, pp. 125-153, 1986.

Han, K.S. and Hwang, W., “Fatigue of Composites – Fatigue Modulus Concept and Life Prediction.” Journal of Composite Materials, Vol. 20, pp. 154-165, 1986.

Reifnsider, K.L., Stinchcomb, W.W., O’Brien, T.K. “Frequency Effects on a Stiffness Based Fatigue Criterion in Flawed Composite Specimens.” Fatigue of Filamentary Composite Materials, ASTM STP 646, Reifsnider and Lauraitis, Eds., pp. 171-184, 1977.

Shirazi, A., Varvani-Farahani, A., “A Fatigue Damage Model for (0/90) FRP Composites Based on Stiffness degradation of 0° and 90° Composite Plies.” Journal of Reinforced Plastics and Composites, Vol. 26, pp. 1319-1336, 2007.

Slaughter, A.E., "Design and Fatigue of a Structural Wood-Plastic Composite." Master Thesis, Washington State University, August 2004.

Xiao, X.R. "Modeling of Load Frequency Effect on Fatigue Life of Thermoplastic Composites." Journal of Composite Materials, Vol. 33, No. 12, 1999.

Yang, H.S., Qiao, P., Wolcott, M.P. “Fatigue Characterization and Reliability Analysis of Wood Filled Polypropylene Composites.” Polymer Composites, accepted, 2008.

3.5 Tables

Table 3.1. Stress amplitudes and MTS 407 interface inputs.

Stress Ratio	σ_{max}	P_{max}	σ_{min}	P_{min}	Span (lbs)	Set Point (lbs)
70%	4,838	50.4	480	5.0	22.7	27.7
80%	5,530	57.6	557	5.8	25.9	31.7
90%	6,221	64.8	624	6.5	29.2	35.6

Table 3.2. Stress ratios vs. failure cycles (S-N data).

Stress Ratio	Run 1	Run 2	Run 3	Run 4	**Average**	COV (%)
70%	1,075,702	894,231	1,289,441	1,080,337	**1,084,928**	14.89
80%	65,388	76,305	97,155	120,013	**89,715**	26.88
90%	5,814	5,146	5,946	4,791	**5,424**	10.11

Table 3.3. Fatigue condition levels.

Stress Ratio	Avg. N_{ult}	30% N_{ult}	50% N_{ult}	70% N_{ult}
70%	1,084,928	325,478	542,464	759,449
80%	89,715	26,915	44,858	62,801
90%	5,424	1,627	2,712	3,797

3.6 Figures

Figure 3.1. Side view of fatigue test setup.

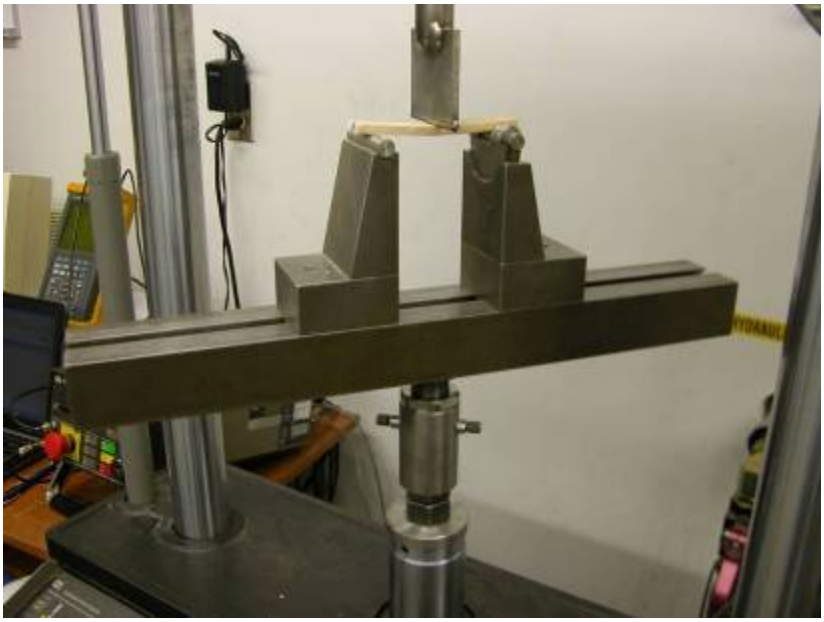

Figure 3.2. Front view of fatigue test setup.

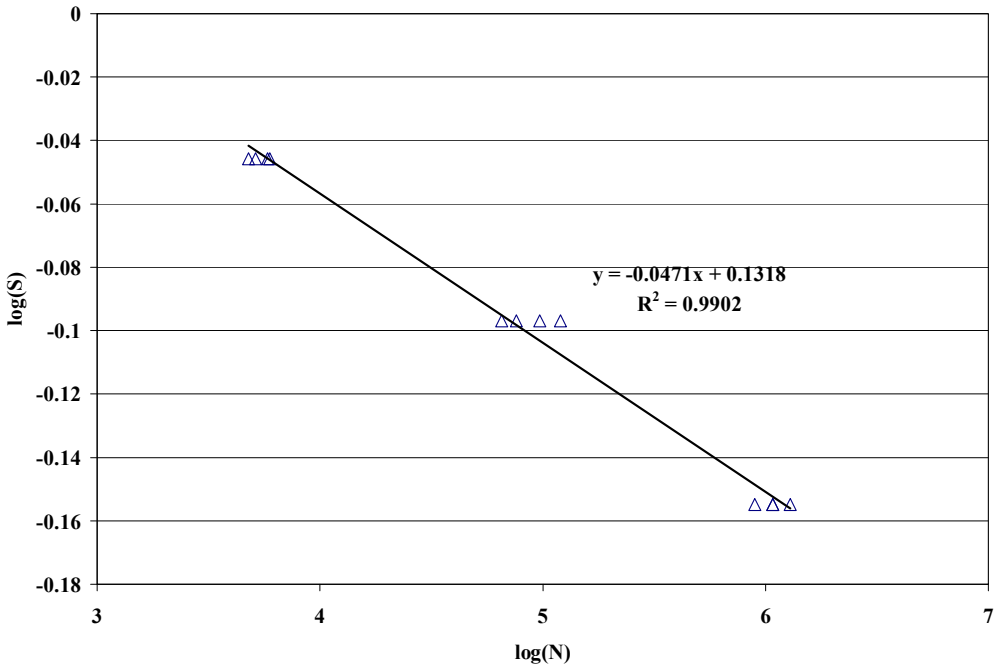

Figure 3.3. S-N curve on logarithmic scale.

CHAPTER 4 – EVALUATION OF FATIGUE-ACCUMULATED DAMAGE

4.1 Introduction and Background

With the ever increasing production and use of wood-plastics in the current materials market, research has been largely focused on evaluating the design capabilities of composites. Synthetic fibers such as glass are playing a more predominant role in composite production with wide implementation in the aeronautic and automotive industries. Perhaps more significant for the purposes of this research, natural fibers are emerging as a common reinforcement and filler in the fabrication of fiber-thermoplastics and have many advantages when compared with synthetic fibers on a performance-cost basis. Natural fibers have low density, high specific strength and stiffness modulus, nonabrasiveness, and wide availability. Natural fibers are also more cost efficient than synthetics in many applications where high composite performance is less important. However, natural fibers also have disadvantages, such as lower allowable processing temperatures, incompatibility between the hydrophilic natural fibers and hydrophobic polymers, and overall moisture absorption in the resulting composite (Tajvidi, et al. 2006). However, some disadvantages can be overcome to an extent. As discussed in detail in earlier chapters, many researchers have observed improvements in the mechanical properties and performance of WPC when a compatibilizer, or coupling agent, is used to enhance the bonding at material interface (Correa, et al., 2007; Danyadi, et al., 2007). Varying the levels and types of fiber content in order to optimize moisture resistance has also shown to be effective. Tajvidi, et al. (2006) showed that out of rice hull, kenaf, maple wood flour, and newsprint fibers at varying content levels, kenaf and wood flour performed the best due to better compatibility between fiber and matrix.

As mentioned previously, thermoplastic materials are susceptible to various modes of dynamic stress during lifetime service, whether they are used in bridge decks, wind turbines, or casings and panels for vehicles. Therefore, it is of prime interest to study the dynamic mechanical properties of these materials. Plastics are notoriously dependent on temperature, as they are generally hard and rigid around room temperature but softer and more malleable at excessive temperatures. Since many mechanical properties of polymeric materials (WPC in this case) are sensitive to temperature, the application of a method that can monitor changes in those properties is critical (Min Min, et al., 2008). Like many other properties, dynamic mechanical properties depend on types of fiber, fiber length, orientation, fiber-to-matrix ratio, and fiber dispersion and loading (Kurvilla, 1993; Kim, 1997).

Dynamic mechanical analysis, or DMA, is an ultra-sensitive technique capable of characterizing the mechanical responses of materials and their properties over ranges of temperature and/or frequency oscillation. DMA has been used broadly to characterize synthetic composite materials as well as wood and wood products. DMA is most commonly used to obtain rheological information about a material in the solid state by subjecting it to dynamic loads over a range of temperatures and/or frequencies. Various loading modes can be achieved by interchanging fixtures made for 3-point bending, single and dual cantilever, tension/compression, and shear. During the DMA test, a sinusoidal strain or predetermined displacement can be applied to the sample while measuring the sinusoidal stress response (Wolcott and Schirp, 2006). The elastic component represents the energy stored in the material and is measured by the response that is in phase with the applied strain. This component is commonly dubbed the storage

modulus and is expressed as E'. The damping or viscous component represents the energy dissipated from stressing the material and is out of phase with the applied strain. This component is referred to as the loss modulus and is expressed as E". The final mechanical parameter of chief concern for this study is the mechanical loss factor, or tan δ, which is the ratio of loss to storage modulus, or E"/E'. This parameter can be especially useful as it may change with material degradation or aging (Liang, et al., 2000; Tajvidi, et al., 2006).

DMA is especially advantageous for developing phenomenological damage models because it can measure changes in properties quickly, utilize very small samples, and can be applied across broad ranges of temperatures and frequencies. Both the elastic and viscous phases monitored in DMA exhibit time-dependent properties in natural fiber-thermoplastics. It's often impractical for most researchers to conduct very lengthy studies as in creep or relaxation test. Therefore, DMA is often the most desirable test method over others, including stress relaxation or creep or creep rupture tests. It is especially useful in characterizing a material's internal morphological behavior when coupled with other techniques like differential scanning calorimetry (DSC) and scanning electron microscopoy (SEM) (; Jiang, et al., 2007; Mouzakis, et al., 2007).

Polymers exhibit two types of morphology in the solid state: amorphous and semicrystalline. In an amorphous polymer, the molecules are oriented randomly and intertwined, and the polymer has a glasslike transparent appearance. In semicrystalline polymers, like the polypropylene and polyethylene used throughout this project, the molecules are arranged together in more ordered regions known as crystallites. Most thermoset polymers are amorphous, while thermoplastics can be amorphous or

semicrystalline. Most studies in polymers utilize the temperature scan function of DMA analyzers in order to observe relaxation processes, which are pronounced by significant changes in any of the dynamic mechanical properties along the scan. Three relaxation processes can usually be found for semicrystalline polymers between liquid nitrogen temperature of -196°C and the crystalline melting point, which varies among polymers (Tajvidi, et al., 2006). The highest transition process is usually denoted with α and is often related to the crystalline fraction. The β process is related to the amorphous phase and usually represents the largest noticeable relaxation, the glass transition temperature, or T_g, although some authors use the γ symbol to denote this phase (Wolcott and Schirp, 2006; Tajvidi, et al., 2006). The low-temperature process is generally considered to originate in the amorphous phase, but may also have an important component associated with the crystalline phase (Turi, 1997 from Tajvidi, et al., 2006). For the purposes of this study, the only process of concern is the glass transition to ensure that the temperature sweep is working correctly and to verify that T_g is consistent with other studies performed on similar composites.

There are three main objectives for this portion of the study: (1) to test the conditioned samples in quasi-static flexure to observe changes in MOE, (2) to run a broad temperature sweep and observe glass transition temperature, and (3) to run "mini-sweeps" of virgin and conditioned specimens obtained in the last chapter to observe and characterize their dynamic mechanical properties after accumulating damage. This data will be used in Chapter 5 to develop a 1-D continuum damage mechanics (CDM) model using a kinetic law.

4.2 Test Methods

4.2.1 Materials

The material used in this chapter was the coupled wood-polypropylene (PPC) described in Chapters 2 and 3. Refer to Sections 2.2 and 3.2.1 for further details. The 36 conditioned specimens of 3 different stress ratios and 4 different condition levels obtained using the fatigue protocol in Chapter 3 were tested along with some unconditioned specimens for comparisons and modeling. A 3-point bending apparatus was chosen for quasi-static and DMA analysis in order to maintain consistency with the samples' conditioning.

4.2.2 Quasi-Static Flexure

Fatigue conditioning was performed on 2 samples of each S-N combination, a total of 18 samples. Once the samples were conditioned to the appropriate levels, i.e., the certain percentage (%) of fatigue life (N) as established in Chapter 3, they were tested in quasi-static flexure to measure MOE and then sent to DMA, keeping the tension and compression sides of the samples consistent. The quasi-static flexure tests were conducted using the same 2-kip Instron frame and 3-point bending apparatus from Chapter 2, pictured in Figure 2.3. The samples were loaded at the standard rate of 2.7 mm/min and up to 50% of their previously measured average strength, which was about 6,500 psi, or 72 lbs. They were loaded only to this point to ensure that they did not break so they could be used in DMA. Also, MOE was measured by taking the slope of the stress-strain data between 10% and 20% of MOR just as it was in Chapter 2 and

therefore, higher loading was not really necessary. The results of the quasi-static tests are presented in Table 4.1 and a graph of N/N_{ult} vs. MOE is presented in Figure 4.1.

4.2.3 Sample Preparation

The fatigued samples were 127 x 25.4 x 6.25 mm (5" x 1" x 0.25") after leaving the MTS frame and being tested in flexure on the Instron. Therefore, they needed to be cut to fit the specified dimensions of DMA. The samples were originally going to be tested using only an RSA II Solids Analyzer and environmental controller, but the Tritec 2000 DMA-8 turned out to be a better choice for obtaining the DMA data around ambient temperatures. However, the RSA II has a more efficient and accurate temperature controller that does not involve the use of manually applied liquid nitrogen, so it was used for the broad temperature sweeps for observing T_g. See Appendix E for further information and images of the testing equipment. The samples were originally cut to fit the RSA II specifications outlined in the manual of 52 mm in length, 12 mm in width, and a maximum of 3.2 mm in thickness. These dimensions were also suitable for the DMA-8 and in fact did not actually need to be so thin but worked well for applying very small strains. The samples were cut evenly about the widthwise centerline and straight up the middle lengthwise using a Microlux 3 ¼" table saw, generating 2 DMA samples per 1 fatigued coupon (36 total). The compression side of the flexural fatigued samples was shaved off using a Sherline 2000 3-D milling machine (depicted in Appendix E). The tension and compression sides of the flexural samples would have similar stress distributions in the linear elastic range but may not in the viscoelastic range. The rationale for shaving off one whole side was that the outer layer of the fatigued sample on

the tensile side was under high stress compared to the portion near the neutral axis. If any damage were accumulated during the process, micro-cracks would likely manifest on the outer tensile surface first.

4.2.4 DMA Testing

DMA testing conformed to ASTM D5023 (2007) standards for DMA in 3-point bending. As mentioned before, a 3-point bending apparatus was installed onto the face of the DMA-8. Figure 4.2 shows the test setup as taken directly from the Tritec manual from the top, front, and side views labeled A, B, and C, respectively. The samples were placed securely but delicately into the machine by adjusting tiny screws on the face of the apparatus. This was performed with great care each time to ensure that the initial static displacement on the samples was as minute and consistent as possible but also to create enough force so that when low temperatures caused the sample to shrink, they would not fall out of the fixture.

The first thing that needed to be done before conducting any temperature sweeps was a strain sweep. The purpose of a strain sweep is to find a suitable oscillation strain that ensures linearity throughout the test and is high enough to cause substantial displacement. The test was conducted from 0.001 to 0.05 mm at a constant frequency of 1.0 Hz and at room temperature, which was 26°C for this particular room. The results are displayed in Figure 4.3, which shows the stress and modulus with respect to displacement. By inspection, the stress data remains undeniably linear up until about 0.01 mm when there appears to be a slight change in slope. The data remains linear the rest of the way but has a steeper slope. Just to be safe, a strain of 0.01 was selected to be

used throughout the entirety of the DMA study. An identical approach was taken for a strain sweep on the RSA II and yielded the same results. The significant and applicable facets of this study were conducted using the DMA-8, so those procedures are more carefully outlined here.

Temperature sweeps were performed on the RSA II analyzer for purposes of verifying the glass transition temperature in compliance with ASTM E1867 (2006) and ASTM E1640 (2004). Broad sweeps were conducted on 2 virgin (unconditioned) samples from -30°C to 60°C at a constant frequency of 1.0 Hz and strain of 0.01% with a heating rate of 2°C/minute and a soak time of 1 minute. These are standard parameters commonly used for temperature sweeps. The two sweeps are shown in Figures 4.4 and 4.5. Each chart depicts loss modulus, storage modulus, and tan δ as a function of temperature.

The next experiment was the small-range temperature sweeps conducted on the DMA-8, under ASTM E5023 (2007). The purpose of this test was to gather data corresponding to normal ambient temperatures of around 21°C, but the room was generally hotter than 26°C and the temperature controller for the DMA-8 was not capable of equilibrating lower than that for long periods of time. Therefore, in order to ensure that the actual sample temperature was close to the desired temperature, a sweep was conducted to monitor the activity at and around 21°C. The tests were hence conducted from 10°C to 40°C on all 36 conditioned samples. The DMA-8 software interface prompted the user to enter the sample dimensions, desired temperature range (10°C to 40°C), maximum strain displacement (0.01 mm), frequency (1.0 Hz), and the heating rate (2°C/minute). The samples were then loaded and tightened to an appropriate static

displacement (usually 0.04 mm). The temperature control chamber was then fastened to the face of the machine and hooked up to a small liquid nitrogen (LN2) tank that had a release valve. Once all parameters were input, the LN2 valve was turned on and LN2 flowed around the control chamber, gradually lowering the temperature. Once the rate of temperature decrease was desirable, the valve was shut off while the chamber continued to cool. The chamber usually reached 8 or 9 degrees before beginning to automatically warm back up. Once the temperature was around 10°C, the experiment was started. The results for the 36 samples at each S-N grouping and 2 unconditioned samples are displayed in Tables 4.2 – 4.5 and correspond to virgin, S = 70%, 80%, and 90% with %N fatigue life, respectively. The "Data ID" column shows each individual sample, labeled in the form of N-S-Name. For example, sample "1a" conditioned at S = 70% and N = 30% would be labeled 30-70-1a. Tables 4.6 and 4.7 summarize the data for storage modulus and tanδ at temperatures of around 21°C, respectively. Figures 4.6 and 4.7 show plots for that data.

4.3 Results and Discussion

Table 4.1 and Figure 4.1 display the results of quasi-static flexural testing of the conditioned samples. Modulus of elasticity decreased as the fatigue cycles increased for the bottom two stress ratios, as expected. However, the 90% stress ratio was more erratic in that it decreased from N = 30% to N = 50% but then spiked for N = 70%. This data is actually not all that surprising. The ultimate cycles to failure for the 70% and 90% stress ratios was roughly 1,000,000 and 5,000, which is almost 2 orders of magnitude. Since the higher stress ratio samples required such a low number of cycles compared to the

other samples, one cannot fully expect a trend in damage accumulation measured by the quasi-static flexural tests. When fatigue conditioning at S = 90% and N = 70%, the samples often did not even make it through enough cycles to use them in DMA. They sometimes broke prematurely, which raises questions about the accuracy of N_{ult}. Also, at higher stress ratios the MTS frame proved to be more out of tune than it was at smaller loads, so the peak stress may have been slightly inaccurate. Although the stresses were monitored to the best of the researcher's ability, the tests were so short that only a small amount of force-time data was able to be recorded. The data from the other fatigue levels were more plausible, and the amount of scattering of all the data in this experiment was quite acceptable (8.06% or less). At S = 80%, the stiffness degraded from N = 30% to N = 50% but remained almost the same from N = 50% to N = 70% (increase of 2,600 psi, only a 0.4% increase). At S = 70%, the stiffness dropped 3.4% from N = 30% to N = 50% and dropped 3.0% from N = 50% to N = 70%. Overall, the drop in MOE was not really significant for any case, but the tests resulted in enough evidence to conclude that damage was likely to have accumulated, due to the reduced stiffness. According to quasi-static tests, it is reasonable to conclude that fatigue conditioning at high stress ratios does not necessarily produce reliable samples for measuring damage. Future research should focus on stress ratios between 50% and 80%. Further tests, i.e., DMA, were needed to verify evidence of damage accumulation in the samples for this study.

The first test conducted using DMA was the broad temperature sweep from -30°C to 60°C to verify glass transition temperature (T_g) of unconditioned samples. The drops in E' curves and the peaks of tanδ plots are used to report on the physical transitions in most polymers. Usually, the transitions are observed at the maximum rate of turndown in

storage modulus and/or at the peaks in tanδ, depending on the material's thermal sensitivity (Cristea, et al., 2008). According to Figures 4.4 and 4.5, an obvious peak in tanδ occurs right at 0°C. This finding was consistent with other previous studies, which have shown that the glass transition occurs between -10°C and 0°C in polypropylenes, depending on a variety of factors, such as fiber reinforcement and fiber content (Abraham, et al., 2008; Tajvidi, et al., 2006; Larena, et al., 2006). The verification of this parameter was useful in maintaining confidence in the methods for dynamic mechanical analysis and showed that the specific wood-PP composition was suitable and representative of the behavior in other polypropylenes.

The second test performed using DMA was the short temperature sweeps conducted from 10°C to 40°C on all samples, both virgin and conditioned. Refer to Tables 4.2 – 4.5 and Figures 4.6 and 4.7 for the dynamic mechanical parameters obtained from this experiment. The results were very good, with the exception of the samples conditioned at S = 90% stress ratio, and reasonably consistent with the quasi-static degradation discussed earlier. The abnormally high numbers in storage modulus compared to MOE measured in quasi-static tests were due to the fact that such a small strain was applied in DMA. This means that stiffness was measured very early in the stress-strain slope, resulting in higher values than would be obtained by taking an extended average of the slope (between 10% - 20% of MOR, typically).

Average E' (storage modulus) of the unconditioned samples was measured at 1.03 x 10^6 psi. For S = 70%, the storage modulus was measured at 930,823 psi, 858,589 psi, and 763,327 as condition cycles increased, an overall drop of 18%. For S = 80%, storage modulus was 1,089,690 psi, 923,915 psi, and 857,791 as cycles increased, which was a

total drop of almost 25%. At the highest stress ratio of 90%, E' dropped 25% from 1.05 x 10^6 psi to 813,704 psi between N = 30% and 50% but it then increased 2.2% at N = 70%, which is consistent with the conclusions observed in the quasi-static flexure test, since the DMA samples were cut from the flexural samples. While it doesn't exactly make sense that a sample's storage modulus would increase with conditioning, the same justification applies for E' that was used for MOE earlier. The 90% stress ratio was probably unreliably fatigued during conditioning and the resulting data should not be deemed as too significant. However, both DMA and quasi-static tests showed the same trend as N was increased for S = 90% (Figures 4.1 and 4.6), so it can be concluded that the problem was most likely due to inaccuracy in the hydraulic test frame at higher loads during the fatigued-conditioning process.

Similar to the expected trend observed in E', Figure 4.12 shows that tanδ increased with N for all samples except for those conditioned at S = 90%. In other words, the ratio of E"/E' increased as damage accumulated within the composite. We will see how these results can be used to create a 1-D CDM model in the next chapter. The decrease of storage modulus, increase of loss modulus, or increase of tanδ obtained from the DMA tests of the samples conditioned at different stress ratios and fatigue cycles (i.e., a percentage of fatigue life, %N) indicates that the elastic component of material was reduced due to fatigue accumulated damage, and most energy is dissipated as the material degraded with increasing fatigue conditioning. The experimental results validate that the DMA test is more effective to assess the damage accumulation and material degradation when compared to the quasi-static test.

4.4 Concluding Remarks

In this chapter, the effect of fatigue damage accumulation was evaluated using either the quasi-static flexure or DMA tests. The PPC samples were conditioned under the fatigue loading at different stress ratios (i.e., S = 70%, 80% and 90%) with different percentages of fatigue life (N) which were established in Chapter 3. It showed that the flexural stiffness properties from the quasi-static tests as well as the storage modulus from the DMA tests decreased as the condition levels of stress ratio and cycle increased. Both the reduced stiffness and reduced storage modulus indicated that the damage was accumulated via fatigue in the material. The higher stress ratio and higher percentage of fatigue life (%N) conditioning generally corresponds to increasing stiffness reduction, indicating the degraded material properties due to fatigue. The DMA tests were more sensitive to damage accumulation and produced larger changes in the observing variables (e.g., storage or loss modulus and tanδ), when compared to the quasi-static tests. Thus, the DMA tests may be a better test method to condition the test samples and evaluate their damage accumulation. The material degradation data in terms of either reduced stiffness or reduced storage modulus could be compared with the predictions by a continuum damage mechanics (CDM) model to calibrate its validity, as proposed and illustrated in next chapter.

4.4 References

Abraham, T.N., Karger-Kocsis, J., Siengchin, S. "Dynamic Mechanical Thermal Analysis of all PP Composites Based on β and α Polymorphic Forms." Journal of Material Science, Vol. 43, pp. 3697-3703, 2008.

ASTM D5023-07. "Standard Test Method for Plastics: Dynamic Mechanical Properties: In Flexure (Three-Point Bending)." American Society for Testing and Materials.

ASTM E1640- 04. "Standard Test Method for Assignment of the Glass Transition Temperature by Dynamic Mechanical Analysis." American Society for Testing and Materials.

ASTM E1867-06. "Standard Test Method for Temperature Calibration of Dynamic Mechanical Analyzers." American Society for Testing and Materials.

ASTM E2368-04. "Standard Practice for Strain Controlled Thermomechanical Fatigue Testing." American Society for Testing and Materials.

Correa, C.A., Hage Jr, E. "Role of Maleated Coupling Agents on the Interface Adhesion of Polypropylene – Wood Composites." Journal of Thermoplastic Composites, Vol. 20, pp. 323-339, 2007.

Cristea, M., Gaina, C., Gaina, V., Ionita, D.G. "Dynamic Mechanical Analysis on Modified Bismaleimide Resins." Journal of Thermal Analysis and Calorimetry, Vol. 93, pp. 69-76, 2008.

Danyadi, L., Moczo, J., Pukanszky, B., Renner, K. "Wood Flour Filled Polypropylene Composites: Interfacial Adhesion and Micromechanical Deformations." Journal of Polymer Engineering and Science, Vol. XX, pp. 1246-1255.

Jiang, H., Kamdem, D.P. "Thermal and Dynamic Mechanical Behavior of Poly(vinyl-chloride)/Wood Flour Composites." Journal of Applied Polymer Science, Vol. 107, pp. 951-957, 2008.

Kim, T., Lee, Y., and Im, S. "The Preparation and Characteristics of Low-density Polyethylene Composites Containing Cellulose Treated with Cellulase." Polymer Composites, Vol. 18, pp. 273-282, 1997.

Kurvilla, J., Sabu, T., Pavithran, C. "Dynamic Mechanical Properties of Short Sisal Fiber Reinforced Low-density Polyethylene Composites." Journal of Reinforced Plastic Composites, Vol. 12, pp. 139-155, 1993.

Larena, A., Jimenez de Ochoa, S., Dominguez, F. "Dynamic-Mechanical Analysis of the Photo-Degradation of Long Glass Fiber Reinforced Polypropylene: Mechanical Properties' Changes." Polymer Degradation and Stability, Vol. 91, pp. 940-946, 2006.

Liang, J.Z., Li, R.K.Y., Tjong, S.C. "Dynamic Mechanical Analysis of Low-Density Polyethylene with Glass Beads." Journal of Thermoplastic Composite Materials, Vol.13, pp. 12-20, 2000

Min Min, A., Chantera, T.R., Chuah, T.G. "Thermal and Dynamic Mechanical Analysis of Polyethylene Modified with Crude Palm Oil." Materials and Design, Vol. 29, pp. 992-999, 2008.

Mouzakis, D. E., Galiotis, C., Zoga, H. "Accelerated Environmental Ageing Study of Polyester/glass Fiber Reinforced Composites (GFRPCs)." Composites Part B, Vol. 39, pp. 467-475, 2008.

Tajvidi, M., Falk, R.H., Hermanson, J.C. "Effect of Natural Fibers on Thermal and Mechanical Properties of Natural Fiber Polypropylene Composites Studied by Dynamic Mechanical Analysis." Journal of Applied Polymer Science, Vol. 101, pp. 4341-4349, 2006.

Turi, E.A. (ed.). "Thermal Characterization of Polymeric Materials." 2nd Edition; Academic Press: New York, 1997.

Wolcott, M.P., Schirp, A. "Fungal Degradation of Wood-Plastic Composites and Evaluation Using Dynamic Mechanical Analysis." Journal of Applied Polymer Science, Vol. 99, pp. 3138-3146, 2006.

4.5 Tables

Table 4.1. Average MOE and COV from quasi-static flexural tests of conditioned samples.

	S = 90%	S = 80%	S = 70%
N = 30%	579,174 (3.43%)	627,182 (6.83%)	609,166 (0.53%)
N = 50%	544,655 (0.41%)	611,220 (3.71%)	588,322 (1.45%)
N = 70%	594,644 (1.75%)	613,868 (6.18%)	570,795 (8.06%)

Table 4.2. DMA data for unconditioned samples.

Data ID	Temp. (°C)	Freq. (Hz)	Max Δ (mm)	E' (psi)	E" (psi)	tan(δ)
Virgin 1	21.3	1.0	0.010	1,054,909	55,514	0.05262
Virgin 2	21.2	1.0	0.010	1,005,654	58,685	0.05836
Avgerage	**21.3**			**1,030,281**	**57,100**	**0.05549**
COV				3.38%	3.93%	7.30%

Table 4.3. DMA data for 70% stress ratios.

Data ID	Temp. (°C)	Freq. (Hz)	Max Δ (mm)	E' (psi)	E" (psi)	tan(δ)
30-70-1a	21.0	1.000	0.010	962,633	43,049	0.04472
30-70-1b	21.3	1.000	0.010	969,971	40,235	0.04148
30-70-2a	21.2	1.000	0.010	899,310	45,931	0.05107
30-70-2b	21.7	1.000	0.010	891,377	43,319	0.04860
Average	**21.3**			**930,823**	**43,133**	**0.04647**
COV (%)				4.43	5.40	9.10
50-70-1a	21.2	1.000	0.010	800,847	40,999	0.05119
50-70-1b	21.0	1.000	0.010	872,171	36,424	0.04176
50-70-2a	21.0	1.000	0.010	874,563	48,998	0.05603
50-70-2b	20.9	1.000	0.010	886,776	47,450	0.05351
Average	**21.0**			**858,589**	**43,468**	**0.05062**
COV (%)				4.54	13.42	12.30
70-70-1a	20.9	1.000	0.010	739,462	42,119	0.05696
70-70-1b	21.1	1.000	0.010	750,608	40,104	0.05343
70-70-2a	21.5	1.000	0.010	868,253	46,812	0.05392
70-70-2b	20.8	1.000	0.010	694,984	49,165	0.07074
Average	**21.1**			**763,327**	**44,550**	**0.05876**
COV (%)				9.69	9.35	13.85

Table 4.4. DMA data for 80% stress ratios.

Data ID	Temp. (°C)	Freq. (Hz)	Max Δ (mm)	E' (psi)	E" (psi)	tan(δ)
30-80-2a	21.1	1.000	0.010	1,004,240	50,677	0.05046
30-80-2b	21.9	1.000	0.010	1,196,351	51,020	0.04265
30-80-3a	20.8	1.000	0.010	1,068,246	51,623	0.04833
30-80-3b	21.1	1.000	0.010	1,089,922	48,088	0.04412
Average	**21.2**			**1,089,690**	**50,352**	**0.04639**
COV (%)				7.33	3.10	7.82
50-80-1a	20.8	1.000	0.010	905,543	46,710	0.05158
50-80-1b	20.9	1.000	0.010	905,976	43,295	0.04779
50-80-2a	21.0	1.000	0.010	914,509	39,638	0.04334
50-80-2b	20.9	1.000	0.010	969,632	49,026	0.05056
Average	**20.9**			**923,915**	**44,667**	**0.04832**
COV (%)				3.33	9.17	7.62
70-80-1a	21.0	1.000	0.010	777,586	52,160	0.06708
70-80-1b	21.2	1.000	0.010	850,468	50,884	0.05983
70-80-2a	21.2	1.000	0.010	869,660	44,015	0.05061
70-80-2b	21.4	1.000	0.010	933,449	45,613	0.04886
Average	**21.2**			**857,791**	**48,168**	**0.05660**
COV (%)				7.48	8.23	14.99

Table 4.5. DMA data for 90% stress ratios.

Data ID	Temp. (°C)	Freq. (Hz)	Max Δ (mm)	E' (psi)	E"(psi)	tan(δ)
30-90-3a	21.0	1.000	0.010	1,167,317	61,141	0.05238
30-90-3b	21.0	1.000	0.010	890,422	45,881	0.05153
30-90-4a	21.2	1.000	0.010	1,079,709	52,936	0.04903
30-90-4b	20.9	1.000	0.010	1,063,123	61,802	0.05813
Average	**21.0**			**1,050,143**	**55,440**	**0.05277**
COV (%)				11.03	13.60	7.30
50-90-2a	21.1	1.000	0.010	805,826	43,915	0.05450
50-90-2b	20.8	1.000	0.010	892,835	56,272	0.06303
50-90-3a	20.9	1.000	0.010	748,330	49,167	0.06570
50-90-3b	20.8	1.000	0.010	807,828	57,040	0.07061
Average	**21.0**			**813,704**	**51,598**	**0.06346**
COV (%)				7.32	12.07	10.64
70-90-3a	21.1	1.000	0.010	840,045	42,293	0.05035
70-90-3b	21.0	1.000	0.010	930,064	48,702	0.05236
70-90-4a	21.0	1.000	0.010	782,377	44,908	0.05740
70-90-4b	21.1	1.000	0.010	783,815	40,199	0.05129
Average	**21.1**			**834,075**	**44,025**	**0.05285**
COV (%)				8.32	8.32	5.95

Table 4.6. Average E' for each fatigue condition measured at 21°C.

	Average E' (psi) at 21°C		
	S = 70%	S = 80%	S = 90%
N = 30%	930,823	1,089,690	1,050,143
N = 50%	858,589	923,915	813,704
N = 70%	763,327	857,791	834,075

Table 4.7. Average tan δ for each fatigue condition measured at 21°C.

	Average tan δ at 21°C		
	S = 70%	S = 80%	S = 90%
N = 30%	0.04647	0.04639	0.05277
N = 50%	0.05062	0.04832	0.06346
N = 70%	0.05876	0.05660	0.05285

4.6 Figures

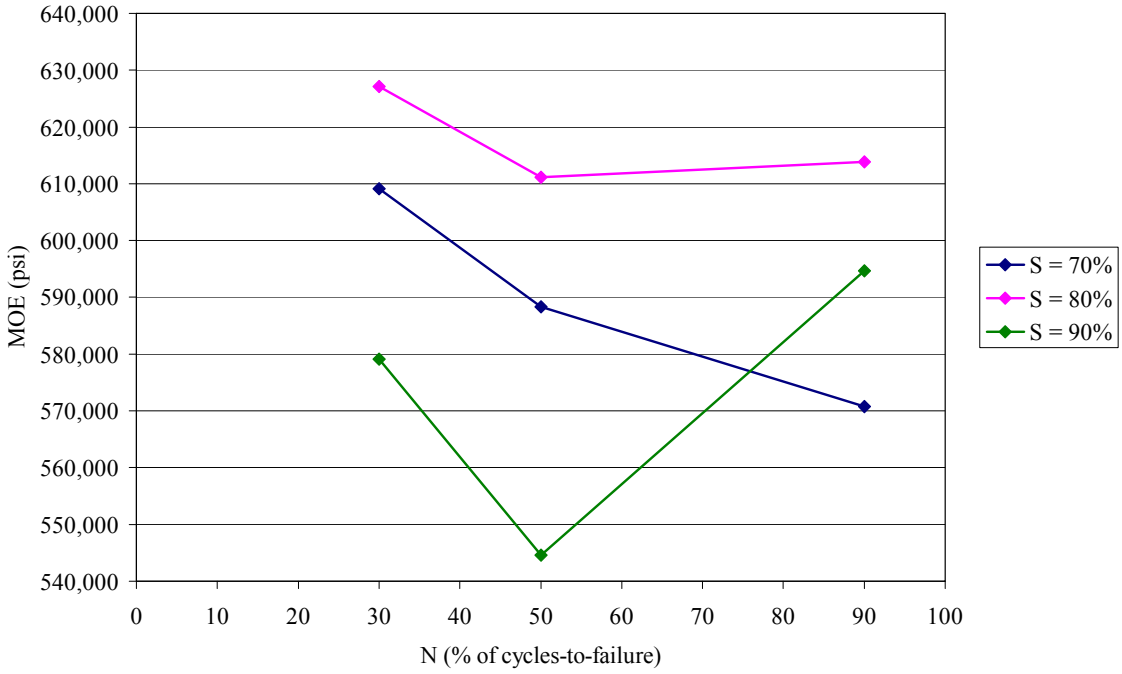

Figure 4.1. Average MOE vs. $\%N_{ult}$ for each stress ratio.

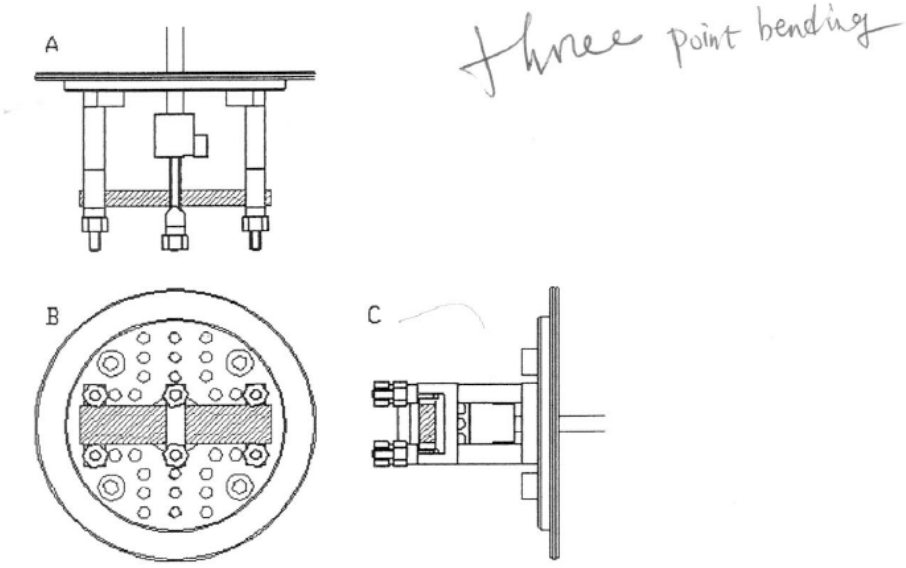

Figure 4.2. Top (A), front (B), and side (C) views of the 3-point bending apparatus used on Tritec DMA-8.

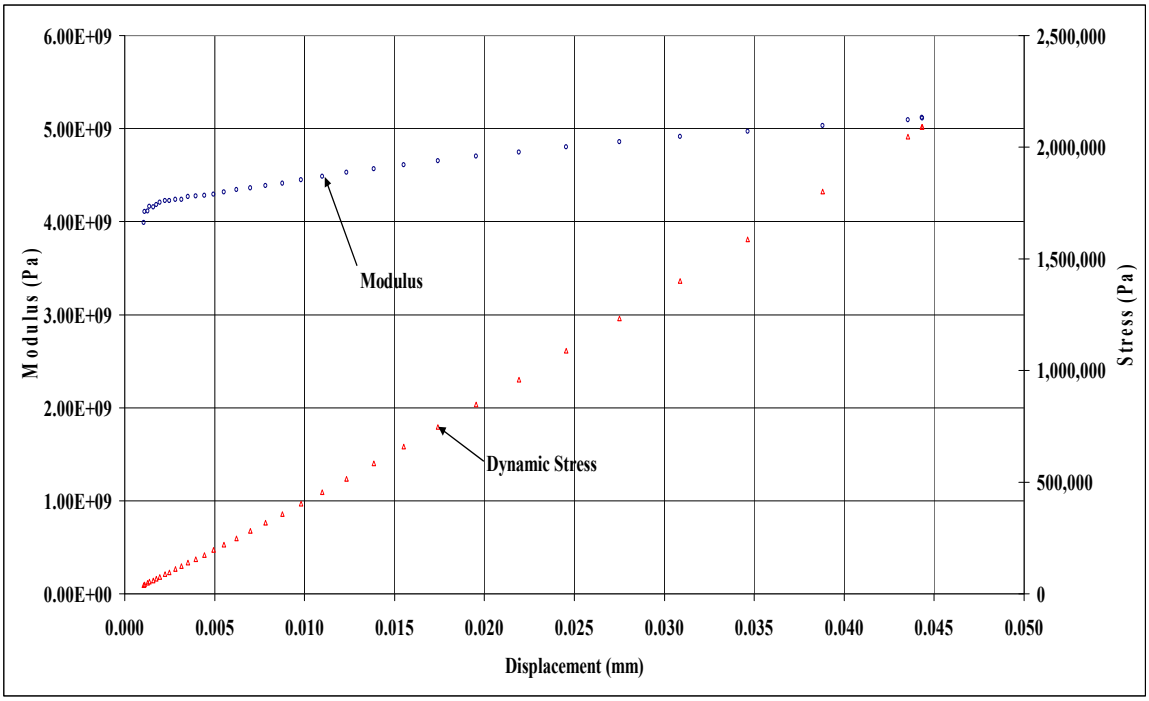

Figure 4.3. Dynamic strain sweep.

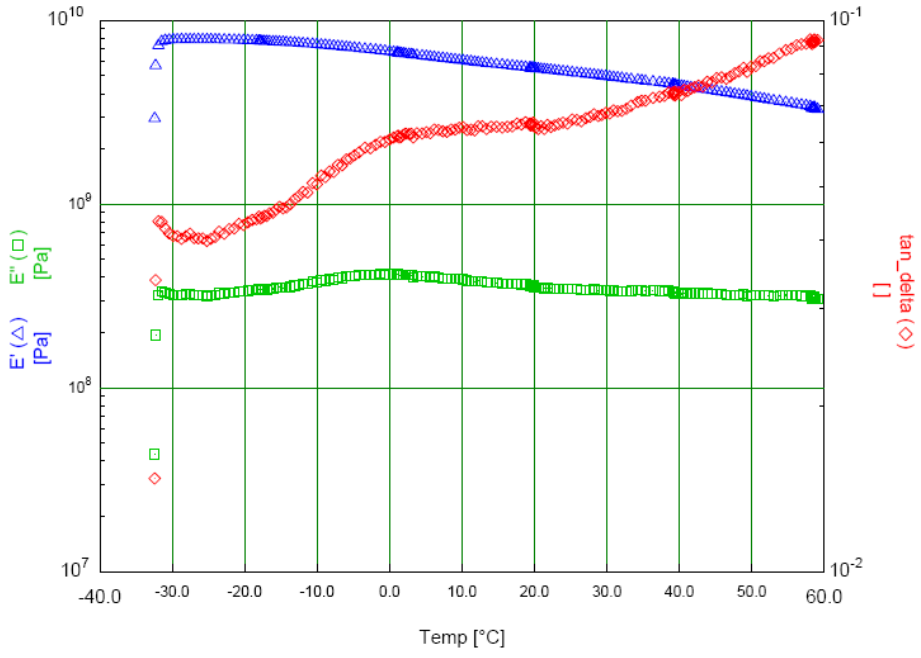

Figure 4.4. Virgin sample 1 temperature sweep.

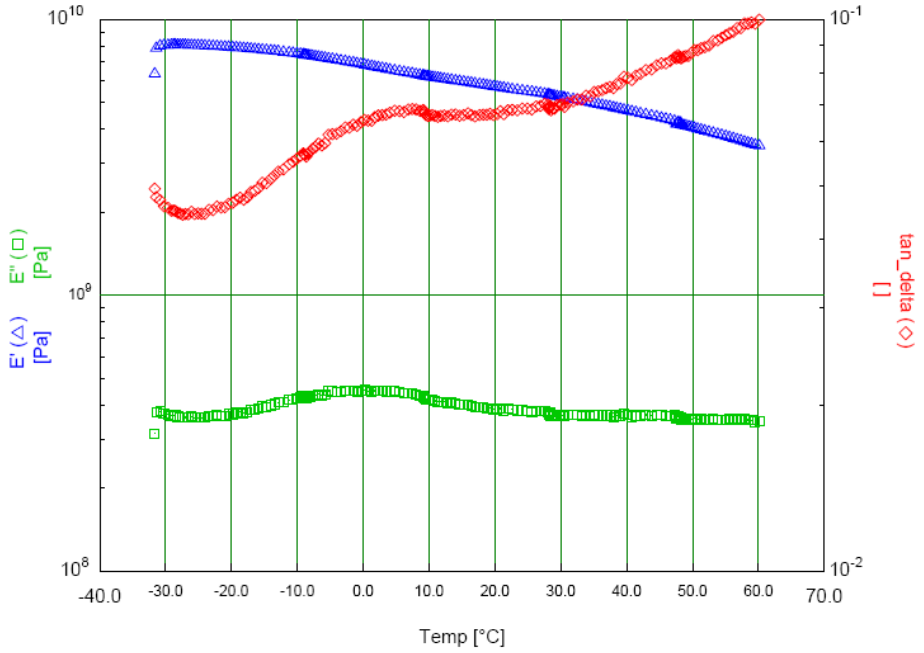

Figure 4.5. Virgin sample 2 temperature sweep.

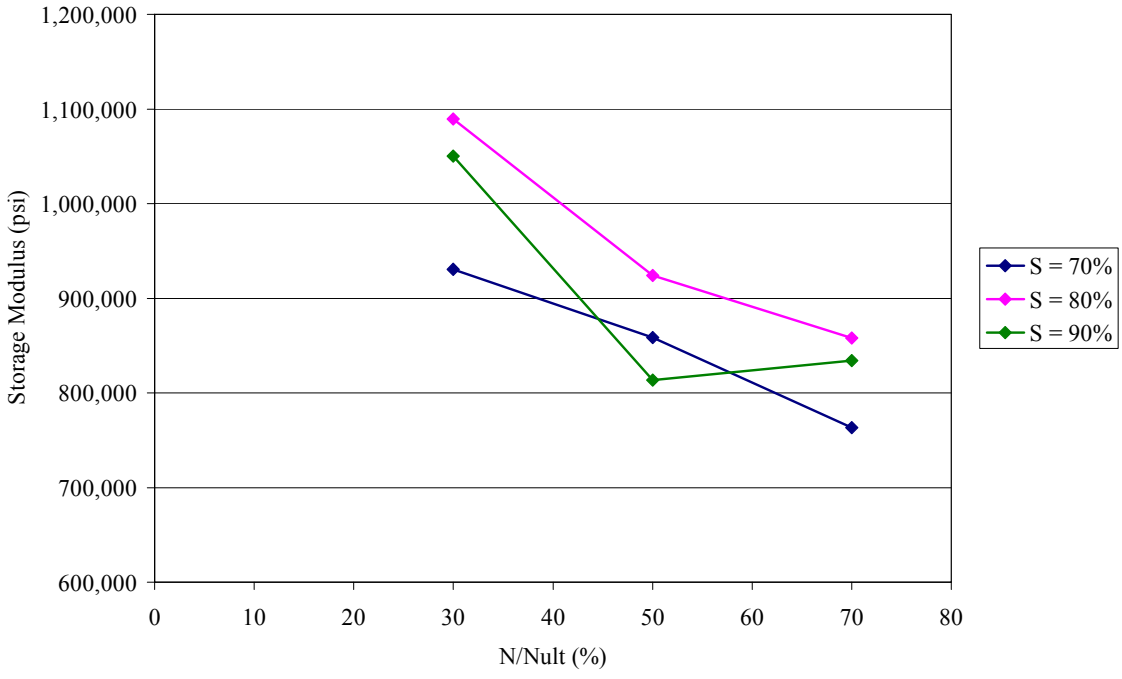

Figure 4.6. E' vs. N/N_{ult} for each stress ratio.

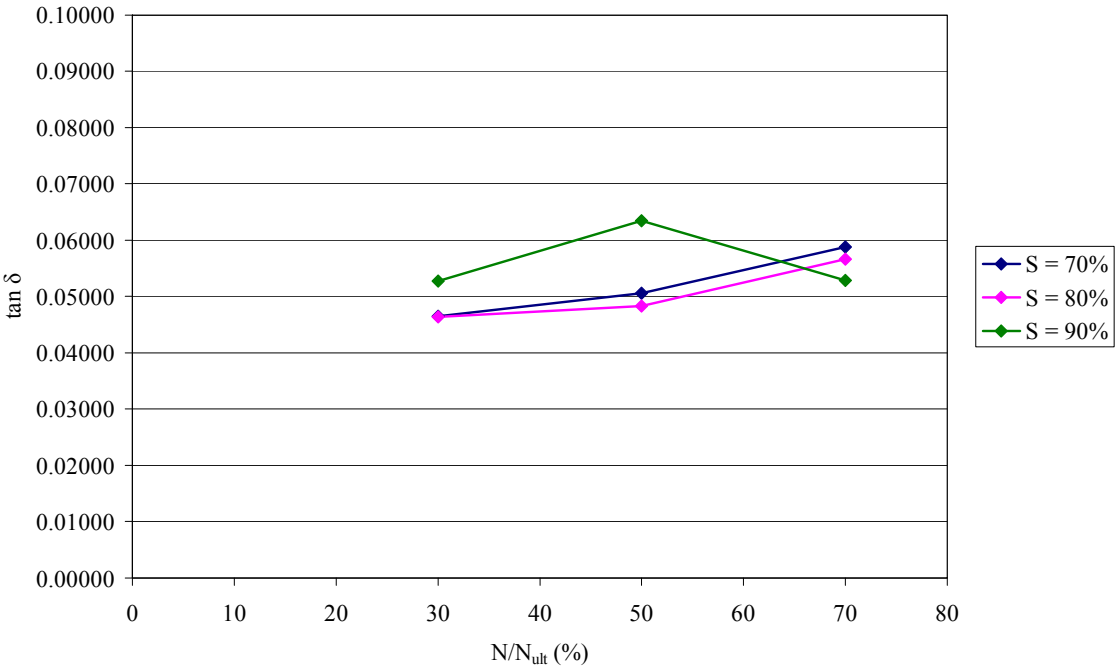

Figure 4.7. Tanδ vs. N/N_{ult} for each stress ratio.

CHAPTER 5 – MODELING OF FATIGUE-ACCUMULATED DAMAGE

5.1 Introduction and Background

It is a well-known fact that wood-plastic composites are established in the national and global marketplace for non-structural applications. What most people, including some professionals working in design today, are not aware of is that they are steadily becoming an applicable material for use in structural elements as well. Studies such as this and other work directly related to the development of design philosophy and procedures are helping pave the way for expanded use of WPC in current markets and the creation of new opportunities. With sustainability emerging as a primary concern in structural design, the environmental and economic attributes of WPC make it a viable subject for continued research and development. However, any new and industrious material is always accompanied by ambiguity or unknowns, from deformation characteristics and load-duration behavior to basic material response under an enormous range of variables such as cyclic stress, temperature, UV light, etc. The study and quantification of those variables are the very means by which researchers and professionals to narrow the gap between uncertainty and reliability, which many might argue is the foundation of engineering.

Damage and its evolution have been a popular area of interest to researchers of composites and still a fervently studied topic that requires a close look. Damage accumulation and both the experimental and theoretical modeling of the phenomenon are highly investigated fields. Many papers have been published in attempts to characterize damage in composite laminates and fiber-reinforced polymers (FRP and GFRP for glass) with varying levels of success (Gao, 1994; Dano, et al., 2006), but there is no or little

research that focuses explicitly on WPC. The mode of damage accumulation is also very important in how it is described and what models are implemented to do so. Modes of accumulating damage range from UV exposure, fungal deterioration, cyclic fatigue, temperature and humidity, etc. Not all studies in damage accumulation incorporate a physical means of damaging the material, but still make valid contributions to methods of modeling damage. For example, Gao (1994) related fatigue failure of graphite/epoxy laminates to the fundamental damage in its constituent laminae using a nonlinear damage model. Hwang and Han (1986) analytically evaluated cumulative damage by applying concepts of fatigue modulus, resultant strains, and multi-stress life prediction. One viable technique as proposed in this study (see Chapter 4) is to physically damage a composite material and then characterize it using dynamic mechanical analysis (DMA) and curve fitting. The chosen method for inflicting material damage in this study is single-amplitude fatigue, but it is important to note that much has been accomplished using other means. Temperature, humidity, and UV radiation have been shown to stiffen and slightly reduce the strength of GFRP composites using DMA and scanning electron microscopy (SEM) (Mouzakis, et al., 2007). Some more unconventional methods aim to classify specific industrial situations. One such study showed that fungal incubation caused yellow poplar to severely deteriorate in stiffness but the wood-plastic composite of the same species actually stiffened due to a reinforcing effect of the fungal hyphae (Schirp, et al., 2006). These types of findings can greatly improve the use and efficacy of WPC today.

Chapters 3 and 4 of this study established fatigue and dynamic mechanical analysis (DMA) data for one WPC (i.e., , coupled polypropylene - PPC) in flexure.

Samples were fatigued to failure at 3 different stress ratios and then 4 samples at each stress ratio were conditioned to 30%, 50%, and 70% of the ultimate failure cycles. The conditioned samples were then tested either in quasi-static flexure to measure the stiffness (E) or in dynamic mechanical analysis to measure storage modulus (E') and the lag angle (tanδ). Based on the testing data and the evidence of reductions in material and dynamic mechanical properties from these chapters, it is suggested that fatigue-accumulated damage is manifested through cyclic fatigue and micro-mechanical damage. The objectives for this chapter are as follows:

1) Model the accumulated fatigue damage for each fatigue stress ratio through a random distribution and a Weibull distribution.
2) Propose a kinetic law using the cumulative density function to designate a damage parameter and develop prediction models for both reduced stiffness and storage modulus.
3) Compare the CDM model results with test data obtained from quasi-static flexure and dynamic mechanical analysis.

5.2 1-Dimensional Damage Mechanics

5.2.1 Introduction to Damage Mechanics

Various modes of damage have been observed in composites such as matrix cracking, matrix-fiber debonding, fiber rupture, failure of interfacial adhesion in composite laminates, etc. Many studies have been done to measure and predict these failure modes with respect to strain, load, cyclic frequency, and number of cycles and to characterize their effects on stiffness, strength, and time to failure. It is difficult to

incorporate all variables into practical design procedures, which is why many authors choose to employ damage mechanics in an attempt to generalize failure at the meso-scale, or of the sample as a whole.

In principle, damage is a measurable parameter. It could be possible to physically measure damage from a noted reduction in cross-sectional area, volumetric change, or more practically, differences in the degradation and integrity of material properties. At a micro-scale, damage is in fact occurring through the failure modes usually at micro level as discussed above, but how to measure it precisely is the conundrum. In thermodynamic terms, temperature is a measurable damage parameter that may be used to describe the seemingly random agitation of atoms and other subatomic particles. While it is very difficult to characterize this agitation directly, one can measure temperature easily and then attempt to connect the dots. The same concept applies to composite materials, in that a carefully selected parameter may describe damage evolution.

For the applications of this study, damage mechanics is especially useful in describing damage under time- or cycle-dependent loading. For example, in flexural fatigue and creep models, it is difficult to portend the exact moment of rupture or track the damage evolution leading up to it. When a structural member is subjected to prolonged creep, it is most likely that damage begins to form through micro cracks on the tensile surface of a sample in bending that eventually manifest into macro cracks, resulting in a more gradual failure through the whole cross-section. The principles of fracture mechanics imply that if macro cracks can be observed forming in the material, failure could possibly be prevented. However, a sample subjected to fatigue will behave differently, but the mode of damage accumulation may be very similar. If the initiation

of such cracks are small and unpredictable, then they will go unnoticed, resulting in a sudden and brittle failure (especially in coupled polypropylene), which is disastrous in the design of critical members like beams and columns. For the purposes of this study, fracture mechanics is not a practical method because it does not effectively deal with multiple micro cracks. That is where Continuum Damage Mechanics (CDM) becomes an imperative resource. The principles are referred to as "continuum" because the material is treated as such, though there are multiple discontinuities (like micro cracks) actually present in the materials; whereas fracture mechanics attempts to identify the changes in field variables as functions of crack location and propagation. Fracture mechanics is a more useful approach in attempting to predict when and where a crack may appear and to approximate the number of cycles or level of stress it will take to either fracture a specimen or to reduce its stiffness in such a way that it is rendered structurally inept. CDM, on the other hand, intends to ignore the existence of cracks, rather treating the damage material as a continuum with reduced mechanical properties. This study utilizes a phenomenological approach in developing a kinetic law to simulate damage evolution and to thus describe fatigue damage. The most notable and measurable effect that fatigue damage has on a wood-plastic composite is stiffness, or the reduction of stiffness. However, rather than using a measured reduction in stiffness to define damage, we will use statistical data fitting of measured fatigue life to define and predict cumulative damage.

5.2.2 1-Dimensional CDM

The principles of 1-D Damage Mechanics are only functional under certain conditions. It does not work for multi-stress or multi-axis states of damage accumulation, but only when one stress dominates and in one direction, i.e., uni-axial tension or flexure with tension or compression as a dominated failure mode. The ideology behind these concepts relies on the fact that exact deformations in any directions other than the one being stressed (or strained) cannot be accounted for. Therefore, the principle of strain equivalence is applied to allow the application of damage mechanics regardless of the differences in nominal and effective stresses acting internally on the material as it is being loaded. Since Poisson's effect is essentially accounted for through strain equivalence, structural analysis can be performed using the nominal geometry, but taking into account the increase in effective stress, and therefore, the depreciation of stiffness.

5.2.3 Damage-Induced Reductions in Stiffness and Storage Modulus

The development of a one-dimensional damage mechanics model typically involves 3 major components: the damage variable, a damage activation function, and a damage evolution equation, or kinetic law. For the purposes of this study, the damage activation function can be ignored because due to the stress-strain nonlinearity observed throughout quasi-static testing, it can be reasonably assumed that some damage begins to grow early in any applied loading and does not commence at a damage threshold. The statistical model used in this study does not require the establishment of an elastic domain or a damage threshold for feasibility

It is necessary to build a phenomenological approach by first deriving the method for an isotropic material under a unidirectional stress, say tension (for simplicity). The method below displays the principles behind this derivation of a damage parameter and how it is used to indicate reduced material properties in composites. However, as previously mentioned, this study employs statistical data fitting of fatigue life to establish a damage parameter, but the application is the same. The following relationship states that the apparent stress in a sample is proportional to the axial load over the initial undamaged area.

$$\bar{\sigma} = \frac{P}{A_0} \tag{5.1}$$

As the damage is accumulated in the material, a small reduction in cross-sectional area can be observed. The ratio of this loss in area to the initial area is stated as the measurable damage parameter,

$$\omega = \frac{A_{LOST}}{A_0} \tag{5.2}$$

The actual stress in the material through damage accumulation, or the effective stress, cannot be directly measured since the stresses vary through assumedly formed micro cracks. If damage is the result of interfacial debonding; however, then there would be no change in cross-sectional area. Even though the formation of micro cracks is the more likely cause for damage, the same concept can be applied, and effective stress can be related to a damage variable ω as

$$\sigma = \frac{P}{A_0 - A_{LOST}} = \frac{P}{A_0(1-\omega)} = \frac{\bar{\sigma}}{1-\omega} \tag{5.3}$$

or

$$\overline{\sigma} = \sigma(1-\omega) \tag{5.4}$$

Applying the principle of strain equivalence, it is assumed that apparent and effective stresses can both be related by the same elastic deformation, but the damaged material has lost a fraction of its undamaged stiffness.

$$\hat{E}\,\varepsilon = E\varepsilon(1-\omega) \tag{5.5}$$

or

$$\hat{E} = E(1-\omega) \tag{5.6}$$

Of course, the main motif behind this study is that the stress-strain relation of WPC is highly nonlinear, and therefore, does not necessarily obey Hooke's Law for any significant portion of loading. Hence, the CDM damage variable ω was selected based on curve fitting and statistical distribution and then applied to equation (5.6) in the same way, the procedures of which are outlined in the following section.

5.2.4 Kinetic Law

The rate of damage accumulation is generally represented by a kinetic equation. Introducing some relationship that quantifies this variable over a selected domain, i.e., stress, time, number of cycles, temperature, etc., constitutes a proposed kinetic law. This study proposes that the kinetic law for measuring fatigue damage may be given as the cumulative density function through Weibull or random distributions. Both statistical methods will be detailed here and discussed in Section 5.3.

The random distribution function is very simply applied, where the damage parameter is

$$\omega = \frac{1}{N_{ult}} \tag{5.7}$$

This means that at the maximum number of cycles statistically represented, the damage parameter would be equal to 1, or 100% of damage accumulated, which would theoretically constitute failure. At 30% of maximum cycles to failure, the damage is $N_{30\%}/N_{max}$, at 50% of maximum cycles to failure, the damage is $N_{50\%}/N_{max}$ and so on. Refer to Table 5.1 for N_{max} and corresponding condition levels used to determine this damage parameter.

The procedure for the Weibull distribution is a little more involved in that the recorded fatigue life data in each sample set is curve-fitted by estimating the cumulative density function to obtain Weibull parameters. Then the cumulative density at each fatigue level is recalculated using the parameters. This function is implemented as follows, beginning with the general form of the probability density function (Tanimoto, et al, 1979):

$$f(N) = \frac{\beta}{\alpha}\left(\frac{N}{\alpha}\right)^{\beta-1} e^{-\left(\frac{N}{\alpha}\right)^{\beta}} \tag{5.8}$$

where α is the scale parameter that locates the life distribution and β is the shape parameter that serves as the inverse measure of the dispersion in fatigue life results. By integrating the probability density function f(N) in equation (5.8), the cumulative density function can be determined as

$$P_f(N) = \int f(N)dN = 1 - e^{-\left(\frac{N}{\alpha}\right)^{\beta}} \tag{5.9}$$

$P_f(N)$ is the probability of failure that will represent the cumulative damage parameter ω. The scale and shape parameters can be determined by taking the natural logarithm twice in each side of equation (5.9) as

$$\ln\left[\ln\left(\frac{1}{1-P_f(N)}\right)\right] = \beta\ln(N) - \beta\ln(\alpha) \tag{5.10}$$

This expression can be considered as a linear function in the form of Y=BX+C where Y is the double logarithmic on the left side, B is β, X is ln(N), and C is βln(α). $P_f(N)$ can be estimated for regression plotting purposes using one common technique, the mean rank. The mean rank is a nonparametric estimate of the cumulative distribution function based on failure order. There are several variations for this estimation one can utilize, such as median rank, approximation to White's plotting positions, and the Kaplan Meyer estimates (Dodson, 2006). Yang, et al. (2008) utilized the median rank and Kashaba (2003) utilized the mean rank, both yielding successful results. It is more or less up to the author to judge which estimation is preferred, based on scattering of data. The mean rank is given by the following expression:

$$P_f(N) = \frac{i}{n+1} \tag{5.11}$$

In equation (5.11), i is the failure serial number and n is the total number of test samples in each set. Plotting the expression in equation (5.10) for each stress ratio, 70%, 80%, and 90% and performing a linear regression yields constants for B and C. See Figures 5.1 – 5.3. Then α is solved for algebraically from

$$\alpha = e^{\left(\frac{-C}{\beta}\right)} \tag{5.11}$$

Once the fitting parameters have been obtained, equation (5.9) is used to calculate the damage parameter ω for the appropriate fatigue level in each set sample set. For example, $\omega_{50\%}$ for a given stress ratio (30, 50, or 70%) is found by entering $N_{50\%}$ and the corresponding α and β into equation (5.9) and so forth. Table 5.2 shows the regression equations and the values for α and β and Table 5.3 shows the calculated damage parameters for all 9 conditions using both statistical methods. Further calculations were performed to yield the mean-time-to-failure (MTTF),

$$MTTF = \alpha\Gamma\left(1+\frac{1}{\beta}\right) \tag{5.12}$$

the standard deviation (SD),

$$SD = \alpha\sqrt{\Gamma\left(1+\frac{2}{\beta}\right)-\Gamma^2\left(1+\frac{1}{\beta}\right)} \tag{5.13}$$

and the coefficient of variation (COV),

$$COV = \frac{SD}{MTTF} \tag{5.14}$$

in each sample set. These values are also observed in Table 5.2. Once all damage parameters are obtained, equation (5.6) is employed for each condition, yielding a modeled reduced stiffness and storage modulus at each condition, which can be found in Table 5.4. Figures 5.4 – 5.9 are especially useful, graphically displaying measured and modeled reduced stiffness and test-model error overlap. Figures 5.4 – 5.6 show the actual and modeled degradation in stiffness for the sample sets tested at S = 70, 80, and 90%, respectively. Naturally, Figures 5.7 – 5.9 serve the same purpose for storage modulus.

5.3 Results and Discussion

This discussion refers to Figures 5.4 – 5.6 in comparing the curves for reduced stiffness and Figures 5.7 – 5.9 in comparing the curves for reduced storage modulus. All plots show the COV calculated in equation (5.14) and the COV for the test data determined in previous chapters in the form of error bars. The test data is shown in solid blue, the Weibull model in dashed red, and the random model in solid green. It is important to note in comparing the model curves with test data that actual predicted values of E and E' compared with measured values are of less significance than the trend in reduction among cycle levels in each set, especially for the random case. The reason for this is the initial modulus that receives the damage reduction in equation (5.6) is based on an average of tested virgin samples that have a significant amount of data dispersion themselves. The individual samples that get fatigued may have a higher or lower initial modulus, but that concept is neglected in comparison. For example, the average initial flexural modulus of PPC was around 636,000 psi. A damage parameter that is based on fatigued samples is applied to this value to find a predicted reduced stiffness. Those same fatigued samples get tested in flexure up to 50% of their "ultimate" modulus to measure a real reduced stiffness. However, if this particular sample had an actual initial stiffness of 500,000 psi or 750,000 psi, which is possible but unlikely, then the many things slightly change with a small trickle effect. That's why it is informative to compare the values, but the degradation trend is a better indicator of accuracy.

By inspection, the random model predicts a much more drastic reduction rate in both properties than is actually observed. The model is simply based on intuition (a phenomenological approach) that the % of damage accumulation is linearly proportional

to the % of reduction in material properties. The proposed damage parameter for the random model is based on the ratio of the fatigue condition level to the maximum failure cycle in each sample set. Since the fatigue condition level prior to conditioning was calculating by taking fractions of the average ultimate failure cycle in each set, the damage parameters are very similar for each stress ratio, when in physical reality that should not be the case for an accurate model. When the damage parameter is applied to equation (5.6), the virgin stiffness and storage modulus for each stress ratio (which are the same before any conditioning is applied) take a large reduction that is nearly independent of stress ratio and nearly dependent on the difference between average N_{ult} and maximum N_{ult} in each set. For the fatigue data in this study, those differences happened to be substantial, but not large enough to constitute pure randomness. The random model does not really have an applicable error associated with it either, other than that directly related to the error in the fatigue life data, which ranged between 10 and 27%.

The Weibull model, on the other hand, provided more reliable results. Observing the plots and comparing the red and blue curves, one can note that the general model trend makes sense and compares well with the tested data, with the exception of the S = 90% set. The error bars that reflect variation in each data point are indicated, with the line weights and types matching that of their series. Each chart for 70% and 80% stress ratios shows some overlap in the error bars, which is very positive considering the randomness observed in fatiguing. The Weibull prediction gives a slight initial reduction in material properties between $30\%N_{ult}$ and $50\%N_{ult}$ with more exaggerated but still gradual progression up to $70\%N_{ult}$, which is most likely the way damage propagates

through the material. Observed and modeled E/E_0, E'/E'_0, and the overall losses in initial stiffness and storage modulus can be observed in Table 5.5. The comparisons are fairly adequate in general, but are especially close for the lowest stress ratio, S = 70%, suggesting that both the fatiguing process and the modeling become unstable at higher applied stress ratios.

The reduction data in Table 5.5 for S = 90% should be disregarded since the material properties of interest fluctuated against the noted trend of the other loading amplitudes. This set and the ensuing curve fitting to obtain Weibull parameters was flawed from the beginning, since tests consistently showed an increase in stiffness and storage modulus between N = 50% to N = 70%. This data set actually provided evidence counterintuitive to the concept of damage accumulation and, if accompanied by more test samples or similar results from additional stress ratios, would beg for an answer to how a WPC could stiffen upon being fatigued. However, this increase should be considered a fluke or an outlier in the evident trend of fatigue damage accumulation in WPC, and that trend is that fatigue life cycles can be used to estimate loss in material properties through the imposition of a statistical kinetic law.

5.4 Concluding Remarks

Based on the testing data and the evidence of reductions in material and dynamic mechanical properties from the previous two chapters, fatigue-accumulated damage was assumed to have manifested in the samples through cyclic fatigue and micro-mechanical damage, although a damage mode was not specifically modeled. In this chapter, the accumulated fatigue damage for each stress ratio was modeled via random distribution

and a two-parameter Weibull distribution. A kinetic law using the cumulative density function was proposed in order to establish a continuum damage parameter. Prediction models for both reduced stiffness and storage modulus revealed that the effects of the randomness in fatigue life data observed in Chapter 3 are two-fold in terms of how we think about damage in WPC.

First, the Weibull distribution was able to shape and scale the somewhat erratic phenomenon of this composition being able to withstand anywhere between 1,000 cycles and over 1.2 million cycles over a relatively small stress increase. The Weibull parameters that governed the values of the damage parameters were solved for through regression of the real test data, so even large scattering can be reasonably accounted for by estimating the shape of the distribution. The shape parameter loses little accuracy with scattering, making it a valuable tool for fitting the behavior of lots of short-fiber composites, not just WPC. This evidence alone makes the task of tracking fatigue damage accumulation far less daunting for future authors and designers.

Second, the fatigue life data collected in this study was some of the most random data available for WPC (samples lasting over 1,000,000 cycles at moderate stress ratio), but yet was still not random enough to be accurately modeled by a random distribution. The differences between developed damage parameters for each stress ratio were small since average N_{ult} was usually fairly close to maximum N_{ult}. No matter how random the fatigue data may be, damage evolution itself may only be modeled with a random distribution for many samples under the same stress ratio. Linearly relating fatigue cycles to % loss in E without using a damage parameter that reflects stress ratio could theoretically work if the mode of damage accumulation were assumed to be linear.

However, since stress and strain have a proven nonlinear relationship, an intuitive author would have to conclude that stress-induced damage accrues nonlinearly as well. A distribution must be used that takes into account the entire distribution, i.e. all data points, for each stress ratio so that the dispersion can actually be reflected in the damage parameter.

In this study, quality control was of chief concern, and the equipment seemed to work well. All necessary entities were tuned and tested prior to obtaining actual data. As mentioned in Appendix C, the stress amplitudes in fatigue were carefully monitored graphically and electronically. The randomness in the scattering of the data and the difficulty that entailed collecting reliable fatigue data can be attributed to that inherent to all short-fiber composites. Short-fiber composites are known to have low fiber-polymer interface strength (which a coupling agent cannot fully compensate), low fiber pull-out strength, and although they are treated as homogenous and isotropic, they truly are not at a micro scale. Applying damage mechanics at a macro level merely estimates behavior patterns at a micro level and then relates it back to a structural member as a whole, without accounting for the infinite ways that the short fibers are oriented and how they can fail.

5.5 References

ASTM E739-02. "Standard Practice for Statistical Analysis of Linear or Linearized Stress-Life (S-N) and Strain-Life (e-N) Fatigue Data." American Society for Testing Materials.

Dodson, B. "The Weibull Analysis Handbook." ASQ Quality Press, Milwaukee, WI. 2nd Edition, 2006.

Gao, Z. "A Cumulative Damage Model for Fatigue Life of Composite Laminates." Journal of Reinforced Plastics and Composites, Vol. 13, pp. 128-141, 1994.

Han, K.S., and Hwang, W., "Cumulative Damage Models and Multi-Stress Fatigue Life Prediction." Journal of Composite Materials, Vol. 20, pp. 125-153, 1986.

Han, K.S. and Hwang, W., "Fatigue of Composites – Fatigue Modulus Concept and Life Prediction." Journal of Composite Materials, Vol. 20, pp. 154-165, 1986.

Khashaba, U. A., "Fatigue and Reliability Analysis of Unidirectional GFRP Composites under Rotating Bending Loads." Journal of Composite Materials, Vol. 37, pp. 337-331, 2003.

Mouzakis, D. E., Galiotis, C., Zoga, H. "Accelerated Environmental Ageing Study of Polyester/glass Fiber Reinforced Composites (GFRPCs)." Composites Part B, Vol. 39, pp. 467-475, 2008.

Wolcott, M.P., Schirp, A. "Fungal Degradation of Wood-Plastic Composites and Evaluation Using Dynamic Mechanical Analysis." Journal of Applied Polymer Science, Vol. 99, pp. 3138-3146, 2006.

Yang, H.S., Qiao, P., Wolcott, M.P. "Fatigue Characterization and Reliability Analysis of Wood Filled Polypropylene Composites." Polymer Composites, accepted, 2008.

5.6 Tables

Table 5.1. Maximum cycles and condition levels for random distribution.

S (σ/σ_{ult})	N_{max}	30%N_{avg}	50%N_{avg}	70%N_{avg}
70%	1,289,441	325,478	542,464	759,449
80%	120,013	26,915	44,858	62,801
90%	5,946	1,627	2,712	3,797

Table 5.2. Curve fitting data and Weibull parameters.

S (σ/σ_{ult})	Regression Equations	β	α	MTTF	SD	COV (%)
70%	y = 5.423x - 75.763	5.423	1,168,157	1,077,579	229,146	21.26
80%	y = 3.110x - 35.832	3.110	100,791	90,152	31,720	35.19
90%	y = 8.041x - 69.558	8.041	5,711	5,380	795	14.78

Table 5.3. Damage parameters (%) obtained from Weibull distribution (left) and random distribution (right).

	$\omega = P_f(N)$			$\omega = 1/N_{ult}$		
	S=70%	S=80%	S=90%	S=70%	S=80%	S=90%
N = 30%	0.09777	1.63	0.0041	25.24	22.43	27.36
N = 50%	1.549	7.75	0.25	42.07	37.38	45.61
N = 70%	9.23	20.52	3.68	58.90	52.33	63.86

Table 5.4. Measured and modeled values of stiffness and storage modulus for both Weibull and random distributions.

	Measured E (psi)			**Measured E' (psi)**		
	S = 90%	S = 80%	S = 70%	S = 90%	S = 80%	S = 70%
$N_{30\%}$	579,174	627,182	609,166	1,050,143	1,089,690	930,823
$N_{50\%}$	544,655	611,220	588,322	813,704	923,915	858,589
$N_{70\%}$	594,644	613,868	570,795	834,075	857,791	763,327
	Weibull Model E (psi)			**Weibull Model E' (psi)**		
	S = 90%	S = 80%	S = 70%	S = 90%	S = 80%	S = 70%
$N_{30\%}$	636,032	625,672	635,436	1,030,239	1,013,458	1,029,274
$N_{50\%}$	634,466	586,784	636,058	1,027,702	950,467	1,014,321
$N_{70\%}$	612,631	505,565	577,370	992,334	818,910	935,219
	Random Model E (psi)			**Random Model E' (psi)**		
	S = 90%	S = 80%	S = 70%	S = 90%	S = 80%	S = 70%
$N_{30\%}$	475,506	493,411	462,014	770,220	799,223	748,366
$N_{50\%}$	368,470	398,315	345,949	596,845	645,187	560,365
$N_{70\%}$	261,435	303,218	229,884	423,471	491,150	372,364

Table 5.5. Stiffness and storage modulus reductions for all conditions.

	Weibull Modeled E/E_0 & E'/E'_0			Measured E/E_0 & E'/E'_0		
	S = 90%	S = 80%	S = 70%	S = 90%	S = 80%	S = 70%
$N_{30\%}$	1.000	0.984	0.999	0.911	0.986	0.958
$N_{50\%}$	0.997	0.923	1.000	0.856	0.961	0.925
$N_{70\%}$	0.963	0.795	0.908	0.935	0.965	0.897
Reduction	**3.68%**	**20.52%**	**9.23%**	**6.51%**	**3.49%**	**10.26%**

5.7 Figures

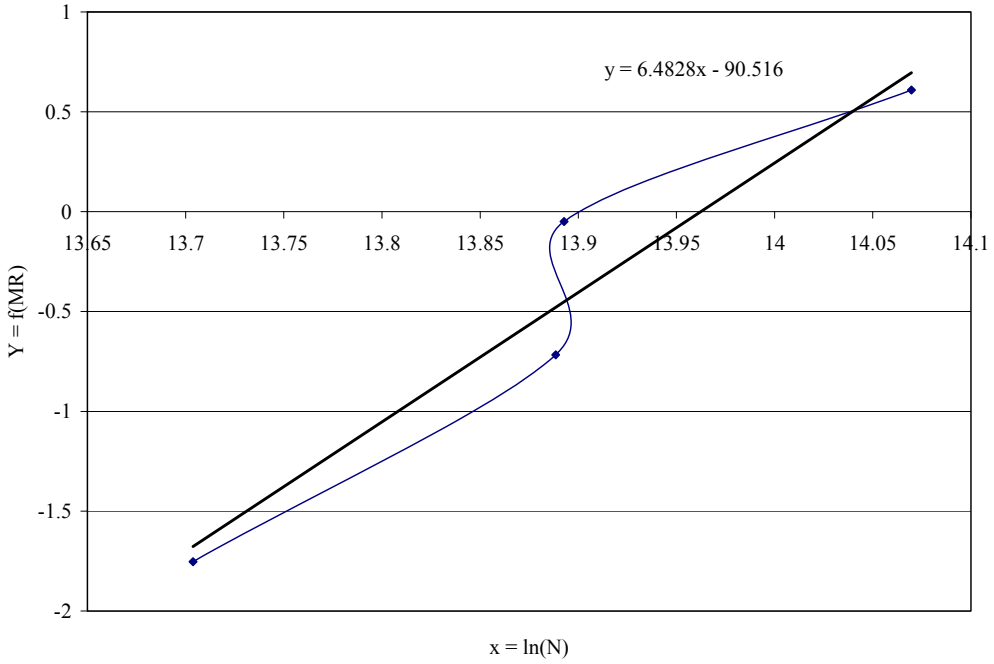

Figure 5.1. Linear regression for 70% stress ratio.

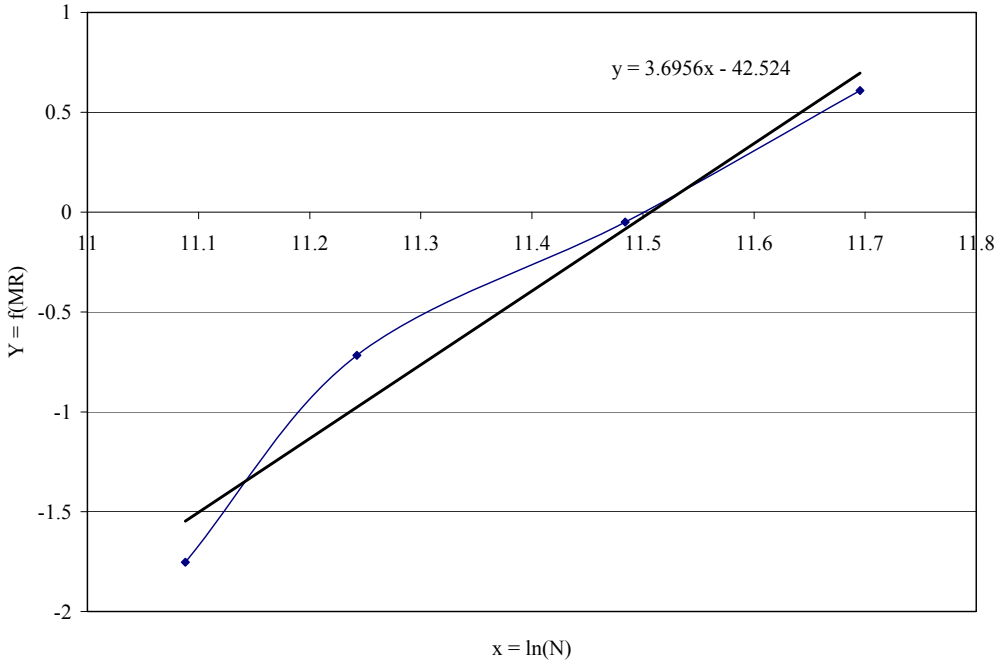

Figure 5.2. Linear regression for 80% stress ratio.

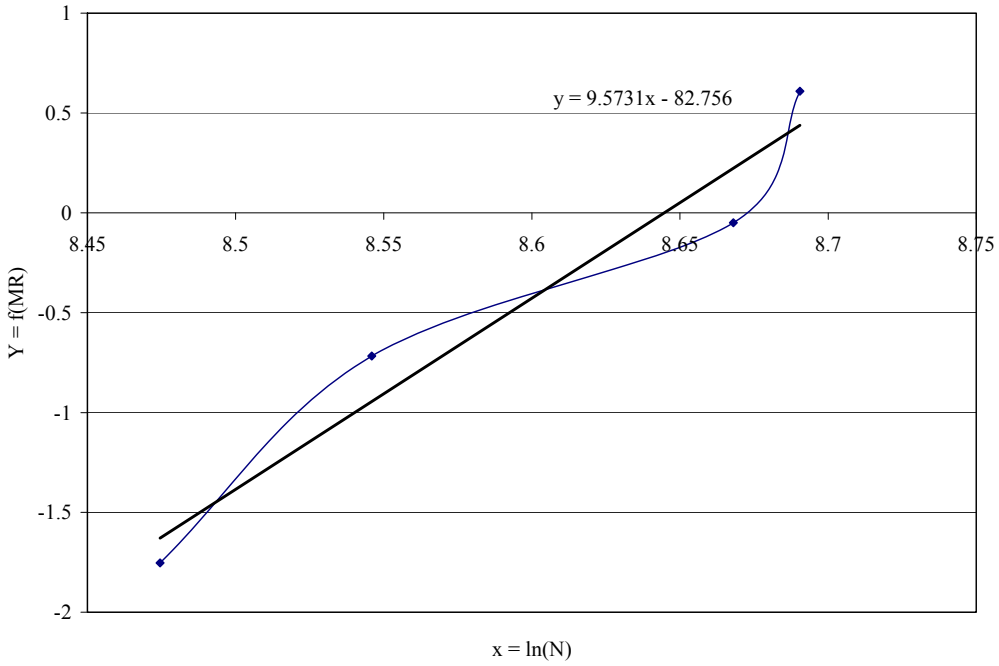

Figure 5.3. Linear regression for 90% stress ratio.

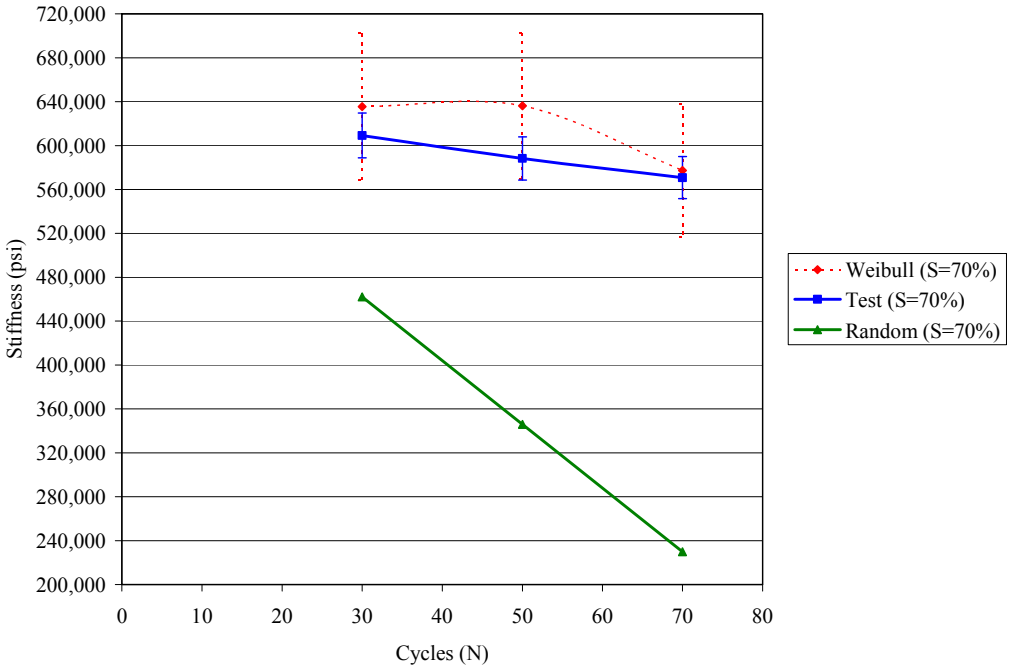

Figure 5.4. Modeled vs. measured stiffness for S = 70%.

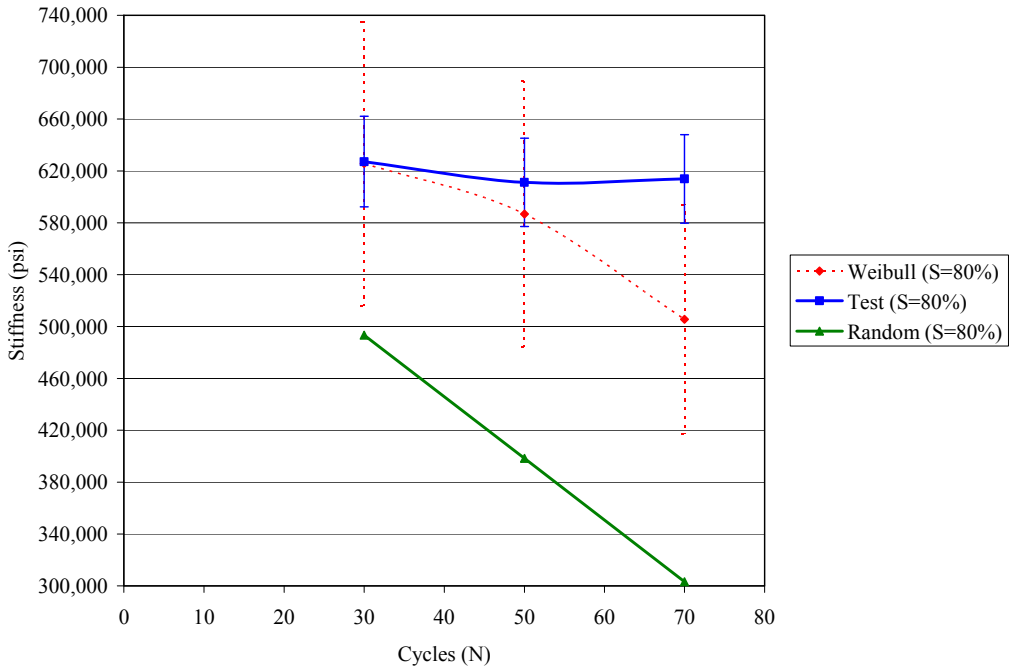

Figure 5.5. Modeled vs. measured stiffness for S = 80%.

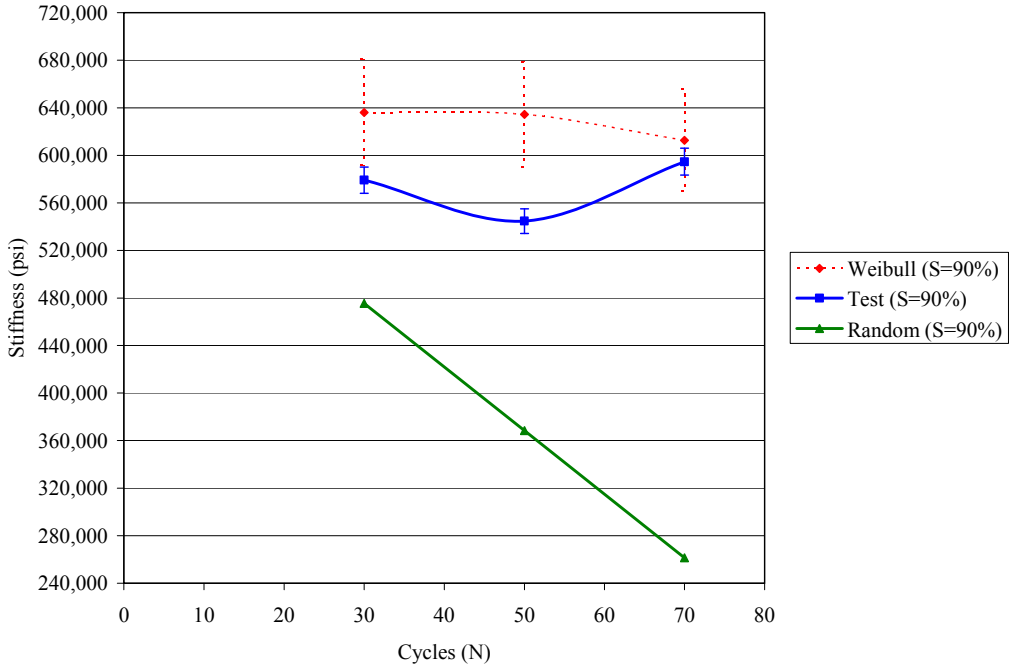

Figure 5.6. Modeled vs. measured stiffness for S = 90%.

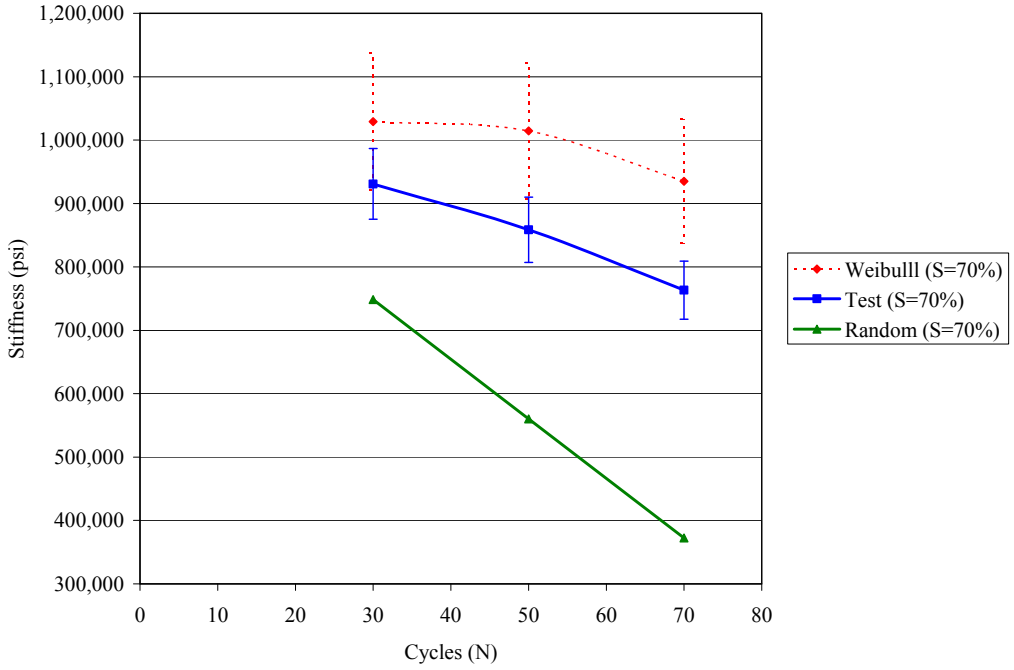

Figure 5.7. Modeled vs. measured storage modulus for S = 70%.

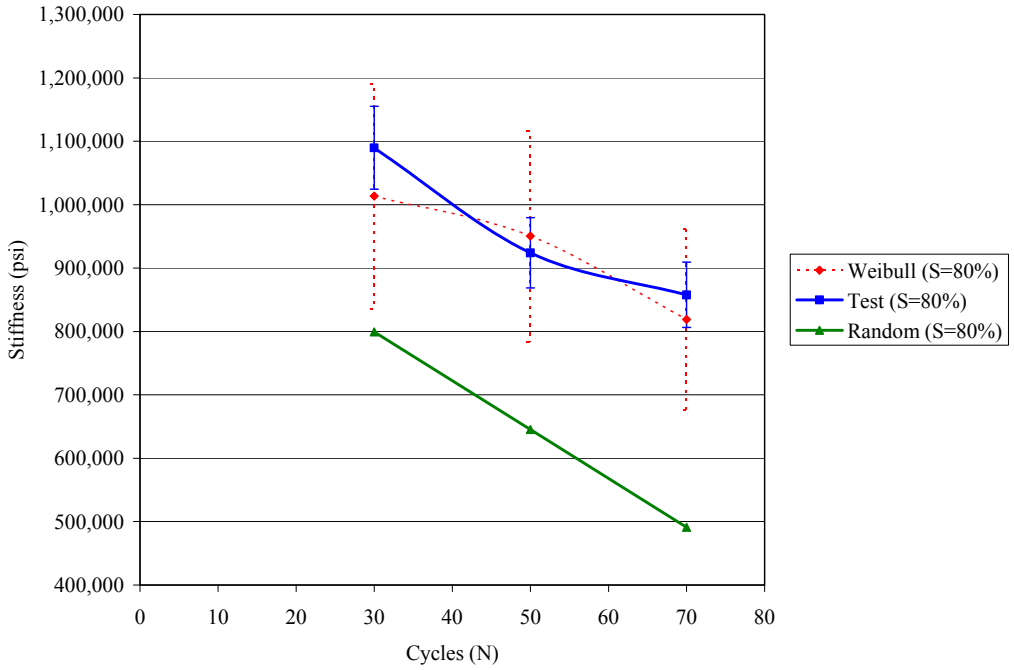

Figure 5.8. Modeled vs. measured storage modulus for S = 80%.

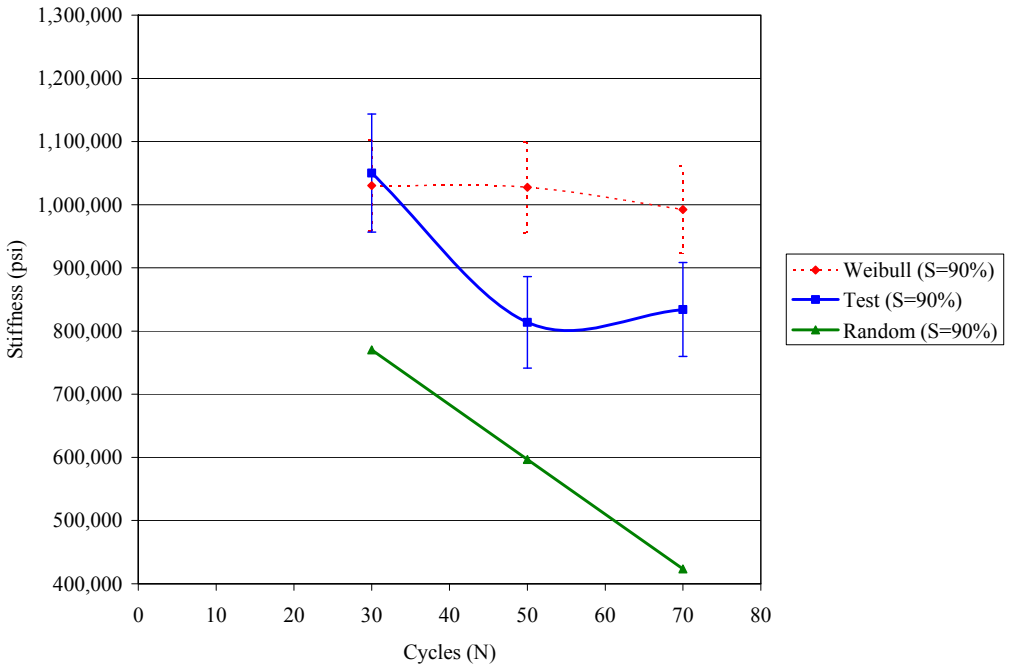

Figure 5.9. Modeled vs. measured storage modulus for S = 90%.

CHAPTER 6 – CONCLUSIONS AND RECOMMENDATIONS

Wood-plastic composites were thoroughly investigated in this study and have recently been a popular subject for many authors. They provide a unique and interesting new material that is durable and highly resistant to corrosion, fungal decay, bacteria and marine-inhabited organisms. WPC also has its disadvantages in that it lacks in relative stiffness, is susceptible to sunlight in numerous ways, and possesses the design ambiguities of all short-fiber reinforced composites. The need for continued education, research, and development of accurate design philosophy is evident. WPC is a useful and some would argue a rare type of composite in that it utilizes natural wood fibers, which should warrant the attention of all engineers, future engineers, and any persons interested in a sustainable material that can be manufactured from recycled products and has a healthier impact on the environment. This paper investigated and attempted to provide feasible solutions to two of the difficulties that currently limit the widespread use of WPC in the structural and construction market: the prediction and characterization of stress strain-behavior and modeling of damage accumulation.

A large and significant portion of this study was accomplished in Chapter 2, which was focused on stress-strain material nonlinearity. Quasi-static mechanical properties of coupled and uncoupled polypropylene (PPC and PP, respectively) and high density polyethylene (HDPE) were evaluated in tension and flexure. PP and HDPE in flexure were comparable in all respects, from physical characteristics such as color, texture, and their observed ductile fracture, to mechanical properties like stiffness and ultimate strength. PPC performed better than its uncoupled counterpart but exhibited a more brittle snapping at rupture due to the improved interface adhesion by the coupling

agent. Consistent results were achieved for all mixtures loaded in tension. Again, PPC performed the best of all compositions with nearly double the yield strength as HDPE, which made it a good material to use in later chapters.

It was also evident in this part of the study that an increased rate of applied stress improved mechanical properties as verified through flexural tests at strain rates of 2.7, 5, 10, 20, 30, and 40 mm/min, but only at the expense of reliability and increased uncertainty in the true failure mechanism. Properties were affected by uncontrollable or limited variables in these tests, such as sample collection rate and the effect of simulated dynamic loads at the highest rates. For both experimental and analytical purposes, it is recommended that both the mechanical properties (e.g., modulus of elasticity and ultimate strength) increase with increasing load rate, and the data measured between 2 to 30 mm/min are reliable in design application.

The most revealing work in this chapter verified that the hyperbolic tangent function can be used to fit the tensile and flexural stress-strain data and demonstrated great potential for load-deflection analysis in axial and bending members. The function's constants were highly accurate in representing modulus of elasticity and rupture for all test scenarios. The relationship can be used to predict strains as a function of stress at a wide range of points on the modeled curves with excellent precision, but tends to slightly underestimate initial stiffness in tension and flexure. The P-Δ models presented for tension and bending can be implemented to numerically calculate member elongation and displacements at any point along any rectangular beam.

The concept of hyperbolic tangent fitting as a nonlinear stress-strain constitutive relation has been successfully explored by previous authors under different test scenarios,

compositions, and other circumstances. It has been verified in this study that the nonlinear P-Δ behavior of the structural members can be modeled using the function at coupon level, thus eliminating the necessity of the full-scale structural tests and aiding engineering design of WPC members. It should be noted here that structural members that may be susceptible to critical impact loads should not be designed to resist those loads using the methods of Chapter 2 without further analysis, as they proved less accurate at higher load rates.

Once the static behavior was well-established, the fatigue behavior of one mixture (PPC) was evaluated. The fatigue characterization and analysis in Chapter 3 served to establish the cycle life (N) of the WPC under various stress amplitudes (S), which would be used as a baseline to condition the samples and thus accumulate fatigue damage. In Chapter 4, the effects of fatigue damage accumulation were evaluated using quasi-static flexure and DMA tests to measure degradation of stiffness and storage modulus, respectively. The methods showed that the flexural stiffness properties from the quasi-static tests as well as the storage modulus from the DMA tests followed intuition and decreased as the condition levels of stress ratio and cycle increased. The DMA tests were especially sensitive to damage accumulation and produced more drastic changes in the dynamic mechanical properties (e.g., storage and loss modulus and tanδ) when compared to the quasi-static flexural tests. The dynamic properties from the DMA tests might be a better indicator of damage accumulation than the ones from the quasi-static tests due to their sensitivity and ability to control variables. For future interests, it is suggested that the stress inflicted and controlled by DMA could be used to more effectively induce and

measure the cumulative damage so that the modeled and tested data would be based on identical parameters, tolerances, strains, etc.

Based on the test data, the fatigue-accumulated damage was assumed to have manifested in the samples through cyclic fatigue and micro-mechanical damage, although a damage mode was not specifically recognized as predominant. The higher stress amplitude and higher percentage of conditioning (%N) generally resulted in more degradation, but the micro-specific parameters of fracture mechanics were considered basically immeasurable, suggesting that the degraded material properties may be related through Continuum Damage Mechanics (CDM). The accumulated fatigue damage for each stress ratio was modeled via random distribution and a two-parameter Weibull distribution. A kinetic law using the cumulative density function was proposed in order to establish a continuum damage parameter. Prediction models for both reduced stiffness and storage modulus were used to compare modeled reductions to tested reductions. The results for the Weibull distribution method were quite promising, especially in terms of showing the rate of degradation, but the random distribution was deemed inapplicable to this particular study, although possibly valid for many other short-fiber reinforced composites.

In summary, two unique mechanical behaviors (i.e., nonlinear material behavior and fatigue-accumulated damage) of WPC were investigated in this study. For nonlinear material characterization of WPC, the load rate effect and hyperbolic tangent function to fit nonlinearity and scale-up of material data to predict the global structural response were studied. They provided better understanding of nonlinear stress-strain relation of WPC under quasi-static load, predicted the deformation of structural components, and

potentially improved design practice for serviceability of WPC. For fatigue-accumulated damage evaluation of WPC, a comprehensive study on fatigue baseline establishment, sample conditioning, and 1-D CDM model were conducted, and a test protocol for sample conditioning via fatigue and assessment by flexural and DMA testing were established. The cumulative probability density function of a 2-parameter Weibull distribution was used to mimic kinetic damage evolution in WPC and a 1-D CDM model was proposed to successfully predict the fatigue-accumulated damage in WPC.

Though a genuine effort was made, some aspects of physical behaviors still need to be further investigated, and they are recommended as follows. WPC specimens at structural level should be tested to validate the scale-up P-Δ predictions based on the hyperbolic tangent function-fitted nonlinear stress-strain relation obtained at the material level. Also, more and diverse experimental tests should be conducted to further validate the proposed 1-D CDM model and establish the CDM model as a reliable and viable methodology in predicting damage accumulation and material degradation in WPC due to different environmental and load factors, such as fatigue shown in this study.

APPENDIX A – QUASI-STATIC TESTING

A.1 Summary

The purpose of the work in this portion of the Appendix is to provide any supplemental calculations, tables, figures, and other additional information that may present a more comprehensive understanding of the methods undertaken in this chapter. This section will outline the data reduction process in further detail for the quasi-static testing of all compositions and loading modes. Calculations for stress and strain in both flexure and tension are provided in A.2. Excerpts from the spreadsheets used to reduce the stress-strain data in flexure and tension are located in A.3 and A.4, respectively.

A.2 Calculations

Below are the equations used for calculating bending stress and strain and tensile stress at every point on the load-deflection curve obtained from LabView. The tensile strains were measured as a percentage by an extensometer attached at the mid-span of the samples and then converted into unitless values by dividing by 100. All stresses and strains were calculated at each time step and compiled into the stress-strain curves displayed in section 2.6.

$$\sigma_b = \frac{3PL}{2bd^2} \tag{a.1}$$

$$\varepsilon_b = \frac{6\Delta d}{16} \tag{a.2}$$

$$\sigma_t = \frac{P}{bd} \tag{a.3}$$

where:

σ_b = bending stress (psi)

σ_t = tensile stress (psi)

P = measure load (lb)

L = span (in)

b = average measured width (in)

d = average measured depth (in)

ε = strain (in/in)

Δ = measured deflection (in)

A.3 Data Reduction

Figure A.3.1 was taken from Sample 1 of HDPE tested in flexure at the standard load rate of 2.7 mm/min. LabView provided base data in time, load, and displacement for flexural tests, and then stress and strain are calculated at every point in accordance with A.2. Figure A.3.2 was taken from Sample 1 of PP tested in tension at 2.7 mm/min. LabView provided base data in load, displacement, and strain, and then stress was calculated at every point in accordance with A.2. The ultimate stress and 10% and 20% of the ultimate stress (MOR) were calculated from the peak load and equations (a.1) and (a.3). MOE is then calculated by taking the slope of the stress-strain values between 10% and 20% of MOR, outlined in red in the Figures below.

Sample 1			C1 (MOE)	σ_{ult}
Avg. Width	0.993		610860.1	3821.84
Avg. Depth	0.254			
10% ult	20% ult			
382.18	764.37			
Time (sec)	Load (lb)	Disp. (in)	Stress (psi)	Strain (in/in)
2.538	0.000	0	0.000	0
3.039	0.054	-0.001	5.050	9.51E-05
3.539	0.269	-0.001	25.250	9.51E-05
4.039	0.913	-0.002	85.841	0.00019
4.539	1.450	-0.003	136.360	0.000285
5.039	1.987	-0.004	186.860	0.00038
5.539	2.470	-0.005	232.282	0.000475
6.039	3.060	-0.006	287.767	0.00057
6.539	3.651	-0.007	343.345	0.000665
7.039	4.188	-0.008	***393.845***	***0.000761***
7.54	4.779	-0.009	449.424	0.000856
8.041	5.369	-0.009	504.908	0.000856
8.542	5.906	-0.01	555.408	0.000951
9.042	6.443	-0.011	605.909	0.001046
9.542	6.980	-0.012	656.409	0.001141
10.042	7.570	-0.013	711.893	0.001236
10.543	8.107	-0.014	***762.393***	***0.001331***
11.043	8.644	-0.015	812.894	0.001426
11.544	9.181	-0.016	863.394	0.001521
12.044	9.718	-0.017	913.894	0.001616
12.544	10.260	-0.017	964.865	0.001616
13.045	10.740	-0.018	1010.004	0.001711
13.545	11.280	-0.019	1060.787	0.001806
14.045	11.760	-0.02	1105.927	0.001901
14.545	12.240	-0.021	1151.066	0.001996
15.045	12.780	-0.022	1201.849	0.002091
15.545	13.210	-0.023	1242.287	0.002186
16.045	13.690	-0.024	1287.426	0.002282
16.545	14.170	-0.025	1332.566	0.002377
17.045	14.660	-0.025	1378.647	0.002377
17.546	15.140	-0.026	1423.786	0.002472
18.046	15.620	-0.027	1468.926	0.002567
18.546	16.050	-0.028	1509.364	0.002662
19.046	16.540	-0.029	1555.444	0.002757
19.546	16.970	-0.03	1595.882	0.002852

Figure A3.1. Example of flexural stress-strain data reduction.

UNCOUPLED	C_1 (MOE)	σ_{ult}
Sample 1	741238.62	1814.723
Avg Width	0.731	
Avg. Depth	0.128	
10%σult	20%σult	
181.47	362.94	
Load (lb)	Stress (psi)	Strain (%)
0	0	0
3.114	33.280609	0.0013
5.423	57.957849	0.0054
7.785	83.201522	0.0094
10.04	107.30164	0.0107
12.35	131.98957	0.0148
14.55	155.50188	0.0174
16.75	***179.01419***	***0.0188***
18.95	202.5265	0.0228
20.99	224.32883	0.0242
23.03	246.13116	0.0282
25.07	267.93348	0.0309
27.06	289.20144	0.0336
29.1	311.00376	0.0362
31.09	332.27172	0.0376
33.02	352.89843	0.043
34.95	***373.52514***	***0.0456***
36.72	392.44186	0.0456
38.6	412.5342	0.0497
40.81	436.15339	0.0537
42.63	455.60448	0.055
44.4	474.5212	0.0577
46.17	493.43793	0.0617
47.52	507.86594	0.0644
49.66	530.737	0.0658
51.28	548.05062	0.0685
52.99	566.32609	0.0711
54.55	582.99846	0.0738
56.16	600.2052	0.0779
57.77	617.41194	0.0792
59.38	634.61867	0.0792
60.99	651.82541	0.0859
62.5	667.96341	0.0846
63.95	683.46016	0.0899
65.45	699.49128	0.0926
66.9	714.98803	0.094
68.35	730.48478	0.0953
69.8	745.98153	0.1007
71.25	761.47828	0.102

Figure A3.2. Example of tensile stress-strain data reduction.

APPENDIX B – LOAD RATES

B.1 Summary

The purpose of the work in this portion of the Appendix is to provide any supplemental figures, explanations, and other additional information that may present a more comprehensive understanding of the methods and purposes of this chapter. The effect of load rate, also denoted dD/dt for "change in displacement over change in time", was studied for one composition in one loading mode. High density polyethylene (HDPE) was tested in flexure on the 22-kip MTS 810 loading frame in a strain-controlled environment. The load rates used in this research were 2.2, 5, 10, 20, 30, and 40 mm/min. Stress-strain curves for each load rate are provided in section B.2 in Figures B.2.1 – B.2.6.

B.2 Load Rates

The following figures are the stress-strain curves at each load rate. Each chart also includes the generic hyperbolic tangent function as a reference for sections including that topic. It was included here in order to avoid redundancy in showing the same six graphs again in B.3. The average C_1 and C_2 coefficients of all five samples at each load rate were used to create the general curve, which steps in strain increments of 0.0001 in/in and is represented by a thin solid black line denoted "X".

The linear regression technique utilized in 2.3.3 refers to the log-scale curves for MOE and MOR vs. load rate. Figures B.2.7 and B.2.8 below display the curves on a standard scale, but also do not include the load rate of 40 mm/min.

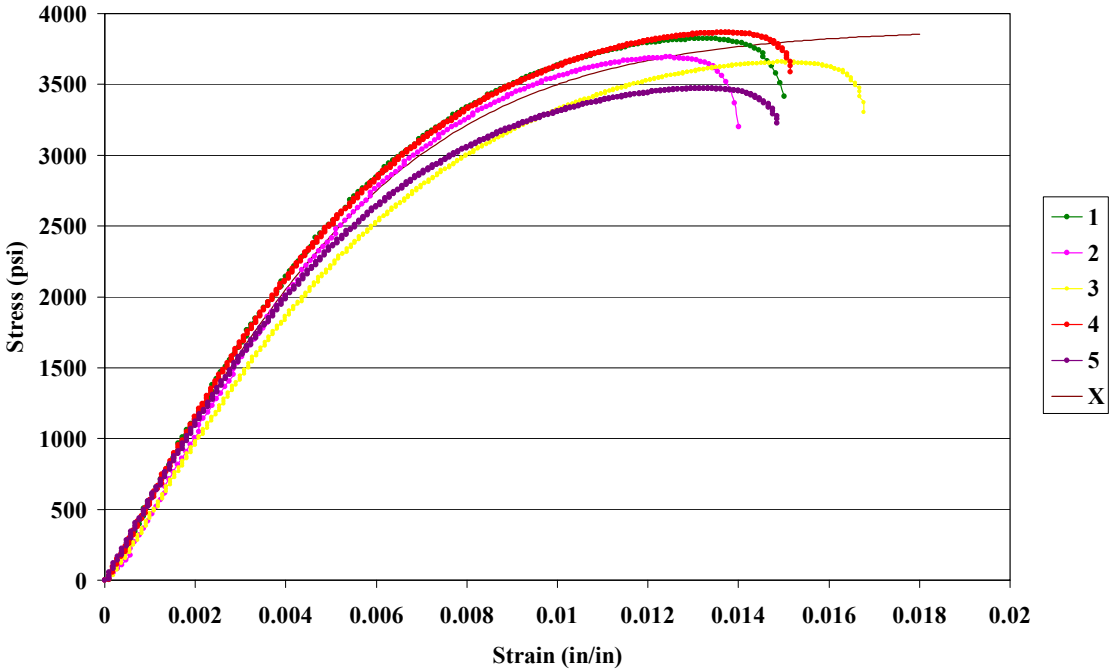

Figure B2.1. Stress vs. strain for HDPE in flexure at 2.7 mm/min (standard).

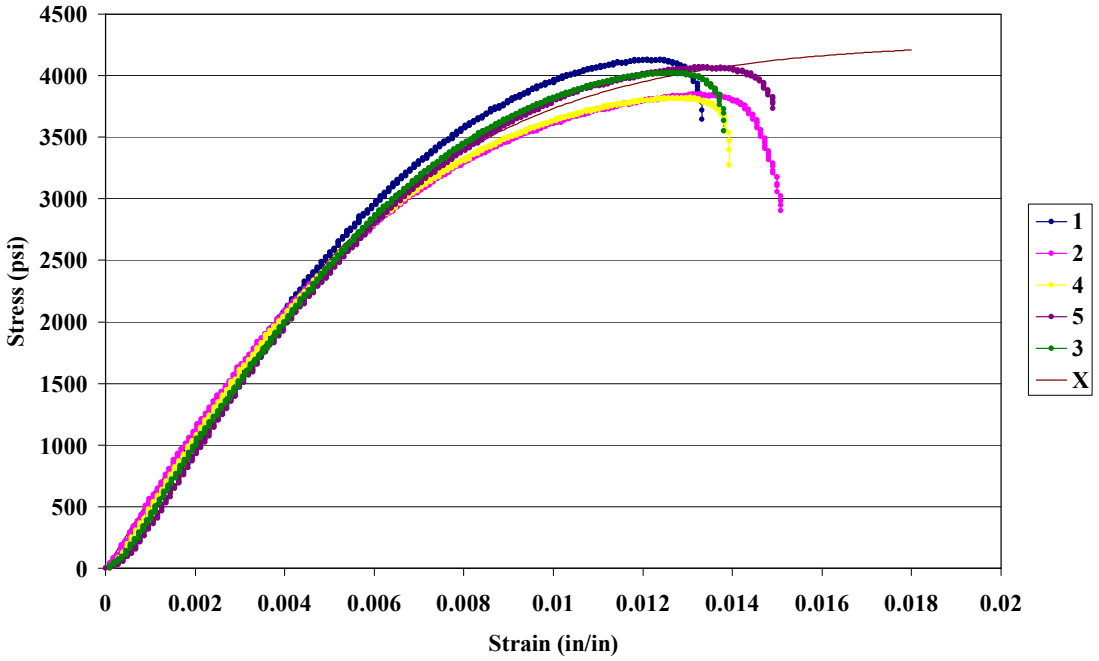

Figure B2.2. Stress vs. strain for HDPE in flexure at 5 mm/min.

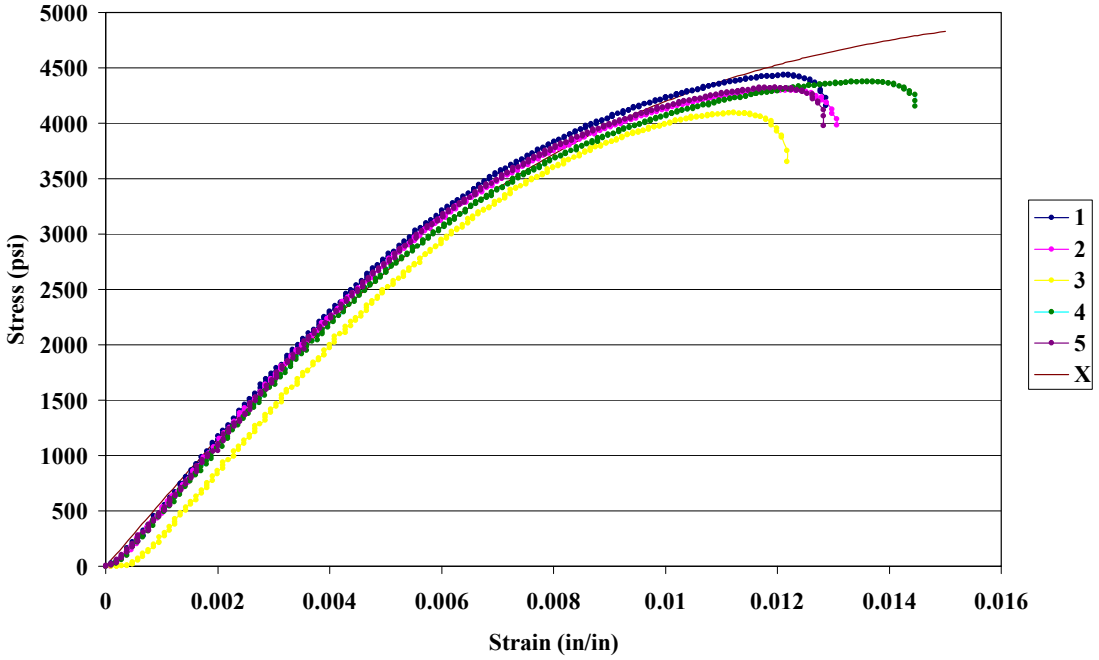

Figure B2.3. Stress vs. strain for HDPE in flexure at 10 mm/min.

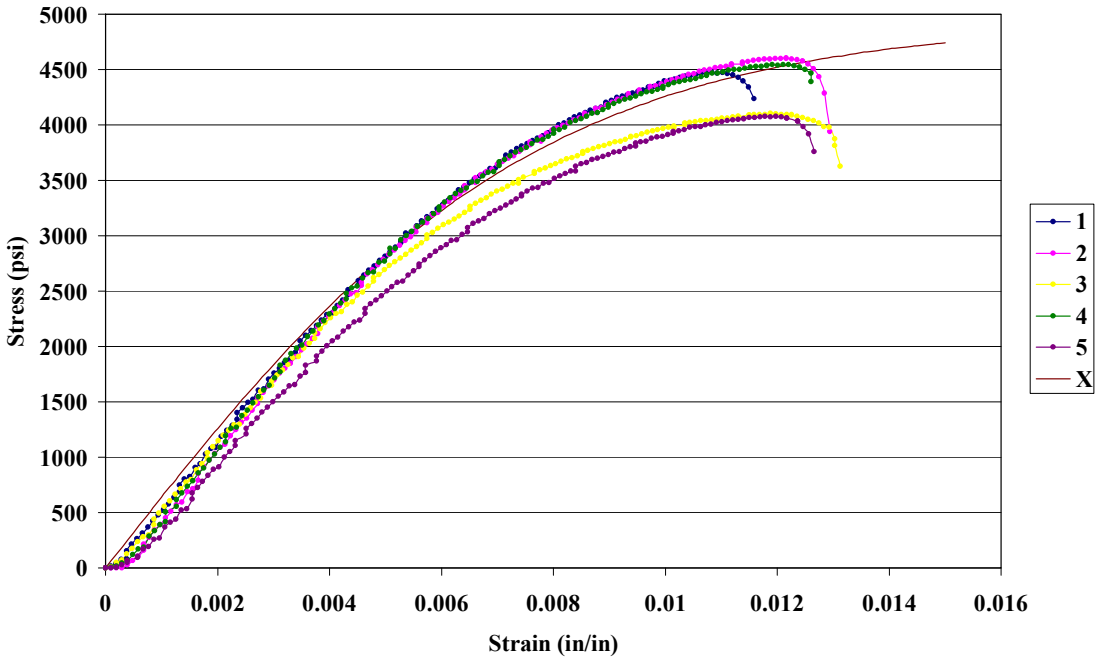

Figure B2.4. Stress vs. strain for HDPE in flexure at 20 mm/min.

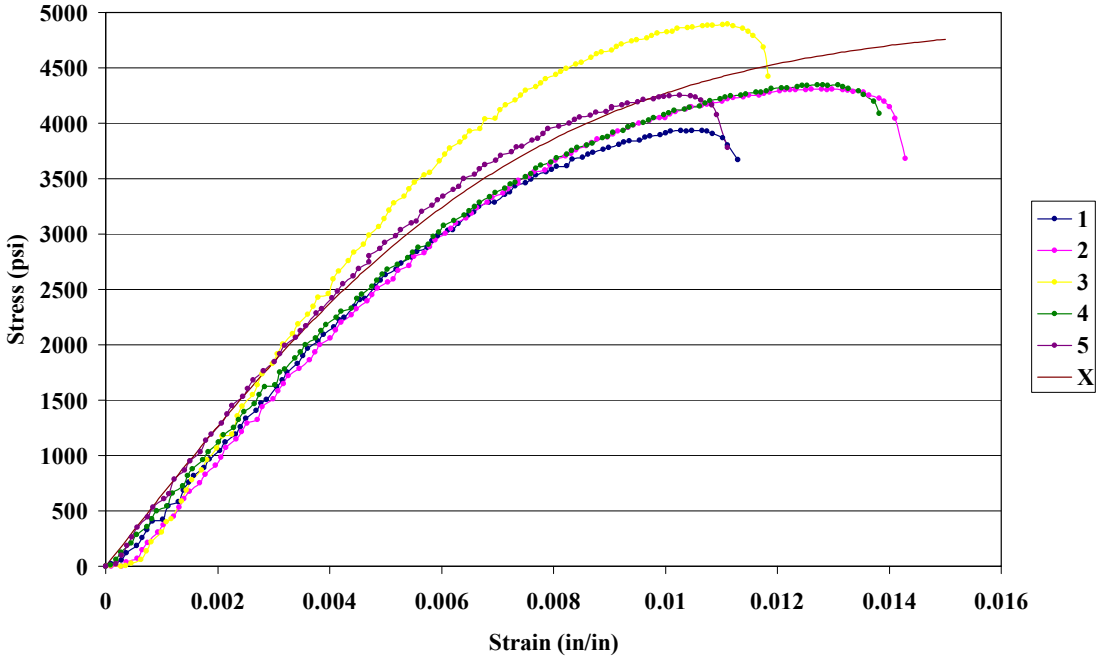

Figure B2.5. Stress vs. strain for HDPE in flexure at 30 mm/min.

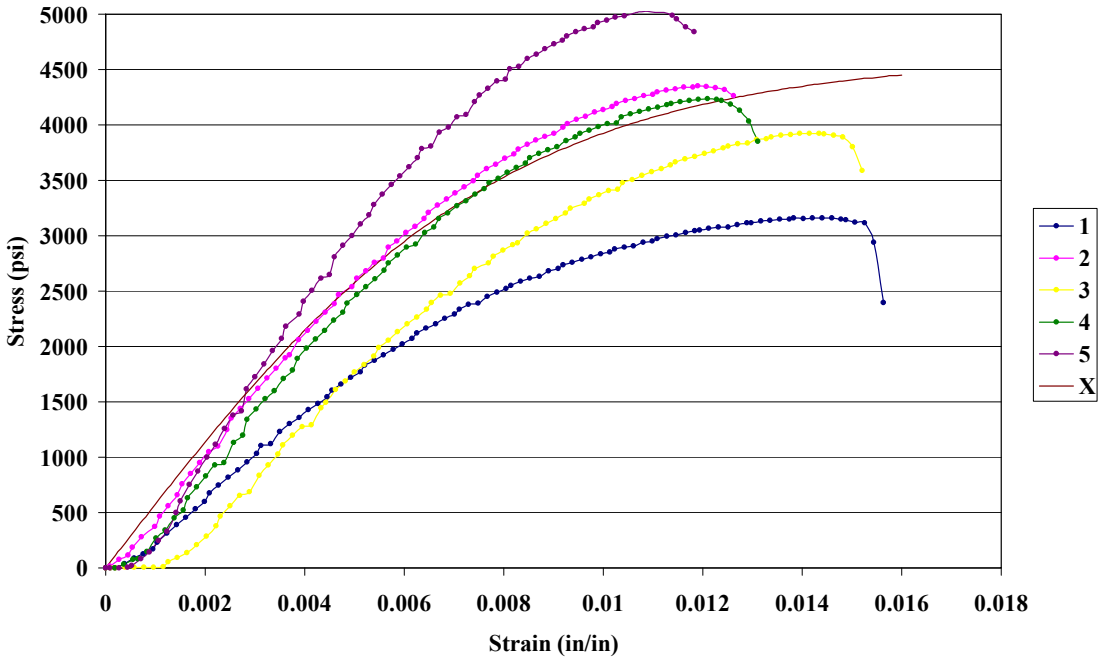

Figure B2.6. Stress vs. strain for HDPE in flexure at 30 mm/min.

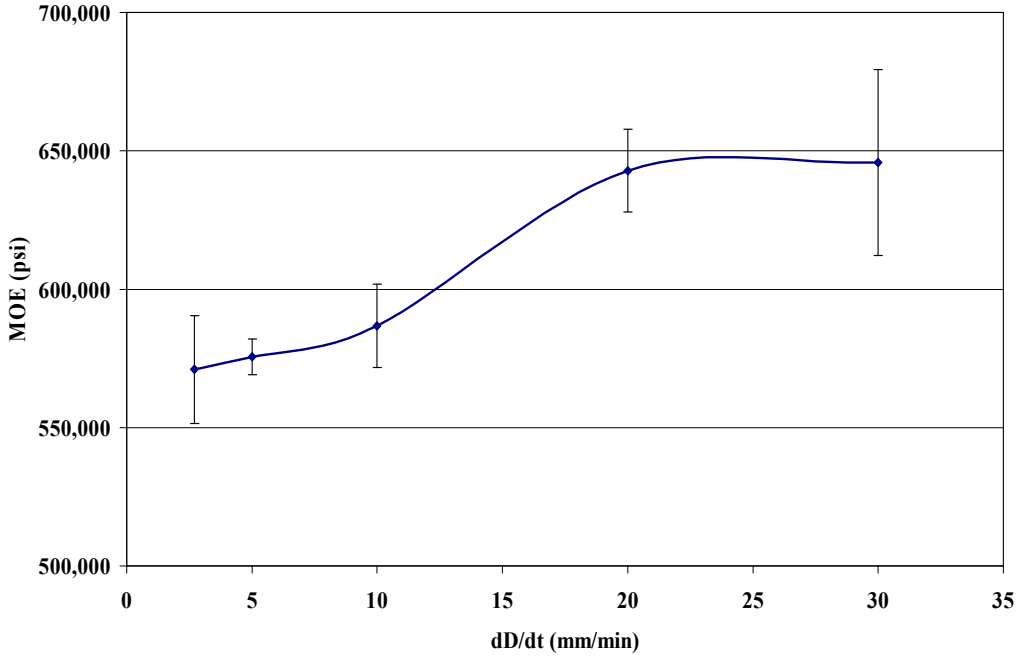

Figure B2.7. MOE vs. load rate for HDPE in flexure ($2.2 \leq dD/dt \leq 30$).

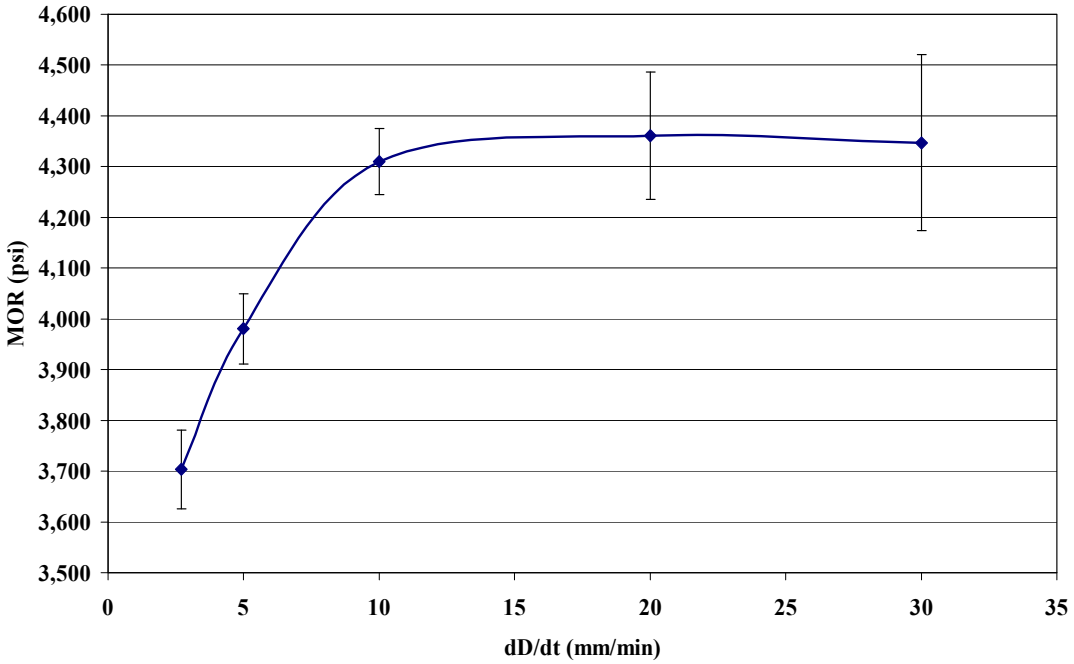

Figure B2.8. MOR vs. load rate for HDPE in flexure ($2.2 \leq dD/dt \leq 30$).

APPENDIX C – HYPERBOLIC TANGENT FUNCTION

C.1 Summary

The purpose of the work in this portion of the Appendix is to provide any supplemental tables or figures, computer algorithms, equations, and other additional information that may present a more comprehensive understanding of the methods and purposes of this chapter.

The purposes of the hyperbolic tangent function under the applications of this research were two-fold. The first objective was to use it to fit the observed nonlinear stress-strain behavior and estimate reductions in stiffness for 3 WPC blends under tension and flexure. In Microsoft Excel, the columns of measured stress and strain were converted to hyperbolic tangent stresses and Chi-Squared values at each data point as outlined in Section 2.3.4. Visual Basic was used to minimize the sum of the Chi-Squared column by testing possible values of C_2 in a selected range against each other until the correct C_2 was found. The second was to derive plausible methods for predicting service deflections for axial and pure bending cases of one WPC composition, coupled polypropylene.

C.2 Data Reduction

Figure C2.1 was taken from Sample 1 of HDPE tested in flexure at the standard load rate of 2.7 mm/min. The "HyperTan" column calculates the hyperbolic stresses per Eq. (2.3) and the "Chi" column calculates the Chi-Squared difference per Eq. (2.4) at each data point. As C_2 is incrementally varied, the cell entitled "Chi Sum" calculates the summation of those differences at every step and compares the coefficient to the one stored from the last step. The C_2 that minimizes "Chi Sum" represents the best possible fit for a given data set. In Figure C2.1, the "HyperTan" stresses closely resemble the actual observed stresses because C_2 matches σ_{ult} almost identically. Section C3.2 of this appendix demonstrates how the Visual Basic Editor and this spreadsheet are utilized to find the desired coefficient. This excerpt is representative of the procedure used for all samples in all scenarios of the study.

Sample 1		C_1 (MOE)	C_2	σ_{ult}	Chi Sum	
Avg Width	0.993	610860	3820	3821.84	319.05	
Avg Depth	0.254				Calculate	
10% ult	20% ult					
382.18	764.37					
Time (sec)	Load (lb)	Deflection	Stress	Strain	HyperTan	Chi
2.538	0.000	0	0.000	0		
3.039	0.054	-0.001	5.050	9.51E-05		
3.539	0.269	-0.001	25.250	9.51E-05		
4.039	0.913	-0.002	85.841	0.00019		
4.539	1.450	-0.003	136.360	0.000285		
5.039	1.987	-0.004	186.860	0.00038		
5.539	2.470	-0.005	232.282	0.000475		
6.039	3.060	-0.006	287.767	0.00057		
6.539	3.651	-0.007	343.345	0.000665	Starting @ 10%σ_{ult}	
7.039	4.188	-0.008	393.845	0.000761	404.9619	0.305162
7.54	4.779	-0.009	449.424	0.000856	462.2824	0.357671
8.041	5.369	-0.009	504.908	0.000856	519.3924	0.40392
8.542	5.906	-0.01	555.408	0.000951	519.3924	2.49744
9.042	6.443	-0.011	605.909	0.001046	576.2668	1.524702
9.542	6.980	-0.012	656.409	0.001141	632.881	0.874664
10.042	7.570	-0.013	711.893	0.001236	689.2107	0.746498
10.543	8.107	-0.014	762.393	0.001331	745.2324	0.395181
11.043	8.644	-0.015	812.894	0.001426	800.9227	0.178922
11.544	9.181	-0.016	863.394	0.001521	856.2593	0.059448
12.044	9.718	-0.017	913.894	0.001616	911.22	0.007848
12.544	10.260	-0.017	964.865	0.001616	965.7836	0.000875
13.045	10.740	-0.018	1010.004	0.001711	965.7836	2.024758
13.545	11.280	-0.019	1060.787	0.001806	1019.929	1.636701
14.045	11.760	-0.02	1105.927	0.001901	1073.638	0.971076
14.545	12.240	-0.021	1151.066	0.001996	1126.889	0.518742
15.045	12.780	-0.022	1201.849	0.002091	1179.664	0.417192
15.545	13.210	-0.023	1242.287	0.002186	1231.947	0.086779
16.045	13.690	-0.024	1287.426	0.002282	1283.719	0.010705
16.545	14.170	-0.025	1332.566	0.002377	1334.966	0.004313
17.045	14.660	-0.025	1378.647	0.002377	1385.67	0.035603
17.546	15.140	-0.026	1423.786	0.002472	1385.67	1.048468
18.046	15.620	-0.027	1468.926	0.002567	1435.819	0.763391

Figure C3.1. Example of hyperbolic tangent fit data reduction for HDPE in flexure.

C.3 Visual Basic

The following is an excerpt from the Visual Basic code that was used to find C_2 for Sample 1 of HDPE in flexure at 2.7 mm/min. This excerpt was repeated for all samples within a test and all codes were identical in sequence and procedure. The only items that changed between mixtures and loading modes were the range of data (9, 10) and the reference cells (16, 17, 28), which would obviously vary from sheet to sheet in the Excel file.

```
1       Private Sub cmdSubmit1_Click()
2
3       Application.ScreenUpdating = False
4
5       Dim ChiVals() As Double
6       Dim ChiMin, ChiCheck, C2, v1, v2, i, j As Double
7
8       'For 2.2mm Test 1 ----------------------------------------------------
9       v1 = 3000
10      v2 = 15000
11
        12      ReDim ChiVals(v2 - v1 + 1, 1)
13
14      'Coarse Filter for min Chi Sum
15      For i = v1 To v2
16      Sheets("2.7 mm data").Cells(2, 4).Value = i
17      ChiVals(i - v1 + 1, 1) = Sheets("2.7 mm data").Cells(2, 6).Value
18      Next i
19
20      ChiCheck = ChiVals(1, 1)
21      For j = LBound(ChiVals) To UBound(ChiVals)
22      If ChiVals(j, 1) <= ChiCheck Then
23      ChiCheck = ChiVals(j, 1)
24      C2 = j + v1 - 1
25      End If
26      Next j
27
28      Sheets("results").Cells(3, 2).Value = C2
29      'END Test 1 -----------------------------------------------------
```

C.4 P-Δ using Matlab

The following Matlab code was used to develop force-displacement curves for the pure bending case outlined in section 2.4.3. The comments are inserted to help explain the methodology in the algorithms.

```
%%%%%%%%%%%%%%%%%%%%%%%%%%%%%%%%%%%%%%%%%%%%%%%%%%%%%%%%%%%%%%%%%%%%%%%%%%%%
The loop below applies the function w(x,F) across a vector of forces
for a location of x=2 and plots the resulting force-deflection data.
%%%%%%%%%%%%%%%%%%%%%%%%%%%%%%%%%%%%%%%%%%%%%%%%%%%%%%%%%%%%%%%%%%%%%%%%%%%%
inc=1;
Fmax=70;
F=[1:inc:Fmax]';
d=zeros(length(F),1);
tic;
for i=1:length(F)
    y=w(2,F(i));
    d(i,1)=y;
end
toc;
plot(d,F)


function y = w(x,F)
%%%%%%%%%%%%%%%%%%%%%%%%%%%%%%%%%%%%%%%%%%%%%%%%%%%%%%%%%%%%%%%%%%%%%%%%%%%%
% Name:     Deflection under 3point bending for beam with nonlinear
%           materials
% Programmed by:   Wei Fan
% Date:     Sep/29/2008
% Input:    x: locations, can be a vector
%           F: concentrated mid span force for 3 point bending
%%%%%%%%%%%%%%%%%%%%%%%%%%%%%%%%%%%%%%%%%%%%%%%%%%%%%%%%%%%%%%%%%%%%%%%%%%%%
This function numerically solves the curvature cubic expression in
equation 2.17 and integrates the resulting vectors along x twice,
producing single deflection values for a given force and location.
%%%%%%%%%%%%%%%%%%%%%%%%%%%%%%%%%%%%%%%%%%%%%%%%%%%%%%%%%%%%%%%%%%%%%%%%%%%%
%%%%%%%%
for i=1:length(x)
    slopex=@(x)slope(x,F);
    y(i)=quad(slopex,0,x(i));
end
end
```

```
%%%%%%%%%%%%%%%%%%%%%%%%%%%%%%%%%%%%%%%%%%%%%%%%%%%%%%%%%%%%%%%%%%%%%%%%%%%%
The following function finds slope by integrating the curvature values
along x using a built in solver.
%%%%%%%%%%%%%%%%%%%%%%%%%%%%%%%%%%%%%%%%%%%%%%%%%%%%%%%%%%%%%%%%%%%%%%%%%%%%
function y = slope(x,F)
%%% Parameter Input: Span %%%%%%%%%%%%%%%
L=4;
%%%%%%%%%%%%%%%%%%%%%%%%%%%%%%%%%%%%%%%%
for i=1:length(x)
    if abs(x(i))<1e-8
        x(i)=1e-8;
    end
    curvature=@(x)curvatureroot(x,F);
    y(i)=quad(curvature,0,x(i))-quad(curvature,0,L/2);
end
end


%%%%%%%%%%%%%%%%%%%%%%%%%%%%%%%%%%%%%%%%%%%%%%%%%%%%%%%%%%%%%%%%%%%%%%%%%%%%
%%%%%%%%
The following function solves the cubic equation for curvature and
rejects the imaginary components of the solution before storing them in
a vector.
%%%%%%%%%%%%%%%%%%%%%%%%%%%%%%%%%%%%%%%%%%%%%%%%%%%%%%%%%%%%%%%%%%%%%%%%%%%%
%%%%%%%%
function y = curvatureroot(x,F)
%%% Parameter Input%%%%%%%%%%%%%%%%%%%%%%%%%%%%%%%
%%% A material constant, measured modulus of elasticity
c1=636,058;
%%% A material constant, evaluated modulus of rupture
c2=3801;
%%% Sample depth
h=0.25;
%%%%%%%%%%%%%%%%%%%%%%%%%%%%%%%%%%%%%%%%%%%%%%%%%%%%%%
for i=1:length(x)
    c=[-1./3.*c1.^3.*h.^5./80./c2.^2,0,h.^3.*c1./12, F.*x(i)./2];
%%polynomial
    r = roots(c);
    p=r(1);
    for j=2:3
        if (abs(imag(r(j)))<1e-20) && (real(r(j)) < 1e-20) &&
(abs(r(j))<abs(r(j-1)))
            p=r(j);
        end
    end
    if (abs(imag(p))<1e-20) && (real(p) < 1e-20)
        y(i)=real(p);
    else
        error('No real negative root')
    end
end
end
```

APPENDIX D – FATIGUE CONDITIONING

D.1 Summary

The processes of determining fatigue life and conditioning samples prior to dynamic mechanical analysis involved a system of components working together. Some of the tests take many hours, even several days on some certain occasions. Since the system is powered by hydraulic pressure, it is capable of creating massive amounts of force. Therefore, the user must be aware of how the components contribute to the overall operation and how to monitor and control the tests in order to assure quality and above all, safety.

D.2 System Operation

The 22-kip MTS servo-hydraulic frame was connected to the main hydraulic supply and operated by a hydraulic service manifold (Figure D3.1). Supply and return valves can be switched on and off to control the flow of hydraulic oil pressure to the frame. The top of the frame held the 1-kip load cell that was connected to the crosshead used for 3-point bending. The roughly 50 pound base was attached to the bottom of the frame using a 2-nut system similar to those used for the quasi-static tests in this study. A cable connected the load cell to the MTS 407 controller interface where all the user inputs could be toggled. These inputs included AC/DC commands, the proportional-integral-derivative (PID) gain adjustments, command signals, loading ramp rates, etc. Too much detail in this area will become far too monotonous, but the 407 interface controls the entire test. Two BNC cables (AC and DC) were run from the 407 controller

to a switchboard, which was then connected to the computer. Through the 407 interface, the user can enter the set point load/displacement, the span to which it oscillates around, what type of wave to feed, frequency, interlock limits for safety, and countless other electronic settings that make the hydraulic frame operate.

D.3 Quality Control

Conducting a fatigue study with hydraulics in a sensitive multi-component system means that the stress and strain amplitudes are difficult to control and must be carefully monitored. In order to assure that the applied load amplitudes were tolerable, two things were done. First, a specific program was written in LabView that was capable of recording load vs. time and displacement with a high sample collection rate, say greater than 100 Hz. However, the program didn't necessarily record measurements at the max ad min of each cycle since it was impossible to exactly match the sample collection frequency with the loading frequency (due to miniscule error in each). Therefore, it was necessary to record over an extended period of time so as to collect thousands of points and catch as many peaks and valleys as possible. This load vs. time measurement was represented as a block of dispersed data with clear and consistent limits. This procedure was done for every fatigue test and was carefully monitored throughout to check for jumps or dips in the cycles, which were never observed.

Second, a Fluke Model 97 50MHz Scopemeter (commonly referred to as the Fluke) was connected to the 407 interface through BNC cables. Two channels, A and B, relayed the command and feedback signals from the test frame to the screen of the Fluke. If the user commands a sine wave, then a perfect sine wave of the cycling would show up

on the screen as curve “A” and whatever the load cell was actually reading would show up as curve “B”. The more perfectly they overlapped then the more accurate the load amplitudes. See Figure D3.2 for an example.

Figure D3.1. The hydraulic service manifold (HSM).

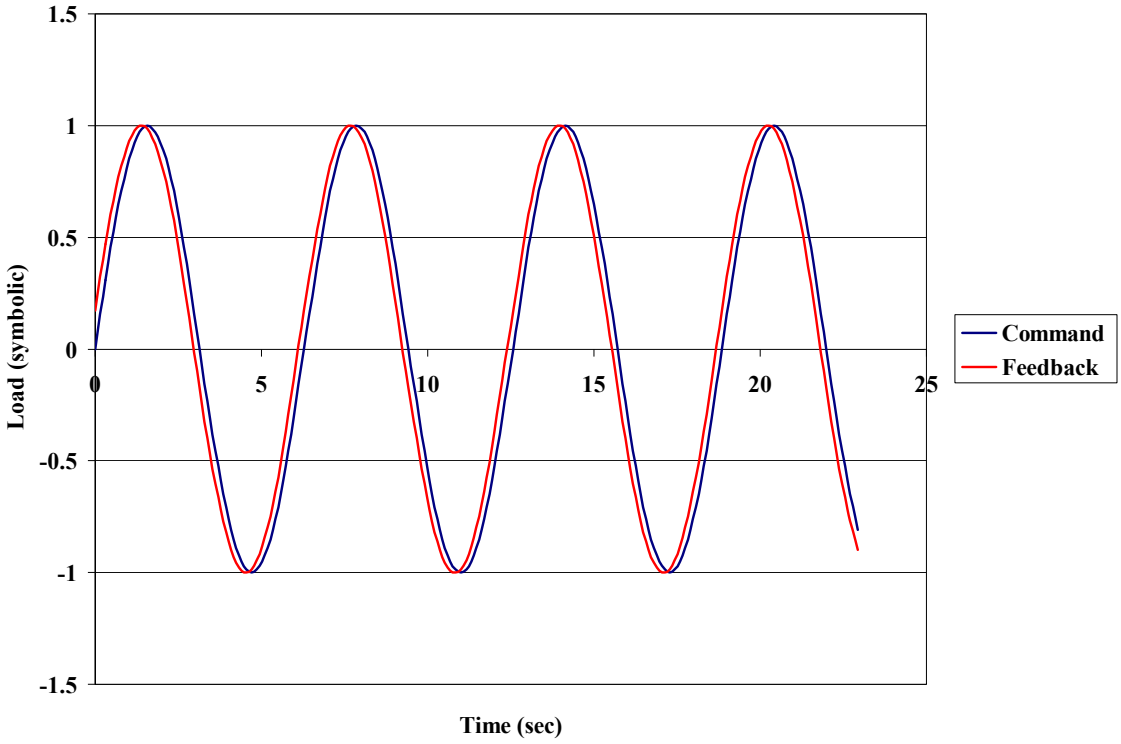

Figure D3.2. Example of Fluke Scopemeter reading.

APPENDIX E – DMA SUPPLEMENTAL IMAGES

E.1 Summary

Dynamic mechanical analysis (DMA) was conducted in Chapter 4 to determine the thermodynamic and initial and degraded properties for coupled wood-polypropylene. Before being sent to DMA, the samples had to be machined down to very small dimensions (52 mm x 12 mm x 3.2 mm ± 2 mm tolerance). The compressive stressed side of the samples was shaved off using a Sherline 2000 3-D milling machine and the samples were cut down to 12 mm wide with a Microlux 3 ¼" tables saw, depicted in Figures E1.1 and E1.2, respectively. An RSA II Solids Analyzer (Figure E1.3) was used to verify the glass transition temperature for the material prior to conducting the rest of the analysis. The purpose of this was to make sure that the mixture extruded was similar in all respects to other wood-polypropylene composites. The observed properties in Chapter 2 and the T_g measured at 0°C did indeed verify that this mixture was consistent with those used in previous studies. A Tritec 2000 DMA-8 (Figure E1.4) was used to conduct strain sweeps and temperature sweeps on the fatigued samples. This data was used to compare dynamic mechanical properties at a certain controlled temperature among the samples with various damage accumulation.

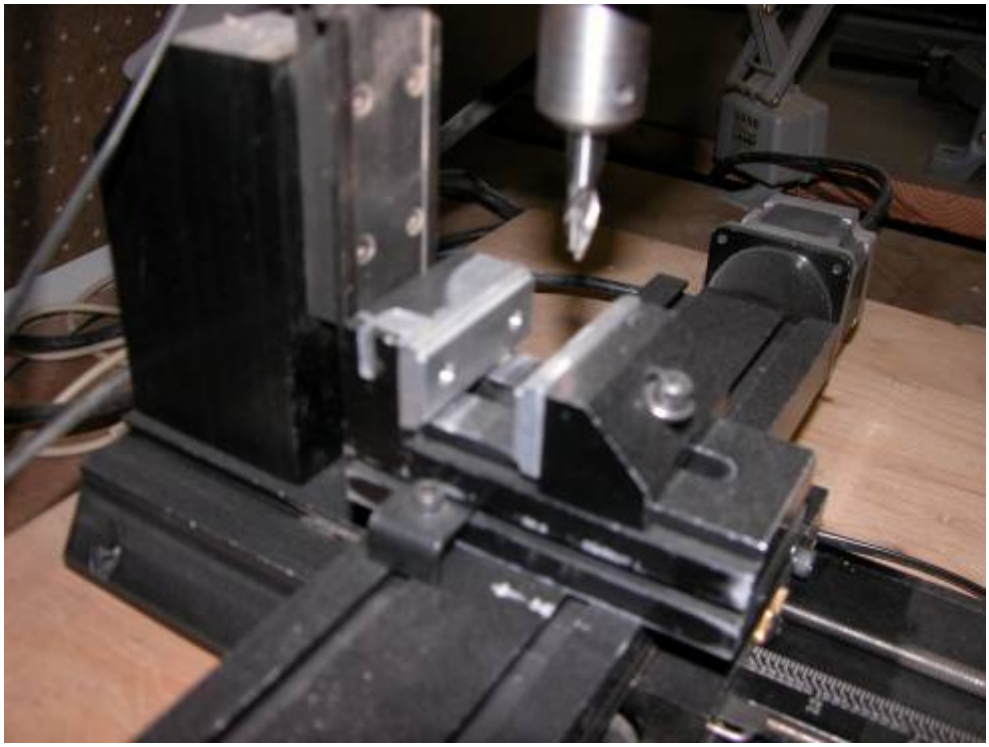

Figure E1.1. Sherline 2000 3-D milling machine.

Figure E1.2. Microlux 3 ¼" table saw.

Figure E1.3. RSA II Solids Analyzer.

Figure E1.4. Tritec 2000 DMA-8.